FINAL REPORT

to

US Department of Energy

CYCLOTRON AUTORESONANCE ACCELERATOR FOR ELECTRON BEAM DRY SCRUBBING OF FLUE GASES

DE-FG02-97-ER 12209

Submitted by: _____

J. L. Hirshfield
Principal Investigator

May 25, 2001

Yale University
Beam Physics Laboratory
272 Whitney Avenue - WNSL
New Haven, CT 06511

DISCLAIMER

Cyclotron Autoresonance Accelerator
for Electron Beam Dry Scrubbing of Flue Gases
DE-FG02-97-ER 12209
April 1, 1997 – December 31, 2000

SUMMARY OF RESEARCH RESULTS

Experimental and theoretical work carried out under this grant embraced several interrelated subjects, all involving use of a cyclotron autoresonance accelerator (CARA). These subjects including the following:

- design and laboratory test of a CARA with specifications suitable for e-beam dry scrubbing of flue gases;
- analysis, design and laboratory test of a CARA for generation of seventh-harmonic radiation at 20 GHz, based on near-coincidental phase matching;
- analysis, simulation, and design of a cavity CARA for generation of eighth-harmonic radiation at 91 GHz;
- analysis, simulation, and design of a laser-driven CARA, dubbed LACARA, for high-gradient acceleration of electrons in a strong guide magnetic field;
- analysis and simulation of a low-frequency CARA for high-gradient acceleration of protons (or muons), using a cascade of resonant cavities; and
- analysis of parameters for an e-beam source suitable for remediation of SO_2, NO_x, and particulates in emanations from coal-burning power plants.

Archival publications resulted on all of these topics, save the last. Reprints of these publications are included at the end of this report. The main results of the 3-1/2 year research program include: (*i*) a deeper understanding of the microwave version of CARA itself; (*ii*) extensions of the CARA concept to higher (infrared) and lower (UHF) frequency drivers for acceleration of multi-MeV electron beams and protons, respectively; (*iii*) use of the gyrating electron beam produced in a microwave CARA in a high-harmonic generator of high-power coherent millimeter-wave power; and (*iv*)

improved understanding of parameters required for an electron-beam source to remove SO_2, NO_x, and particulates in emanations from high-power coal-burning power plants. It can be seen that some of these topics were not anticipated when the original DoE grant proposal was written in 1996. But, as is not uncommon in basic research, serendipity intruded to cause discovery of unexpected phenomena invoking the CARA mechanism. Some of these topics have acquired independent status: the seventh- and eighth-harmonic generators and LACARA are themselves now subjects of DoE-funded research projects. A summary follows of un-published findings regarding e-beam remediation of flue gas emissions.

Dose Requirements. Numerous published studies give a wide range of results on removal of SO_2 and NO_x from flue gases.[1] Here, we cite briefly only representative data. A typical published report[2] describes tests using three 800 kV, 36 kW dc e-beam sources (108 kW total) irradiating the flue gas from a pilot-scale plant with flow rate of 12,000 m^3/hr. The results show that an absorbed dose of about 7 kGy is sufficient for removal of 95% SO_2 in a gas mixture with initial concentrations of 650-950 ppm SO_2 and 150-230 ppm NO_x in the presence of ammonia at a gas temperature of 62-64 °C. The same dose resulted in removal of 95% NO_x in a gas mixture with initial concentrations of 650-950 ppm SO_2 and 140-200 ppm NO_x. Details as to variations with ammonia and water vapor concentration were not provided. More recently, tests in Chengdu, China[3] have been reported on a demonstration plant with a flow rate of 300,000 m^3/hr using two 800 kV, 320 kW dc e-beam sources (640 kW total). Here it is claimed that an absorbed dose of 3.2 kGy is sufficient to reduce SO_2 concentration from 1800 ppm to 65 ppm, but NO_x concentration is only reduced from 400 ppm to 320 ppm. Both ammonia and water vapor addition are used in the Chengdu tests. However, since a power deposition of 640 kW with a flow rate of 300,000 m^3/hr ($\approx$ 83 kg/sec) corresponds to a dose of 7.7 kGy; it appears that the efficiency of beam coupling to the flowing gas in the Chengdu tests is only about 42%. Uncertainty in required dose, a need for high beam coupling efficiency,

[1] *Environmental Applications of Ionizing Radiation,* W. J. Cooper, R. D. Curry, and K. E. O'Shea, eds. (John Wiley & Sons, Inc., New York, 1998).
[2] "Electron-Beam Technology for Purification of Flue Gas," by I. Tokunaga, in ref. 1.
[3] *personal communication,* 2000.

and the desire to optimize removal of SO_2 and NO_x by control of thermal reactions (i.e., reactions that do not depend upon the e-beam at all), suggest that the dose be carefully optimized in concert with other parameters. Accordingly, the technical specifications we employ in the discussion that follows are for a range of parameters as embodied in two systems: one to deliver a dose of 8.6 kGy, the second to deliver a dose of 4.3 kGy.

E-Beam Systems. Simple considerations suggest strongly that optimum e-beam sources for pollution remediation in flue gases should operate with beam energies that are sufficient to allow the beam to penetrate up to 10 m of flowing gas. This follows from the required dimensions of the exhaust flow channel for a full-scale plant. For example, a 300 MWe power plant has an exhaust flow of about 280 m^3/sec. If the flow speed is to not exceed 14-18 m/sec (to maintain nearly laminar flow), and if the height of the flow channel illuminated by the e-beam is not to exceed 2 m (larger windows may be impractical), it follows that the flow channel width must be 8-10 m. [Alternately, multiple flow channels can be used, but this may impose a restriction that not all power plant operators would wish to tolerate.] Penetration of 8 m of atmospheric pressure gas requires the energy of the e-beam to be about 1.6 MeV. For a dose of 8.6 kGy, the total required beam power is 2,400 kW, as can be delivered by six 400 kW e-beam sources.[4] Another consideration is the volume of e-beam source equipment that must be installed within a biological shield. Typical volumes are ~100 m^3/MW for dc rectifier machines built for Ebara Corporation, ~40 m^3/MW for high-power transformer accelerator HPTA, but well below 20 m^3/MW for pulsed rf accelerators discussed here. The 1.2-2.5 MeV, 20 kW ILU-6 rf accelerator requires a 3×4×5 m interior space plus 180 m^3 volume of 1.5 m thick concrete! Pulsed rf accelerators require a small volume of x-ray shielding since elements of the system wherein high voltages and/or high energy e-beams reside are smaller than for alternate technologies. But even beyond the volume requiring heavy shielding, a clear overhead height within the shield must be provided if the e-beam source

[4]The dose level cited in this paragraph, and in what follows, assumes a wet air mass density value for the flue gas of 1.0 kg/m^3. This value is accurate for an air temperature of about 60 °C, but must be corrected for other gas conditions. Dose values cited in this report may require correction by dividing the cited value by the actual gas density in kg/m^3. It is further assumed that the e-beam is totally stopped within the flue gas, thus giving up all its energy.

operates using an insulating gas, such as SF_6. In such a case the pressure tank enclosing the high-voltage components must be installed with sufficient overhead height to allow hoisting the tank from above for maintenance. This could easily double the volume of the shield, with a concomitant increase in capital cost. If, for comparison, one uses 200 m^3/MW for the size of Ebara machines and 20 m^3/MW for pulsed rf accelerators, the interior volume requiring biological shielding for a 300 MWe power plant would be about 480 m^3 for Ebara machines and 48 m^3 for pulsed rf accelerators.[5] Realistic costs for e-beam systems must include the e-beam system itself, plus all ancillary shielding structures required. Taken together, these considerations lead to a set of parameters given in Table I for e-beam irradiation of flue gas mixtures for optimum removal of SO_2 and NO_x. The parameters shown result from normalization, so as to apply to an "equivalent 100 MWe plant." Use of this unit plant proves convenient for estimations applying to plants of different generation capacity: for example 50-100 MWe for a typical industrial demonstration project, 300 MWe for a medium-sized modern plant, and 600 MWe (or larger) for a large-sized modern plant. The parameters in Table I are for a pulsed e-beam source since high wall-plug efficiency at high-power requires pulsed operation (>60% is anticipated). Moreover, pulsed operation leads to e-beam current densities that are higher (for the same irradiation geometry) by the reciprocal of the duty factor, as compared with dc current densities at the same beam power. For example, for a pulsed system with 4% duty factor, the current density would be 25 times higher than for an equal power dc e-beam. This could be significant since it has been suggested that high current density might lead to lower dose for a given degree of SO_2 removal. The current density value of 4 mA/cm^2 shown in Table I is arrived at by assuming that the 6.25 A e-beam is fanned out uniformly to illuminate the full 7.8 cm × 200 cm = 0.156 m^2 area of the window. Alternatively, the beam can be expanded to an area occupying about 7.8 cm × 7.8 cm, and scanned at a 2.5 kHz rate along the window; in this case, the instantaneous current density would be about 100 mA/cm^2. Wide flexibility in optimization of current density is inherent in the design approach described. The configuration for illumination

[5]For 2 MeV x-rays at normal incidence, 100 cm of Barytes concrete yields a transmission factor of 1.1×10^{-7}, while an additional 10 cm of lead decreases this to 3.8×10^{-10}.

of the flue gas channel uses two e-beam sources injected symmetrically from opposite sides of the channel at an angle of 37.6° with respect to the flow direction. The width of the flow channel and the angle of the injected e-beam would vary with the size of the power plant. Replication of this configuration, either along the streaming direction or stacked vertically, would allow compact installation of several 400 kW individual e-beam sources. Six such sources could deliver a dose of 8.7 kGy to the flue gas discharge from a 300 MWe power plant. For 600 kW sources, only four machines would be required for a 300 MWe plant; or only eight for a 600 MWe plant, with a dose of 8.7 kGy. Should a dose of 4.3 kGy prove adequate, half these numbers of e-beam sources would be required.

Table I. Nominal parameters of e-beam system for equivalent 100 MWe plant.

flue gas flow	330,000 m^3/hr = 92.6 m^3/sec ≈ 92 kg/sec = $\dot{M}$
flue gas composition	1800 ppm SO_2, 400 ppm NO_x
e-beam average power	2×400 kW pulsed, @ 1.6 MeV = 800 kW = $\overline{P}$
e-beam peak power, current	P = 10 MW, I = 6.25 A
range of e-beam	Λ = 820 cm, for $\rho = 1\times10^{-3}$ gm/cm^3
maximum dose	$D = P/\dot{M}$ = 8.7 kGy (assuming full beam stopping)
pulse width, rep rate, duty	200 μsec, 200 Hz, 4.0%
flow channel dimensions	height H = 2 m, width W = 5 m
flow velocity	v = 9.26 m/sec
e-beam injection angle	$\theta = \sin^{-1}(500/820) = 37.6$ deg from flow direction
e-beam width and area	w = 7.8 cm, $A = H\times w$ = 0.156 m^2
flue gas exposure time	$\tau = w/v\sin\theta$ = 12.5 msec = 2.5 × pulse period
e-beam peak current density	$j = I/A$ = 4 mA/cm^2
current density for dc beam	0.16 mA/cm^2

Magnicon-Driven RF Pulsed E-Beam Technology. Major elements in the e-beam system include the rf source (magnicon) rf accelerator, beam window and associated fan/scan system, power supply to drive the rf source, and the control/interlock system. The magnicon and accelerator embody features that allow the e-beam system to achieve high average power, high wall-plug efficiency, and adjustable current density, with a

relatively small volume of equipment requiring biological shielding. The conventional source used in most rf accelerators is the klystron, a linear beam amplifier that has enjoyed more than 50 years of development and production since its introduction into radar systems during World War II. Commercially-available klystrons can furnish average power outputs as high as 1 MW in the frequency range of interest for accelerators for pollution remediation, but with efficiency values no higher than about 60%. Motivation for seeking an alternative rf source is in the possibility of high average power output from a single tube, in a device significantly shorter than an equivalent klystron, with efficiency above 70%, and with moderate cost. These virtues are shared by a microwave amplifier called the *magnicon*, a scanning-beam device developed at the Budker Institute of Nuclear Physics (BINP), in Novosibirsk, Russia. Magnicons have a further advantage over klystrons, in that they require no high-power circulator to absorb power that is inevitably reflected from the accelerator; this represents a significant savings in cost and size for a magnicon-driven system. The first magnicon, built to operate at 900 MHz, has an efficiency of 73%, and has been in continuous operation since 1985. Based on the same principle, magnicons at 7, 11, and 34 GHz have been designed and built, with the first of these producing peak output power of 56 MW with an efficiency of 56%. These magnicons have been designed and built by three former BINP scientists, including the group leader, who are Yale University Research Affiliates. The 11 GHz magnicon is undergoing final commissioning tests at Naval Research Laboratory in Washington, DC, under a Cooperative R&D Agreement that was funded by US Department of Energy (DoE). DoE has also funded a program to design a 1.3 GHz magnicon that meets the specifications for driving TESLA, a large superconducting accelerator planned for operation at Deutsches Electronen Synchrotron (DESY), Hamburg, Germany. TESLA requirements are for 10 MW peak power, 200 kW average power, and efficiency greater than 70%. Such specifications are similar to those for the rf source for a 1-10 MeV accelerator for pollution remediation (but with half the average output power), and well surpass specifications of commercial klystrons. Operation of magnicons at average output power levels up to one MW should be possible, as this would require mainly a change in the beam collector design for the magnicon. Indeed, multi-MW-level beam collectors have been successfully used on klystrons and gyrotrons.

RF Accelerator. Since high wall-plug efficiency is required, the accelerator structure is designed so that significant reflection losses will only occur at the rise and fall of the rf pulse; then beam loading of the structure will dominate greatly over ohmic wall losses. Modern design tools available allow design and development of a modified linac standing-wave structure for high efficiency (>90%) operation. This low-loss structure could be designed to accelerate a beam up to 10 MeV with an average current of about 20 mA or, at higher current and the same incident rf power, to yield an e-beam of lower energy, down to 1 MeV with 200 mA average current.[7] Specifications such as these cannot be obtained with CARA without use of an impractically high voltage injected beam. With a design pulse width of 200 μsec and a pulse repetition frequency (prf) of 100 Hz, the duty factor would be 2%. Higher average power would be achieved by increasing the duty factor to 4% (400 kW), thence to 6% (600 kW), through increasing the prf to 200 and 300 Hz. The main changes as the average power rises would be in the power supply and beam collector. This approach allows a single basic accelerator design to be universal. Its design would be easily modified to deliver a desired beam energy and dose in the 1-10 MeV range, thereby making the technology applicable applications beyond flue gas cleanup, such as sterilization of medical goods, pasteurization of foodstuffs, and cleanup of liquid and solid waste streams of variable composition. Other components of the e-beam system include the modulator (power supply), the control system, and the e-beam window. The first two involve established technologies, so that little risk is associated with implementing their design for this application. The e-beam window is the most sensitive element in any e-beam system, and a pulsed rf system is no exception. However, for the system described, the risk with the e-beam window is reduced, as compared with a conventional dc system, since beam losses and shock heating in the window are lower (at the same beam power) for a 1.6 MeV beam as compared with a 800 keV beam. Only small risk is entailed in the development of the magnicon and the accelerator. This risk can be qualified by stating that little doubt exists that the system as described can be built, but a small probability does exists that the cost and/or time needed for completion may exceed expectations.

[7]Industrial use of an e-beam with energy above 10 MeV is usually prohibited, since nuclear activation must be avoided.

PERSONNEL

Individuals involved in the research supported by this grant include the following:

- Dr. Michael A. LaPointe, Associate Research Scientist in Physics,
- Mr. Saveliy Finkelshteyn, Research Technician,
- Mr. Rodney Yoder, Graduate Student in Physics (Yale Ph.D., 2000),
- Ms. Mei Wang, Graduate Student in Physics (Yale Ph.D., 2000),
- Dr. Jay L. Hirshfield, Professor Adjunct of Physics, Principal Investigator.

PUBLICATION LIST

Archival publications that resulted from research carried out with support under DoE grant DE-FG-02-97-ER 12209 include the following. Copies are appended.

"High Power 20 Ghz Rf Source Based On Seventh Harmonic Co-Generation," Changiao Wang, J. L. Hirshfield, and A. K. Ganguly, in *Proceedings of the 1997 Particle Accelerator Conference*, M. Comyn, M. K. Craddock. M. Reiser, and J. Thomson, eds. (IEEE/AIP, 3171, 1997).

"Cyclotron Autoresonance Accelerator For Electron Beam Dry Scrubbing of Flue Gases," J. L. Hirshfield and Changbiao Wang, in *Proc. of the 1997 Particle Accelerator Conf.*, M. Comyn, M.K. Craddock, M. Reisder, and J. Thomson, eds., (IEEE/in AIP, 3863, 1997).

"Cyclotron Autoresonance Acceleration with Seventh Harmonic Co-Generation," J. L. Hirshfield, Changbiao Wang, and A. K. Ganguly, *IEEE Trans. Plasma Sci.* **26**, 567 (1998).

"Multi-Megawatt W-Band RF Source Based on Gyroharmonic Conversion at the Eighth Harmonic," Ch. Wang, J. Hirshfield, O. Nezhevenko," in *Proc. of the 1999 Particle Accelerator Conf.*, A. Luccio and W. MacKay, eds. (IEEE Conf. Proc. **1-5**, 1052, 1999).

"Laser-Driven Cyclotron Autoresonance Accelerator," Changbiao Wang and J. L. Hirshfield, in *Proc. of the 1999 Particle Accelerator Conf.*, A. Luccio and W. MacKay, eds. (IEEE Conf. Proc. **1-5**, 3630, 1999).

"Laser-Driven Electron Cyclotron Autoresonance Accelerator with Production of an Optically-chopped Electron Beam," J. L. Hirshfield and Changbiao Wang, *Physical Review E*, **61** (6), June 2000.

"10-MW, W-Band RF Source for Advanced Accelerator Research," J.L. Hirshfield, O.A. Nezhevenko, Changbiao Wang, V.P. Yakovlev, A.A. Bogdashov, V.L. Bratman, A.V. Chirkov, G.G. Denisov, A.N. Kuftin, S.V. Samsonov, and A.V. Savilov, *AAC2000 Proceedings* (Patrick Colestock, ed.), Santa-Fe, June, 2000 (to be published).

"Multi-Stage, High-Gradient, Cyclotron Resonance Proton Concept," J.L. Hirshfield, Changbiao Wang, and Robert Symons, *AAC2000 Proceedings* (Patrick Colestock, ed.), Santa-Fe, June, 2000 (to be published).

"Gyroresonant Acceleration of Electrons, Muons and Protons," J.L. Hirshfield, invited plenary talk. IRMMW2000, Beijing, September 2000.

HIGH POWER 20 GHz RF SOURCE BASED ON SEVENTH HARMONIC CO-GENERATION*

Changbiao Wang[1], J. L. Hirshfield[1,2], and A. K. Ganguly[2]
[1]Physics Department, Yale University, New Haven, Connecticut 06520-1820
[2]Omega-P, Inc., 202008 Yale Station, New Haven, Connecticut 06520

Abstract

The TE_{72} mode in cylindrical waveguide has its group velocity nearly equal to that of the TE_{11} mode when the operating frequency of the former is seven times of that of the latter. Thus the two modes have almost the same resonant magnetic field, and coherent radiation can be generated at the 7th harmonic when the fundamental energizes a gyrating electron beam by the cyclotron autoresonance interaction. It is shown analytically that the electron's gyration radius, normalized to waveguide radius, must be less than 0.5431 in the cyclotron autoresonance interaction. This analytical prediction is well confirmed by computer simulations. For a 300 kV, 30 A warm beam driven by 20 MW rf power at 2.856 GHz, simulations indicate that 7th harmonic power of up to 16 MW at 20 GHz can be obtained.

1 INTRODUCTION

Gyroharmonic conversion as a process for efficient production of high-power radiation has been investigated and analyzed in a number of prior publications [1-4]. Gyroharmonic conversion is a frequency-multipler concept, for which two approaches have been proposed. In the first [1,2], low frequency rf drive power is used to accelerate an electron beam using the TE_{11} mode by CARA (cyclotron autoresonance acceleration) [5-8], and the beam is then allowed to selectively emit coherent radiation at a harmonic of the drive frequency in a converter section. To cause the accelerated beam from CARA to fulfill both synchronous and grazing conditions in the converter, a drift region is inserted [6], and the harmonic index is specified by proper choice of converter circuit parameters. The second approach to gyroharmonic conversion is co-generation [4], where the lowest mode with almost the same required resonant magnetic field as that of TE_{11} at the drive frequency is the TE_{72} at the 7th harmonic, and transfer of drive power and generation of harmonic power occur in the self-same structure. The harmonic index is selected by the interaction mechanism, instead of only by circuit parameters. Because no drift region is needed in co-generation, strong rf trapping is always present and preserves good gyrophase coherence among the beam particles, resulting in better beam quality and higher interaction efficiency.

* The work was supported by the U. S. Department of Energy, Division of High Energy Physics.

2 PRINCIPLES OF CO-GENERATION AND MAXIMUM GYRATION RADIUS

Co-generation can be understood by examining the cyclotron autoresonance condition that maintains electron synchronism with rf electric fields. The resonance condition for TE_{sl} mode at the sth harmonic is

$$s\omega = s\Omega_0/\gamma + ck_{z,sl}\beta_z \quad \text{or} \quad \Omega_0 = \omega\gamma(1-n_{sl}\beta_z), \qquad (1)$$

where ω is the drive frequency, c is the light speed in free space, γ and β_z are the electron's relativistic energy factor and normalized axial velocity, the refractive index or normalized group velocity for TE_{sl} mode is $n_{sl} = k_{z,sl}c/\omega$ with $k_{z,sl}$ the axial wave number, and the rest gyration frequency is $\Omega_0 = eB_0/m_0$ with e the electron's charge, m_0 the electron's rest mass, and B_0 the axial magnetic field. For a waveguide radius of 3.3 cm and fundamental operation at 2.856 GHz, the refractive index n_{11} is 0.3605 and n_{72} is 0.3521, these differ by only 2.3%. From Eq. (1) we find the resonance magnetic fields for TE_{11} and TE_{72} modes are nearly identical, with difference of less than 1.3% for $\beta_z = 0.99$, 0.5% for $\beta_z = 0.5$, and 0.3% for $\beta_z = 0.3$. Calculations indicates that $TE_{13,3}$, $TE_{24,5}$, and $TE_{30,6}$ are also of near-degenerate [4].

When an electron beam is pumped by drive power in the TE_{11} mode, all electrons rapidly get phase-trapped and accelerated synchronously. At the same time, the beam begins to emit coherent radiation preferably into TE_{72} mode, although $TE_{13,3}$, $TE_{24,5}$, and $TE_{30,6}$ modes also have nearly equal resonant magnetic fields. This is because the larger the azimuthal mode index, the more the electric field distribution is concentrated in the region close to the waveguide wall. Radiation into higher modes decreases with increase in mode index. Moreover, higher harmonics are more sensitive to beam phase spread.

A larger gyration radius is preferred for interaction with high harmonics, since high-order mode field distributions are closer to the waveguide wall. However, the gyration radius is constrained by the synchronous condition Eq. (1), resulting in

$$\frac{r_L}{R_w} \le \frac{\beta}{j'_{11}}\left[\frac{1-n_{11}^2}{1-(n_{11}\beta)^2}\right]^{1/2} < 0.5431, \qquad (2)$$

where r_L is the gyration radius, R_w is the waveguide radius, $j'_{11} = 1.841184$ is the first root of the derivative of Bessel function $J_1(\chi)$, and $\beta = (1-1/\gamma^2)^{-1/2}$ is the

normalized total electron's velocity. Eq. (2), which is in good agreement with computer simulation, states that the normalized gyration radius must be less than 0.5431 regardless of the beam's energy and waveguide radius in CARA.

3 RESULTS OF SIMULATION

Simulation results are presented here for co-generation with parameters given in Table I. For all examples, a single-energy injected electron beam with a guiding center spread of 10% and an rms axial velocity spread of 0.02% is assumed. This velocity spread value is scaled from that for the Litton $K = 1\times10^{-6}\,\mathrm{A-V^{-3/2}}$ 100 kV gun now in operation in the Yale/Omega-P 4th harmonic converter experiment. 512 computational particles are taken, with 8 values of velocity spread, 8 values of phase spread, and 8 values of guiding center spread.

TABLE I: Parameters in simulation of co-generation.

Injection gun voltage	300 kV
Injector gun perveance	$0.18\times10^{-6}\,\mathrm{A-V^{-3/2}}$
Beam current	30 A
rms axial velocity spread	0.02%
Beam guiding center spread	10%
Waveguide radius	3.3 cm
Refractive index (TE_{11} mode)	0.3605
Refractive index (TE_{72} mode)	0.3522
rf drive frequency	2.856 GHz
rf drive power	20 MW
Output frequency	19.992 GHz
Guide magnetic field	< 2.4 kG

To measure performance of co-generation, one can define a direct efficiency, given by

$$\eta_{\mathrm{direct}} = \frac{P_{72}(\mathrm{out})}{P_{11}(\mathrm{in}) + P_{72}(\mathrm{in}) + P_{\mathrm{beam}}(\mathrm{in})}, \qquad (3)$$

where $P_{s1}(\mathrm{in})$ is the TE_{s1} mode input power, $P_{\mathrm{beam}}(\mathrm{in})$ is the input beam power, and $P_{72}(\mathrm{out})$ is the TE_{72} output power. Fig. 1 shows the results for a co-generator with an optimized detuning of $\Delta = -0.02$. Detuning, defined as $\Delta \equiv \Omega_0/(\omega < \gamma >< \beta_z >) + n_{11} - 1/< \beta_z >$, measures how much the magnetic field profile deviates from exact resonanance; introduction of detuning reduces impairment of beam quality caused by initial velocity spread. In this case, at $z = 83.8$ cm, output power at the 7th harmonic is seen to be 5.52 MW, at the fundamental to be 10.45 MW, and at the 13th harmonic to be 0.04 MW. Possible competing modes $TE_{13,3}$, TE_{62} and TE_{82} are seen to have only a minuscule influence on 7th harmonic co-generation. The direct efficiency is 5.52/(20+9) = 19.03%. The failure of normalized average gyration radius $< r_L/R_w >$ to fall below 0.3 indicates that particles have lost good phase synchronism with the TE_{11} mode, and thus can not give up more than a limited amount of transverse momentum.

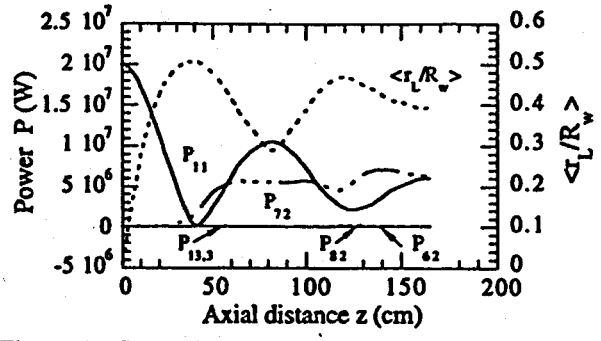

Figure 1: Dependence of rf power P and normalized gyration radius $< r_L/R_w >$ on axial distance z. TE_{11} and TE_{72} modes always coexist and a detuned resonant magnetic field profile is used. Peak value of 7th harmonic power at 20 GHz is 5.52 MW at $z = 83.8$ cm.

To increase efficiency, one can kill the TE_{11} mode after drive power is depleted, using a selective absorber. It is found that use of a segmented straight-line magnetic profile beyond the power-depleted point can also increase 7th harmonic power. As shown in Fig. 2, 7th harmonic output is seen to rise to 10.20 MW at $z = 99$ cm, and the direct efficiency is increased to 35.17%. Comparing Fig. 2 with Fig. 1, we find that mode suppression and adjustment of magnetic profile has considerably improved direct efficiency, but the circuit becomes longer and somewhat more complicated.

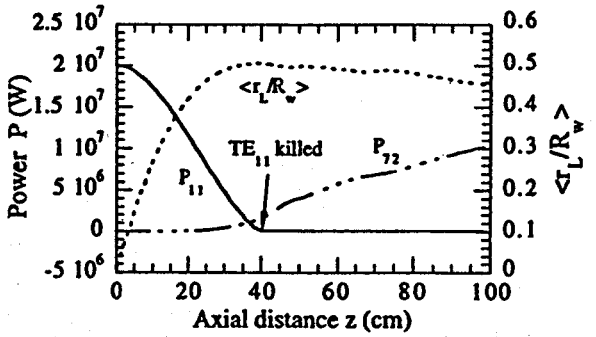

Figure 2: Dependence of rf power P and normalized gyration radius $< r_L/R_w >$ on axial distance z. TE_{11} mode is killed and segmented straight-line magnetic field profile is employed after TE_{11} mode is depleted. 7th harmonic 20 GHz power is 10.20 MW at $z = 99$ cm.

It is found by simulations that injection of a portion of 7th harmonic power with proper phase can effectively reduce gyrophase spread. Fig. 3 shows results with a 7th harmonic injection power of 2.0 MW, but with other parameters the same as in Fig. 1. Now it is seen that the 7th harmonic output at $z = 86.5$ cm is 12.11 MW, indicating a net gain of 10.11 MW, as compared with 5.52 MW output without injection. Fundamental power at $z = 86.5$ cm is 9.27 MW. The significant increase in 7th harmonic output results from much better particle trapping when injection is employed. Now the direct efficiency is 12.11/(9+2+20) = 39.06%.

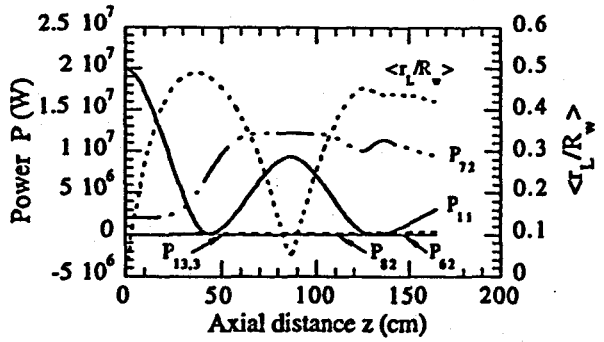

Figure 3: Dependence of rf power P and normalized gyration radius $< r_L/R_w >$ on axial distance z. An injection power of 2.0 MW at 20 GHz is used, with other parameters the same as in Fig. 1. 7th harmonic power at 20 GHz is 12.11 MW at $z = 86.5$ cm.

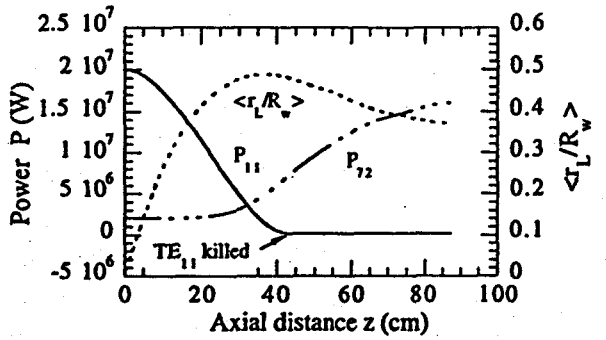

Figure 4: Dependence of rf power P and normalized gyration radius $< r_L/R_w >$ on axial distance z. An injection power of 2.0 MW at 20 GHz is used, with other parameters the same as in Fig. 2. 7th harmonic power at 20 GHz is 15.96 MW at $z = 87.5$cm.

Harmonic injection also benefits co-generation for the Fig. 2 case where TE_{11} mode is killed beyond its power-depleted point. Fig. 4 shows results with a 7th harmonic injection power of 2.0 MW, but with other parameters the same as in Fig. 2. It is seen that 7th harmonic power grows to 15.96 MW at $z = 87.5$ cm, corresponding to a direct efficiency of 51.48%.

In a configuration requiring a large number of sources, such as a high energy electron-positron collider, one could interconnect neighboring sources in tandem, so that any 2.856 GHz output of one source would partially feed the next source; in that case the "makeup" power required for each source (except for the first one) would be reduced. In this case, one can define the output efficiency of a single co-generator in the tandem sequence as

$$\eta_{\text{output}} = \frac{P_{72}(\text{out})}{P_{11}(\text{makeup}) + P_{72}(\text{in}) + P_{\text{beam}}(\text{in})}. \quad (4)$$

A higher efficiency can be achieved through recovery of spent beam energy if a depressed collector is employed [9]. Inclusion of beam energy recovery leads to a definition of an enhanced efficiency, defined as

$$\eta_{\text{enhanced}} = \frac{P_{72}(\text{out}) + \eta_{\text{rec}} P_{\text{beam}}(\text{out})}{P_{11}(\text{makeup}) + P_{72}(\text{in}) + P_{\text{beam}}(\text{in})}, \quad (5)$$

where η_{rec} is the efficiency for recovery of spent beam power, and $P_{\text{beam}}(\text{out})$ is the beam power at the end of the co-generator. For an ideal collector, the recovery efficiency is given by $\eta_{\text{rec}} = (\gamma_{\min} - 1)/(<\gamma> - 1)$, where $\gamma_{\min}$ is the minimum relativistic energy factor in the spent beam. Table II shows comparison for the four configurations of co-generation discussed above. Effects of power injection on co-generation can be found by comparing the Fig. 1 and Fig. 2 cases with the Fig. 3 and Fig. 4 cases respectively; effects of beam energy recovery on co-generation can be found by comparing the output efficiency η_{output} with the enhanced efficiency η_{enhanced}.

TABLE II: Comparison for four configurations of 7th harmonic co-generation at 20 GHz.

	P_{72}-out (MW)	η_{direct} (%)	η_{output} (%)	η_{rec} (%)	η_{enhanced} (%)
Fig. 1	5.52	19.03	29.75	69.1	77.6
Fig. 2	10.20	35.17	35.17	78.6	85.4
Fig. 3	12.11	39.06	55.73	94.4	96.5
Fig. 4	15.96	51.48	51.48	90.2	94.4

4 CONCLUSIONS

Co-generation is a novel means for efficient gyro-harmonic conversion. By injection of harmonic power to improve particle trapping and recovery of spent beam energy to enhance efficiency, simulations have shown that an overall 7th harmonic efficiency of over 90% can be achieved for a 16 MW 20 GHz co-generators with a 300 kV, 30 A electron beam pumped by 20 MW power at 2.856 GHz.

5 REFERENCES

[1] A. K. Ganguly and J. L. Hirshfield, Phys. Rev. E 47, 4364 (1993).

[2] J. L. Hirshfield, A. K. Ganguly, and C. Wang, in *Pulsed RF Sources for Linear Colliders*, edited by R. C. Fernow, AIP Conf. Proc. No. 337, (AIP, New York, 1995), p. 200.

[3] J. L. Hirshfield, C. Wang, and A. K. Ganguly, IEEE Trans. Plasma Sci. 24, 825 (1996).

[4] C. Wang and J. L. Hirshfield, and A. K. Ganguly, Phys. Rev. Lett. 77, 3819.

[5] B. Hafizi, P. Sprangle, and J. L. Hirshfield, Phys. Rev. E 50, 3077 (1994).

[6] C. Wang and J. L. Hirshfield, Phys. Rev. E 51, 2456 (1995).

[7] M. A. LaPointe, R. B. Yoder, C. Wang, A. K. Ganguly, and J. L. Hirshfield, Phys. Rev. Lett. 76, 2718 (1996).

[8] Hirshfield, M. A. LaPointe, A. K. Ganguly, R. B. Yoder, and C. Wang, Phys. Plasmas 3, 2163 (1996).

[9] K. Sakamoto, M. Tsuneoka, A. Kasugai, T. Imai, T. Kariya, K. Hayashi, and Y. Mitsunaka, Phys. Rev. Lett. 73, 3532 (1994).

Cyclotron Autoresonant Accelerator for Electron Beam Dry Scrubbing of Flue Gases

M. A. LaPointe,*# Changbiao Wang,# and J.L. Hirshfield*#

*Omega-P, Inc., 202008 Yale Station, New Haven, CT 06520-2008
#Department of Physics, Yale University, P.O. Box 208124, New Haven, CT 06520-8124

Design and construction is underway for a novel rf electron accelerator for electron beam dry scrubbing (EBDS) of flue gases emanating from fossil-fuel burners. This machine, a cyclotron autoresonance accelerator (CARA), has already shown itself capable of converting rf power to electron beam power with efficiency values as high as 96%. This proof-of-principle experiment will utilize a 300 kV, 33 A Pierce type electron gun and up to 24 MW of available rf power at 2.856 GHz to produce 1.0 MeV, 33 MW electron beam pulses. The self-scanning conical beam from the high power CARA will be evaluated for EBDS and other possible environmental applications.

INTRODUCTION

The irradiation of industrial flue gases from fossil fuel burning plants is one of the most active areas in environmental applications of radiation processing. The viability of using electron beam irradiation for removal of SO_2 and NO_x from flue gas effluents has been tested at demonstration pilot plants in Japan (1-4), Indianapolis, USA and Karlsruhe, Germany (5,6). Details of the radiation processes are beyond the scope of this paper and are presented in detail elsewhere (7). The main capital investment and operating expense in using electron beam dry scrubbing (EBDS) are the electron accelerators. Current accelerator technology has been shown to be cost competitive with non-EBDS technologies only for small and medium sized plants and will become viable for large scale treatment when accelerator costs are reduced (7). To this end the cyclotron autoresonant accelerator (CARA) is being developed as an efficient, compact, potentially lower cost electron source for EBDS and other environmental applications.

380 keV CARA

A 380 keV, 25A CARA has been operating at the Yale Beam Physics Laboratory since 1994 (8). Up to a 100 kV, 30 A, 2.5 μsec beam is produced by a Pierce-type diode gun and injected into a smooth wall cylindrical waveguide. A former SLAC XK-5 klystron operating at 2.856 GHz provides up to 20 MW of pulsed rf power, although for the existing CARA less than 10 MW has been used. The rf power enters the waveguide through a two port, 90° input coupler which launches a TE_{11} rotating wave. An axial magnetic field is provided by solenoid coils surrounding the cylindrical waveguide and energized by individual, computer controlled power supplies. This axial field control allows the electron beam and the rf power to continuously match the Doppler shifted cyclotron resonance condition.

$$\omega(1-n\beta_z)=\Omega/\gamma \qquad (1)$$

where ω is the radian frequency of the rf, n is the wave group velocity and β_z is the axial electron velocity (both normalized to the velocity of light), Ω is the rest electron gyrofrequency in a static magnetic field B, and the relativistic energy factor $\gamma=1+eV/mc^2$ with V being the effective beam voltage.. A schematic representation of the existing CARA is shown in Fig. 1.

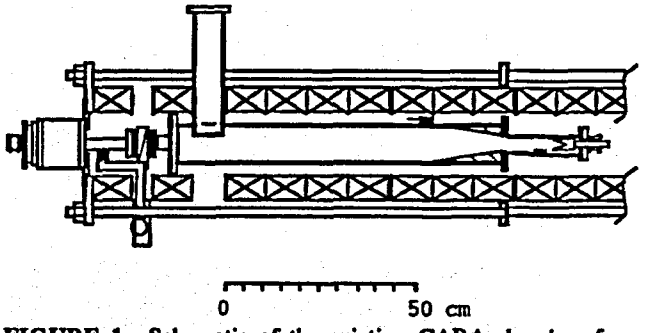

FIGURE 1. Schematic of the existing CARA showing, from left, the Pierce gun, pumping port, gate valve, one of two waveguide inputs, CARA cylindrical waveguide, rf sample point, conical absorber and beam collector. Surrounding CARA are individually powered solenoid coils and an iron flux cage.

The measured rf efficiency of CARA is shown in Fig. 2 over a range of beam and rf power (8). Final beam powers up to 9.6 MW (384 kV, 25 A) have been achieved. RF efficiency values greater than 90% have been routinely achieved with a maximum value of 96% for a high rf power case. RF power losses in the system included reflection at the input coupler were measured to be about 3%, and skin

CP475, *Applications of Accelerators in Research and Industry*,
edited by J. L. Duggan and I. L. Morgan

effect wall losses in the waveguide were calculated to be about 0.02%. The low skin loss is due to the use of a smooth wall traveling wave structure as opposed to a cavity structure.

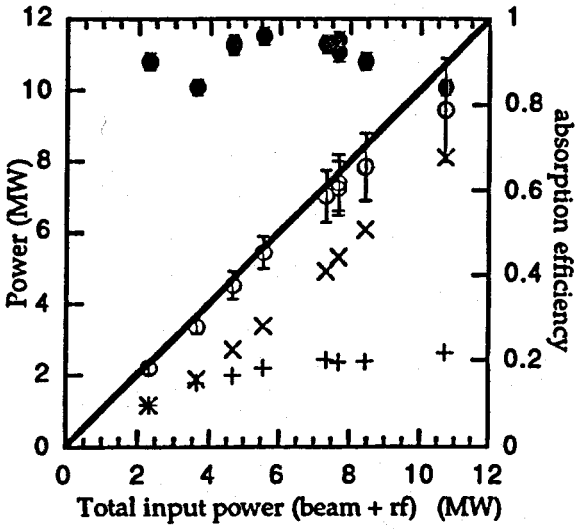

FIGURE 2. Total beam power (O), efficiency (●), CARA injected beam power(+), and initial rf power (×) plotted versus total input power. The solid line corresponds to 100% efficiency. (8)

There is a practical limit on how much energy can be added to the electron beam which is not evident in Eq. 1. As the particles gain energy the magnetic field required to maintain the resonance in the cylindrical waveguide increases. As most of the added energy is in perpendicular motion this increasing field will lead to stalling of the beam ($\beta_z \rightarrow 0$) due to the magnetic mirror effect. It has been shown that this maximum energy is given by (9)

$$\gamma_{max} = \gamma_0 + \left(\frac{\gamma_0^2 - 1}{1 - n_f^2}\right)^{1/2}, \qquad (2)$$

where γ_0 is the injection energy factor and n_f is the normalized group velocity at the end of CARA. Equation 2 assumes that there is enough rf power present to reach the stalling limit; otherwise the maximum energy is limited by rf power depletion.

1 MeV CARA

The maximum energy of the existing CARA ($\gamma_0 = 1.2$, $n_f = 0.95$)according to Eq. 2 would be 1.1 MeV which would satisfy the requirements for EBDS. However, the calculation used to derive Eq. 2 assumed a cold beam (no velocity or energy spread). If one incudes velocity and energy spreads then the maximum energy for stalling part of the beam is decreased. For the 1 MeV CARA under construction a maximum injection energy of 300 keV was chosen for which Eq. 2 gives a maximum final energy of 2.3 MeV and should alleviate any potential partial stalling of the beam.

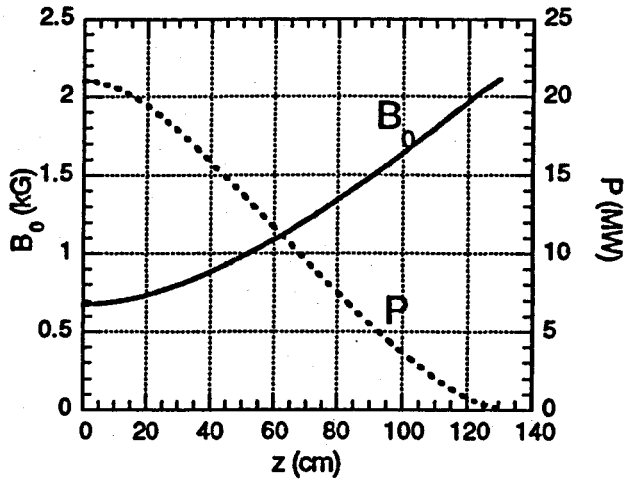

FIGURE 3. Computed magnetic field and rf power profiles. Injected beam is 25 A, 250 keV with zero emittance. Power source is 21 MW at 2.856 GHz. CARA waveguide radius is 4.65 cm and $n = 0.75$. Power remaining at z=130 cm is 0.29% of initial value.

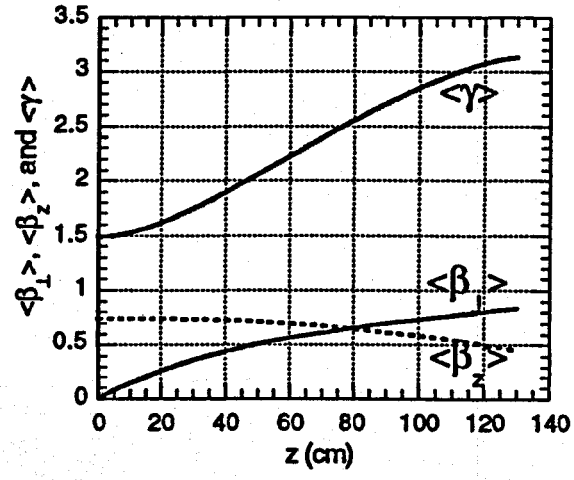

FIGURE 4. Computed energy factor γ and normalized transverse and axial electron velocities $\beta_\perp$ and $\beta_\parallel$, averaged over random initial phase. Beam energy and power are seen to more than quadruple from 250 keV, 6.25 MW to 1.088 MeV, 27.2 MW with 99.7% rf efficiency.

Simulations were performed using a 250 keV, 25A cold injected beam and 21 MW of incident 2.856 GHz rf power. Figure 3 shows the axial magnetic field profile computed to maintain resonance. As is seen the maximum magnetic field required is 2.1 kG which is readily achieved with conventional solenoid magnets. Also shown in Fig. 3 is the rf power depletion. For this cold beam calculation over 99% of the initial rf power is absorbed by the electron

beam. The final beam energy in the simulation is 1.088 MeV as seen in Fig. 4. The evolution of the axial and perpendicular components of the electron velocity are also shown in Fig. 4.

DISCUSSION

From the simulations discussed above it is seen that the CARA under construction will be able to generate 1 MeV electron beams. A schematic layout of the device is shown in Fig. 5. What has also been demonstrated with the existing CARA is that the final beam energy range is selectable by adjusting the input rf power and magnetic field. In practice, the new CARA will be able to generate electron beams in the continuous energy range from the 300 kV injection voltage up to the predicted 1 MeV design voltage.

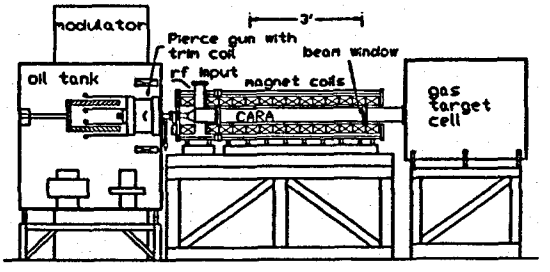

FIGURE 5. A conceptual sketch of the 1 MeV CARA under construction in the Yale Beam Physics Lab showing the injector gun, gun pumping port, gate valve, rf input waveguide (one of two), CARA module, beam output window and gas target cell.

EBDS and other similar applications require that the beam be brought out into atmosphere. For the proof-of-principle experiment the beam will pass through a beam window (most likely tantalum or titanium) and into a gas target cell which will contain up to 3 atm of Argon. The individual electrons, as they leave the magnetic field region, will follow a line at an angle to the axis computed to be approximately 22°. As the beam is also rotating, it will then describe a cone about the axis and will be self-scanning, sweeping a two foot diameter circle five feet from the end of the device.

Although the rf to beam power efficiency is very high for CARA, the limiting efficiency for the device is the rf source. Current state of the art high power production tubes (e.g. SLAC 5045 klystrons, 65 MW, 2.856 GHz) have efficiencies on the order of 60%.(10) A 1.3 GHz magnicon with 200 kW average power and 10 MW peak power has been designed which is predicted to have an efficiency greater than 70%.(11) These two devices are only representative of the very active high power rf development field. Using similar devices to drive a CARA the overall device efficiency can be estimated.

For a 10 μsec pulse width and 300 pps rep rate the 1 MeV, 33A electron beam represents 100 kW of average beam power. To produce this the 300 keV, 33A electron gun requires, assuming 95% modulator efficiency, an average power of 30 kW. For the 23 MW of rf power needed to accelerate the beam to 1 MeV we assume the same pulse width and rep rate and further include the 95% CARA efficiency, 60% rf source efficiency and 95% modulator efficiency. This give an average power requirement of 127 kW for a total power requirement of 157 kW. If we further include the 10 kW power for the magnet system and 5 kW for associated control systems, electronics, etc. then the overall power requirement becomes 172 kW and gives an overall efficiency of 58%.

The relation between beam power, P_{beam}, and absorbed dose, D, is given by (4)

$$P_{beam}[watts] = \frac{1}{\alpha} D[Gy]\dot{M}[kg/s] \qquad (3)$$

where α is the fraction of beam power absorbed and $\dot{M}$ is the mass flow rate under irradiation. In SI units D is measured in gray with 1 Gy = 1 J/kg = 100 rad. For the 100 kW example above, a dose of 1.2 kGy could be administered to a mass flow rate of 50 kg/s (180 tonnes/hr) assuming $\alpha = 0.6$. For EBDS, if the examples found in Ref. 4 are scaled, the 100 kW CARA could process $1-2\times10^4$ m^3/hr of flue gas effluent containing 1000 ppm SO_2 and 400 ppm NO_x.

CONCLUSIONS

It has been shown that CARA is efficient at converting rf power to beam power. A proof-of principle CARA experiment is under construction at the Yale Beam Physics Lab to demonstrate a 1 MeV, 33 A electron beam onto a gas target. Estimates show that the overall efficiency for a CARA system can be in excess of 50%.

ACKNOWLEDGMENTS

This work is sponsored by the U.S. Department of Energy, Division of Advanced Energy Projects.

REFERENCES

1. Machi, S., Tokunaga, O., Nishimura, K., Hashimoto, S., Kawakami, W., Washino, M., Kawamura, K., Aoki, S. and Adachi, K., *Radiat. Phys. Chem.*, 9, 371 (1977).
2. Kawamura, K. and Shui, V.H. in *Industrial Applications of Radioisotopes and Radiation Technology*, IAEA, Vienna, 1982, p 197.
3. Kawamura, Ka., Katayama, T., Kawamura, K., *Radiat. Phys. Chem.*, 18, 389 (1981).
4. Kawamura, K. and Shui, V.H., *Radiat. Phys. Chem.*, 24, 145 (1984).
5. Jordan, S., *Radiat. Phys. Chem.*, 31, 21 (1988).
6. Frank, N., Hirano, S., and Kawamura, K., *Radiat. Phys. Chem.*, 31, 57 (1988).

7. Woods, R.J. and Pikaev, A.K., *Applied Radiation Chemistry-Radiation Processing*, New York: John Wiley & Sons, 1994, Ch 12, pp. 473-489, and references therein.
8. LaPointe, M.A., Yoder, R.B, Wang Changbiao, Ganguly, A.K., and Hirshfield, J.L., *Phys. Rev. Lett.*, **76**, 2718-2721 (1996); Hirshfield, J.L., LaPointe, M.A., Ganguly, A.K., Yoder, R.B., and Wang Changbiao, *Phys Plasmas*, **3**, 2163-2168 (1996).
9. Wang, Changbiao and Hirshfield, J.L., *Phys. Rev. E*, 51, 2456 (1995).
10. Caryotakis, G., IEEE Trans. Plasma Science, 22, 683 (1994).
11. Ganguly, A.K., Nezhevenko, O.A., and Yakovlev, V.P., "Long-Pulse 1.3 GHz Magnicon", in Proc. 6th European Particle Accelerator Conference, Stockholm Sweden, June 22-26, 1998 to be published.

Cyclotron Autoresonance Acceleration with Seventh Harmonic Co-Generation

J. L. Hirshfield, Changbiao Wang, and A. K. Ganguly

Abstract—The TE_{72} mode in a cylindrical waveguide at frequency 7ω has its group velocity v_{gr} nearly equal to that of the TE_{11} mode at frequency ω. In consequence, the two modes have nearly equal resonant magnetic fields for strongly coupled interactions at electron cyclotron resonance. This allows coherent radiation in the TE_{72} mode to be generated at 7ω as a gyrating electron beam is energized using the TE_{11} mode at frequency ω in the same waveguide. It is shown analytically that the electron gyration radius can approach 0.5431 times the waveguide radius during cyclotron autoresonance acceleration, for an axis-encircling beam injected with zero transverse momentum. This fact allows electron acceleration to relativistic energies using the TE_{11} mode to lead to large enough axis-encircling orbit radii for strong coupling with the TE_{72} fields. Results of a particle simulation study are discussed for a 300-kV, 30-A finite-emittance pencil beam injected into a 3.27-cm-radius waveguide, and driven with 20 MW of rf power at 2.856 GHz. The results show that careful choice of the magnetic field profile, and suppression of the TE_{11} mode after its power is depleted, can allow seventh-harmonic output to reach 10 MW at 20 GHz. Furthermore, it is shown that injection at the input of harmonic power can also benefit co-generation, both increasing seventh-harmonic output up to 16 MW and improving spent beam quality. Higher spent beam quality is advantageous for efficient beam energy recovery.

Index Terms—Acceleration, co-generation, cyclotron autoresonance harmonic, gyrating electron beam.

I. Introduction

CONSIDERABLE research effort is underway to develop high peak power, narrowband pulsed rf amplifiers as drivers for large future electron-positron linear colliders [1]. Research programs are active on development of klystrons [2], [3], relativistic klystrons [4], cluster klystrons [5], [6], gyroklystrons [7], magnicons [8], [9], and gyroharmonic converters [10]–[17]. Much of the klystron development is at 11.424 GHz, where Next Linear Collider Test Accelerator is being operated at Stanford Linear Accelerator Center. A new magnicon design at 11.424 GHz has recently been perfected by Omega-P, Inc. in collaboration with Naval Research Laboratory, and a proof-of-principle experiment is now underway. A relativistic klystron [4] and second-harmonic gyroklystron [7] are being investigated for operation at 17.136 GHz. These manifold efforts are in response to wide appreciation that progress toward construction of a TeV-level electron-positron linear collider will be possible only after efficient rf amplifiers are developed at frequencies of 10 GHz or higher, that can deliver at least 100 J per pulse, at a pulse repetition rate of 120–180 pulse/s. Scaling laws suggest that operation at higher frequency (even up to 100 GHz) can yield significant economies in size and cost, particularly in design of multi-TeV machines [18].

Gyroharmonic conversion as a process for efficient production of high-power radiation has been investigated and analyzed in a number of publications [10]–[17], [20]. Gyroharmonic conversion is a frequency-multipler concept, with—so far—two distinct approaches for its realization. In one approach [10]–[17], low-frequency rf drive power is used to accelerate an electron beam using the TE_{11} mode in a cylindrical waveguide by means of cyclotron autoresonance acceleration (CARA) [21]–[24]. The beam then drifts into a converter section, where it can selectively emit coherent radiation at a harmonic of the drive frequency. To allow the accelerated beam from CARA to fulfill the synchronous and grazing conditions in the converter section, the magnetic field in the drift section is tapered up [22]. The operating harmonic index is specified by proper choice of converter circuit parameters and magnetic field profile.

An alternative approach to gyroharmonic conversion [20], which has been dubbed co-generation, exploits the fact that the TE_{72} mode at frequency 7ω has its group velocity v_{gr} nearly equal to that of the TE_{11} mode at frequency ω. As a result, gyroresonant interactions in the two modes require essentially the same resonant magnetic field profile; and thus transfer of drive power to one mode with generation of harmonic power in the other can occur in the self-same structure. The harmonic index (i.e., $s = 7$) is selected by the synchronous interaction mechanism itself, instead of through the circuit parameters. Because no drift region need be inserted for co-generation, strong rf trapping is always present to help preserve gyrophase coherence among the beam particles, resulting in better beam quality and interaction efficiency than when a drift section is interposed. Furthermore, for a traveling-wave co-generator, whatever rf drive power that does not become transformed into harmonic power can be extracted, recycled, and/or perhaps used in a subsequent co-generator stage. (Recycling may require a means of phase stabilization to correct for phase jitter introduced in the co-generator; discussion of phase stabilization among several co-generators is beyond the scope of this paper.) Furthermore, as in conventional linear electron-

Manuscript received August 21, 1997; revised January 8, 1998. The work was supported by the U. S. Department of Energy and the Office of Naval Research.

J. L. Hirshfield is with the Physics Department, Yale University, New Haven, CT 06520-1820 USA and with Omega-P, Inc., New Haven, CT 06520 USA.

C. Wang is with the Physics Department, Yale University, New Haven, CT 06520-1820 USA.

A. K. Ganguly is with Omega-P, Inc., New Haven, CT 06520 USA.

Publisher Item Identifier S 0093-3813(98)04406-3.

beam tubes [25], energy in the spent electron beam emerging from the co-generation interaction can be recovered using a depressed collector. This can occur efficiently in a co-generator, since the energy spread on the beam induced in the acceleration and generation processes can be small. Stanford Linear Collider klystrons at 2.856 GHz with peak power of 65 MW, pulse duration of 3.5 μs, and efficiency of 45% [26] may be used to drive co-generators to provide high power output at 20 GHz. Recent 50-MW klystrons developed to operate at 11.424 GHz could serve as drivers for co-generators yielding high power output at 80 GHz. Either of these high-power sources could play a role in furnishing rf drive power for a future electron-positron linear collider [27].

This paper presents simulation analysis and results for co-generation at 20 GHz using parameters corresponding to planned experiments. Thus a 30-A, 300-kV electron beam pumped by 20 MW of rf power at 2.856 GHz in a traveling-wave structure is considered. The paper is organized as follows. In Section II, the basic principles of co-generation are described, and an analytic expression for the maximum possible gyration radius in a cyclotron autoresonance interaction is derived. In Section III, simulation results for co-generation are given for various magnetic field and circuit configurations, including suppression of the TE_{11} mode beyond its point of maximum absorption, injection of a small level of input harmonic power, and spent beam energy recovery for efficiency enhancement. In Section IV some conclusions are drawn.

II. Basic Principles of Co-Generation and Maximum Gyration Radius

Co-generation can be understood by examining the cyclotron autoresonance condition that must be maintained to keep electrons synchronous with a rotating waveguide mode traveling along a static magnetic field. The condition for resonance in the TE_{sl} mode near the sth gyroharmonic can be written as

$$s\omega = \frac{s\Omega_o}{\gamma} + ck_{z,sl}\beta_z \quad \text{or} \quad \Omega_o = \omega\gamma(1 - n_{sl}\beta_z) \qquad (1)$$

where ω is the drive frequency; c is the light speed in free space; γ and β_z are the electron relativistic energy factor and normalized axial velocity; $k_{z,sl}$ is the axial wave number; $\Omega_o = eB_o/m_o$ is the gyration frequency, with e the electron charge, m_o the electron rest mass, and B_o the axial magnetic field; $n_{sl} = k_{z,sl}c/\omega = [1 - (j'_{sl}c/\omega R_w)^2]^{1/2}$ is the refractive index or normalized group velocity v_{gz}/c for the TE_{sl} mode, with j'_{sl} the lth zero of the Bessel function derivative $J'_s(x)$ and R_w the waveguide radius. For $R_w = 3.3$ cm, the refractive indices are $n_{11} = 0.3605$ and $n_{72} = 0.3522$, a difference of only 2.3%. From (1) it is seen that the resonance magnetic fields for TE_{11} and TE_{72} modes are nearly identical, with a difference of less than 1.3% for $\beta_z = 0.99$, 0.5% for $\beta_z = 0.5$, and 0.3% for $\beta_z = 0.3$. Inspection of the waveguide dispersion relation indicates that the $TE_{13,3}$, $TE_{24,5}$, and $TE_{30,6}$ modes are also nearly degenerate at frequencies 13, 24, and 30ω, respectively, with the TE_{11} mode at frequency ω [20].

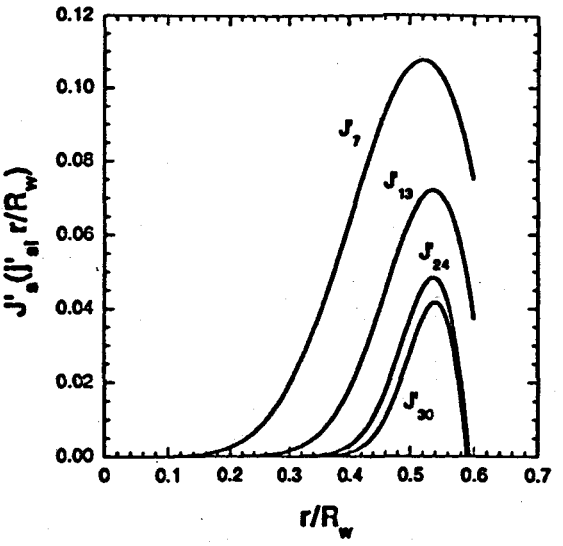

Fig. 1. Amplitudes of Bessel function $J'_s(j'_{sl}r/R_w)$, to which azimuthal electric fields of TE_{sl} mode are proportional, for $(s,l) = (7,2)$, $(13,3)$, $(24,5)$, and $(30,6)$. In the CARA interaction, the azimuthal component is the effective one and the electron's normalized radial coordinate r/R_w is approximately equal to the normalized gyration radius $r_L/R_w < 0.5431$.

When an electron beam is pumped by drive power in the TE_{11} mode, all the electrons rapidly get phase-trapped and accelerated synchronously. At the same time, the beam begins to emit coherent radiation preferably into the TE_{72} mode, although $TE_{13,3}$, $TE_{24,5}$, and $TE_{30,6}$ modes also have nearly equal resonant magnetic fields. This is because the larger the azimuthal mode index, the more the electric field distribution is concentrated in the area close to the waveguide wall. Coupling into those modes decreases with increase in the mode index, for a beam on an axis-encircling orbit of limited radius. Moreover, higher harmonics are more sensitive to beam phase spread. These considerations lead one to anticipate stronger coupling to the TE_{72} mode than to the higher order modes.

The azimuthal rf electric field is the component which interacts effectively with the sth harmonic; this field is proportional to $J'_s(j'_{sl}r/R_w)$, where r is the radial coordinate. Fig. 1 shows dependence of $J'_s(j'_{sl}r/R_w$ on r/R_w for TE_{72}, $TE_{13,3}$, $TE_{24,5}$, and $TE_{30,6}$ modes. At $r/R_w = 0.3$, the relative values of $J'_s/J'_{s\max}$ are, respectively, 0.182, 0.021, 0.0046, and 0.000 048; this shows that only the $TE_{13,3}$ has the potential to compete with the TE_{72}, while $TE_{24,5}$ and $TE_{30,6}$ cannot. When the beam's normalized gyration radius is less than 0.3, even TE_{72} cannot effectively interact with the beam. A larger gyration radius should lead to more effective interaction with rf fields. From this, one interesting question arises: how large can the gyration radius be in the cyclotron autoresonance interaction?

Only the TE_{11} mode is appropriate for CARA acceleration when the injected on-axis beam has negligible transverse momentum. Assuming that the synchronous condition is always satisfied during the acceleration, the gyration radius can be written from (1) as

$$\frac{\omega r_L}{c} = \frac{\alpha\beta}{[(1+\alpha^2)^{1/2} - n_{11}\beta]} \qquad (2)$$

TABLE I
PRAMETERS IN SIMULATION OF CO-GENERATION

Injection gun voltage	300 kV
Injector gun perveance	0.18×10^{-6} A – $V^{-3/2}$
Beam current	30 A
Waveguide radius	3.30 cm
Refractive index (TE_{11} mode)	0.3605
Refractive index (TE_{72} mode)	0.3522
rf drive frequency (at fundamental harmonic)	2.856 GHz
rf drive power	20 MW
Output frequency (at seventh harmonic)	19.992 GHz
Guide magnetic field	< 2.4 kG

where

$$\alpha=\frac{\beta_\perp}{\beta_z}\quad \beta=\left(1-\frac{1}{\gamma_2}\right)^{1/2}\quad \text{and}\quad \beta_z=\frac{\beta}{(1+\alpha^2)^{1/2}} \tag{3}$$

with $\beta_\perp$ the electron's normalized transverse velocity.

Suppose that, at a given value of axial coordinate, the electron's energy γ and waveguide refractive index (group velocity) n_{11} are known. Taking $dr_L/d\alpha=0$ from (2), we obtain the possible maximum gyration radius

$$R_{L\max}=\frac{\lambda_0\beta}{2\pi}(1-n_{11}\beta)^2]^{-1/2} \tag{4}$$

where λ_0 is the wavelength of the drive wave in free space.

The waveguide radius is given by

$$R_w=\frac{\lambda_0 j'_{11}}{2\pi}(1-n_{11}^2)^{-1/2} \tag{5}$$

with $j'_{11}=1.841\,184$. Combining (4) with (5), we obtain

$$\frac{r_{L\max}}{R_w}=\frac{\beta}{j'_{11}}\left[\frac{1-n_{11}^2}{1-(n_{11}\beta)^2}\right]^{1/2}=0.5431\beta\left[\frac{1-n_{11}^2}{1-(n_{11}\beta)^2}\right]^{1/2}. \tag{6}$$

It has been shown, for an injected beam with zero transverse momentum [22] that there is a maximum acceleration energy in the CARA, that is, $\gamma\le\gamma_{\max}$ or $\beta\le\beta_{\max}$. Consequently, the maximum gyration radius at the maximum acceleration energy is given by

$$\frac{r_{L\max}}{R_w}=0.5431\left[\frac{(\gamma_{\max}^2-1)(1-n_{11}^2)}{\gamma_{\max}^2-1)(1-n_{11}^2)+1}\right]^{1/2} \tag{7}$$

where

$$\gamma_{\max}=\gamma_0+\left[\frac{\gamma_0^2-1}{1-n_{11}^2}\right]^{1/2} \tag{8}$$

with γ_0 the normalized initial electron's energy. Combining (6) with (7), we have

$$\frac{r_L}{R_w}\le0.5431\beta\left[\frac{1-n_{11}^2}{1-(n_{11}\beta)^2}\right]^{1/2}\le0.5431\left[\frac{(\gamma_{\max}^2-1)(1-n_{11}^2)}{(\gamma_{\max}^2-1)(1-n_{11}^2)+1}\right]^{1/2}<0.5431. \tag{9}$$

Equation (9) gives the maximum possible gyration radius for a given beam energy and waveguide radius at any point along CARA. For example, if $\gamma_0=1.5871$ (300 kV) and $n_{11}=0.3605$, from (7) we obtain $\gamma_{\max}=2.9083$ (975 kV) and $r_{L\max}/R_w=0.5055$. However, (9) shows that the beam's normalized gyration radius must be less than 0.5431 regardless of the beam's energy and waveguide radius in the CARA interaction. From this, we see that electrons in the CARA interaction can never hit the waveguide wall, but can reach a large enough radius to couple effectively to the fields of the TE_{72} mode.

III. Results of Simulation Studies

In this section, we will present simulation results for a co-generator where a 30-A, 300-kV (i.e., perveance $K=0.18\times10^{-6}\,A-V^{-3/2}$) electron beam is passed through a uniform waveguide with a radius of 3.30 cm. An rf power of 20 MW at 2.856 GHz is used to pump the beam in the TE_{11} mode, and the seventh-harmonic power is generated in the TE_{72} mode. The particle simulation code used was obtained by modifying one used previously to simulate gyroharmonic conversion [10]-[17], so as to handle arbitrary initial beam distributions, multimode competition, and piecewise-linear tapered or resonant guide magnetic-field profiles. For all finite-emittance beam examples given below, a guiding center spread of 10% and an initial rms axial velocity spread of 0.020% are assumed. This velocity spread value is intended to approximately model that for the Litton $K=0.183\times10^{-6}\text{A}\cdot\text{V}^{-3/2}$ 300-kV, 30-A gun now under construction for planned experiments. Computations for this gun give a transverse emittance of 1.73π mm · mrad, corresponding to an rms geometric value for the ratio of transverse-to-axial velocity of 9.8×10^{-4}, and an rms thermal value of 6.0×10^{-3}. The potential depression for this beam is 1.16 kV, corresponding to an estimated rms value for the relative axial velocity spread of 0.027%. Simulation parameters used in all examples are given in Table I.

A. Analysis of Principle of Co-Generation

In order to better understand the principle of co-generation, first let us look at a example employing a cold beam, i.e., a beam without axial velocity spread and guiding-center spread. Harmonic powers in the TE_{62}, TE_{72}, TE_{82}, and $TE_{13,2}$ modes grow from noise, driven by the gyrating beam during acceleration by the diminishing-amplitude fundamental pump field. Fig. 2 shows the evolution of rf power for TE_{11} mode at 2.856 GHz and TE_{72} mode at 20 GHz, and the variation in imposed resonant axial magnetic field, according to (1), where $s = 1$ and $l = 1$; γ and β_z are replaced by their averaged values. A pronounced recurrence phenomenon is observed, with rf power shifting back and forth between the fundamental and the seventh harmonics. To measure performance of co-generation, first let us define a direct conversion efficiency, given by

$$\eta_{\text{direct}} = \frac{P_{72}(\text{out})}{P_{11}(\text{in}) + P_{72}(\text{in}) + P_{\text{beam}}(\text{in})}. \quad (10)$$

At $z = 87.1$ cm, the seventh-harmonic power has reached 10.41 MW and the fundamental power is 8.51 MW, corresponding to a direct conversion efficiency of $10.41/(20+9) = 35.90\%$. The sum of the two powers is only 5.4% less than the 20.0-MW fundamental power injected initially. One finds that 0.91 MW goes into $TE_{13,3}$ mode at the thirteenth harmonic and the rest is lost in the wall. Fig. 3 shows the variations in average beam energy factor $\langle\gamma\rangle$ and normalized gyration radius $\langle r_L/R_w\rangle$, as compared with $r_{L\max}/R_w$ calculated from (6). The beam energy rises to 818 kV at $z = 35.6$ cm, and falls back to 302.53 kV at $z = 87.1$ cm. Thus the beam is seen to have acted essentially as a catalyst, by exchanging power with the rf modes up to this point, but returning nearly to its original state. At $z = 172.9$ cm, the fundamental rf power level has risen to 15.7 MW, and only 3.2 MW resides in the seventh harmonic; again the beam energy is back to 300.13 kV. In the course of this one full recurrence cycle, the magnetic field varies quasisinusoidally between 1.2 and 2.2 kG. The normalized gyration radius varies from 0.0279 to 0.4741. The maximum total of sixth- and eighth-harmonic power at $z = 87.1$ cm is found to be 0.13 kW. The fact that the TE_{72} mode is the only serious competitor to the TE_{72} enforces the claim made previously that group velocity (refractive index) matching is a major factor in co-generation, since $n_{13,3} = 0.3720$, while $n_{62} = 0.1351$ and $n_{82} = 0.4483$. It should be noted from Fig. 3 that $\langle r_L/R_w\rangle$ is always less than $r_{L\max}/R_w$, as predicted by (6). For example, $\langle r_L/R_w\rangle = 0.4876$ and $\langle\gamma\rangle = 2.5899$ at $z = 35.6$ cm, $\langle r_L/R + w\rangle = 0.4741$ and $\langle\gamma\rangle = 2.4733$ at $z = 135.3$ cm, and $\langle r_L/R_w = 0.4964$ and $\langle\gamma\rangle = 2.6912$ at $z = 216.5$ cm while, from (6), $r_{L\max}/R_w = 0.4955$ for $\gamma = 2.5899$, $r_{L\max}/R_w = 0.4908$ for $\gamma = 2.4733$, and $r_{L\max}/R_w = 0.4991$ for $\gamma = 2.6912$.

To investigate effects of finite emittance on co-generation, simulations have been carried out for electron beams with an initial rms axial velocity spread of 0.02% and an initial guiding-center radius spread of 10%. An additional feature in this example is that a detuning of the axial magnetic field from exact resonance is imposed to minimize growth of beam parameter spreads from their initial values. The detuning

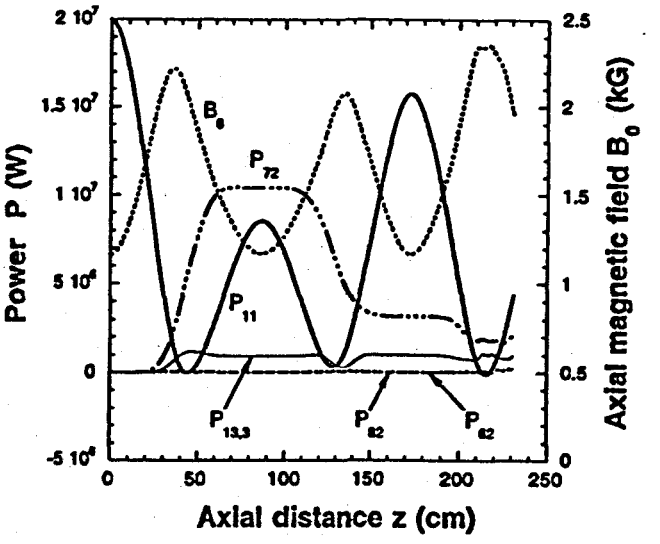

Fig. 2. Co-generation at the seventh harmonic for injection of a 300-kV, 30-A cold beam, and 20 MW of 2.856 GHz rf power, as given in Table I. Seventh-harmonic power at 20 GHz is seen to reach a maximum of 10.41 MW at $z = 87.1$ cm. Fundamental rf power P_{11}, seventh-harmonic power P_{72}, and axial magnetic field B_0 all show quasiperiodic recursions as energy cycles between the beam and the available radiation modes. A small amount of thirteenth-harmonic power $P_{13,3}$ is also seen.

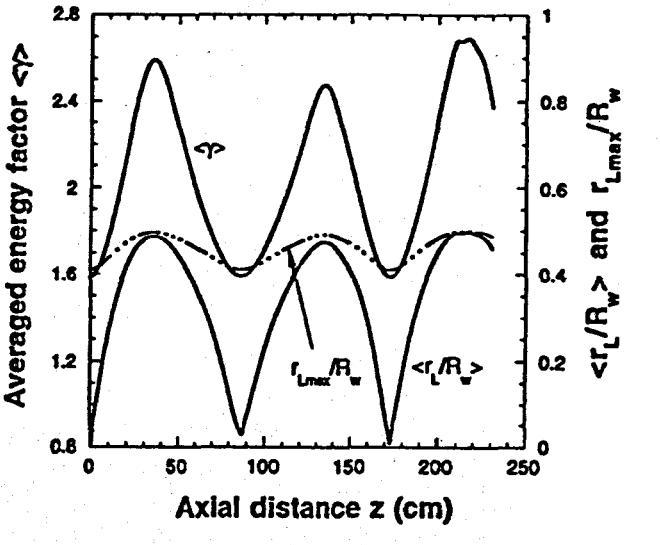

Fig. 3. Ensemble-average relativistic energy factor $\langle\gamma\rangle$ and normalized gyration radius $\langle r_L/R_w\rangle$ for the cold beam example, as in Fig. 2. Recursions are evident. The possible maximum gyration radius $r_{L\max}/R_w$ calculated from (6) is also shown as a reference. Clearly, $\langle r_L/R_w\rangle < \langle r_{L\max}/R_w\rangle < 0.5431$.

parameter is defined by $\Delta = \Omega_0/(\omega < \langle\gamma\rangle\langle\beta_z\rangle) + n_{11} - 1/\langle\beta_z\rangle$. Fig. 4 shows the optimized results, found for $\Delta = -0.02$. In this case, at $z = 83.8$ cm, output power at the seventh harmonic is seen to be 5.52 MW, at the fundamental to be 10.45 MW, and at the thirteenth harmonic to be 0.04 MW. Velocity spread leads to diminished beam-wave interaction, even more so at higher harmonics. Competition from only the $TE_{13,3}$ mode at the thirteenth harmonic is significant for an initial cold beam. But with finite initial beam emittance, possible competing modes $TE_{13,3}$, TE_{62}, and TE_{82} have been demonstrated to have only a minuscule influence on seventh-

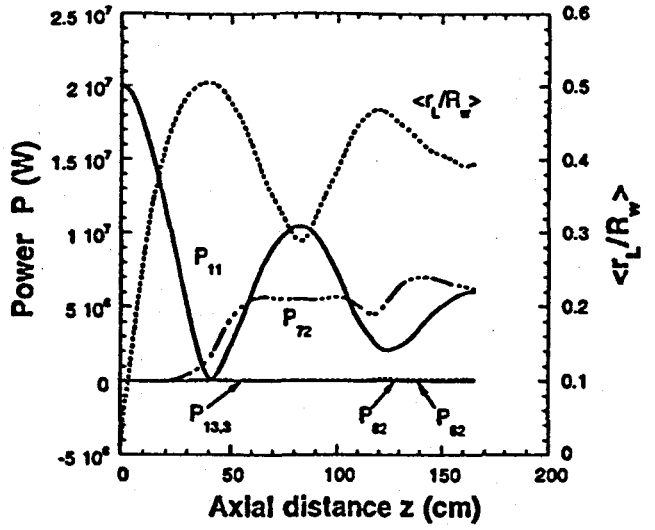

Fig. 4. Same as the Fig. 2, but for a finite-emittance beam, with initial axial velocity spread of 0.02% and initial guiding center spread of 10%. Peak value of seventh-harmonic power at 20 GHz is seen to be 5.52 MW at $z = 83.8$ cm.

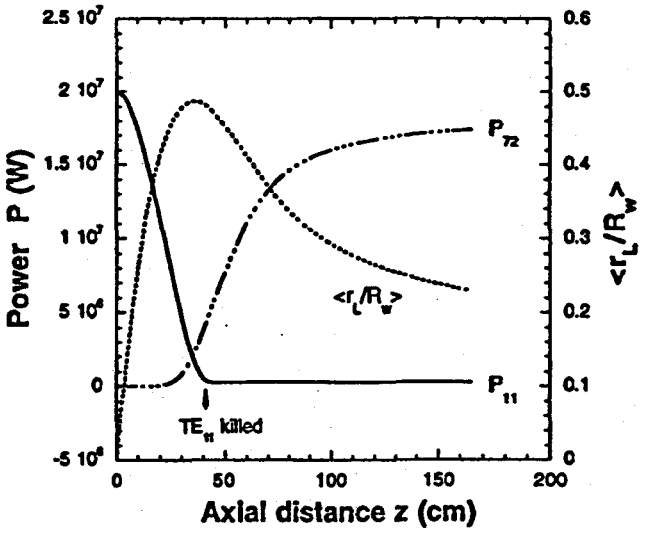

Fig. 5. Ideal seventh-harmonic co-generation for a cold beam, with TE_{11} mode fundamental power suppressed beyond $z = 41$ cm. Detuned magnetic field profile resonant with the TE_{11} mode is imposed. Power at 20 GHz is seen to rise to over 17 MW. Also shown is normalized gyration radius (r_L/R_w). Simulation parameters are given in Table I.

harmonic co-generation. The direct conversion efficiency has fallen from 35.90% for a cold beam to $5.52/(20 + 9) = 19.03\%$. A further significant factor here is seen to be the failure of normalized gyration radius (r_L/R_w) to fall below 0.3, while it fell essentially to zero for the cold beam case. This indicates that particles have lost strict phase synchrony even with the TE_{11} mode, and thus cannot give up more than a limited amount of transverse momentum.

B. Efficiency Enhancement by Mode Suppression and Adjustment of Guide Magnetic Field

From Fig. 4, we find that the power radiated into the TE_{11} mode rapidly exceeds that into the TE_{72} mode, with a maximum of 10.45 MW for TE_{11} and 5.52 MW for TE_{72}, after the point $z = z_{min}$ where the drive power is minimized or used up. When the TE_{11} mode recovers power from the beam, this reduces the beam's gyration radius, and the TE_{72} mode does not continue growing. Can the seventh-harmonic output efficiency be improved by suppressing (or "killing") the TE_{11} mode beyond $z = z_{min}$? To check this idea we first ran the code for a cold beam using a detuned resonant magnetic field with $\Delta = +0.0065$. The modified circuit is assumed to begin at $z = z_{min} = 41$ cm, so that any mode other than TE_{72} is killed beyond this point. As shown in Fig. 5, the output power at the seventh harmonic is seen to rise to 17.22 MW at $z = 150$ cm, corresponding to a direct efficiency of 59.38%. But when finite emittance and guiding center spread are present on the injected beam, and if only a detuned resonant magnetic field profile is chosen, the harmonic power is diminished to 4.71 MW at $z = 55.5$ cm, as shown in Fig. 6. This corresponds to a direct efficiency of only 16.24%. This dramatic drop in efficiency results from a loss of phase synchrony between electrons and the radiation field, as mentioned above, due to an improper choice of magnetic field profile for this warm beam, thus limiting the growth of harmonic power. The average relative gyration radius (r_L/R_w) remains at about 0.5 beyond $z = 40$ cm.

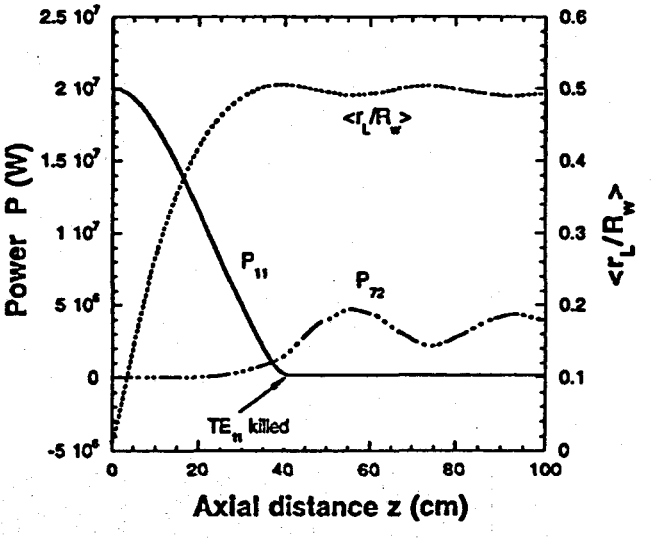

Fig. 6. Same as Fig. 5, but for a beam with finite initial emittance as in Fig. 4. As in Fig. 5, a detuned magnetic field profile resonant with with the TE_{11} mode is imposed. Power at 20 GHz rises only to 4.71 MW at $z = 55.5$ cm.

Different magnetic profiles were tried to improve the interaction efficiency. It was found that use of a segmented straight-line rather than a detuned resonant magnetic field profile after $z = z_{min}$ can restore some of the loss in seventh-harmonic power. This is illustrated in Fig. 7. When a two-segment profile is chosen, the seventh-harmonic output is seen to rise to 10.20 MW at $z = 99$ cm, and the direct efficiency is increased to 35.17%. Comparing Fig. 7 with Fig. 6 we see that careful choice of the magnetic field profile results in a doubling of seventh-harmonic output power. Comparing Fig. 7 with Fig. 4, we also find that mode suppression and adjustment of the magnetic profile has considerably improved direct efficiency, but the circuit becomes longer and somewhat more complicated.

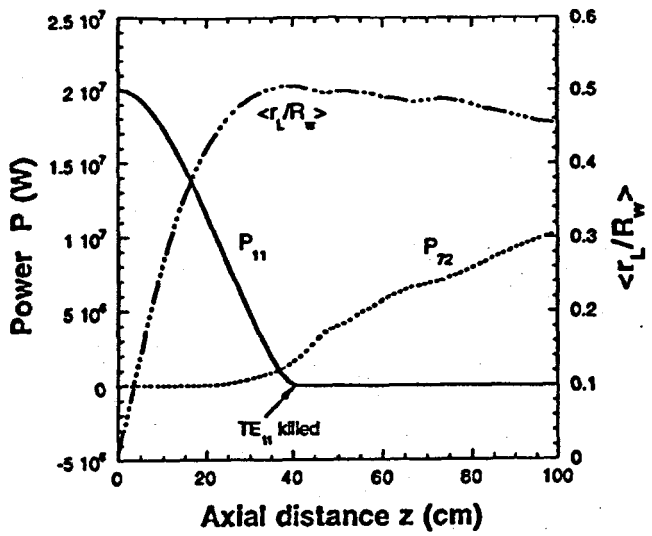

Fig. 7. Same as Fig. 6, for a beam with finite initial emittance as in Fig. 4, but with a detuned resonant magnetic field profile up to $z = 40$ cm, and two straight-line segments for the magnetic field profile up to $z = 99$ cm. Power at 20 GHz at $z = 99$ cm is seen to reach 10.20 MW.

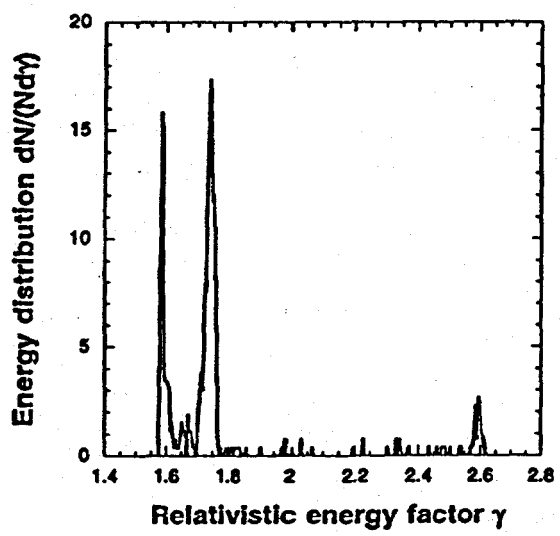

Fig. 8. Energy distribution at $z = 83.8$ cm, the end of the seventh-harmonic interaction, for the example shown in Fig. 4. Simulation contains 512 particles.

C. Efficiency Enhancement by Harmonic Power Injection

Examination of configuration and momentum phase space for an electron beam at the point where seventh-harmonic power reaches its peak value (i.e., at $z = 83.8$ cm in Fig. 4) shows that a large fraction of the beam particles are untrapped, with many particles undergoing large migrations in energy and relative phase. This is illustrated in Figs. 8 and 9, which show the energy distribution function and instantaneous particle coordinates of 512 particles in the z–y plane at $z = 83.8$ cm, i.e., the end of the interaction for the case shown in Fig. 4. Fig. 9 also shows the instantaneous x–y distribution at $z = 0$. A considerable migration in phase and energy is evident for a large fraction of the particles.

Inherent finite emittance of an electron beam is the source of initial transverse velocity spread, and the spread is amplified during the CARA acceleration. Relative gyrophase spread grows with increase in velocity spread after it experiences a rapid compression during trapping. A mean spread in relative phase that is not much smaller than $\pi/7$ is probably sufficient to diminish seventh-harmonic generation significantly. If a means to inhibit this spread in relative phase can be found, one might expect enhancement in seventh-harmonic conversion efficiency and energy recovery from the spent beam.

It was found in the simulations that injection at the input of a portion of the seventh-harmonic power with proper phase can effectively reduce gyrophase spread. Figs. 10–12 show results with a seventh-harmonic injection power of 2.0 MW, with other parameters the same as in Fig. 4. Now it is seen that the seventh-harmonic output at $z = 86.5$ cm is 12.11 MW, indicating a net gain of 10.11 MW, as compared with 5.52-MW output without injection. Fundamental power at $z = 86.5$ cm is 9.27 MW. The significant increase in seventh-harmonic output can be understood by reference to Figs. 11 and 12, where are depicted the energy distribution function and instantaneous x–y coordinates of the beam particles at $z = 86.5$ cm. The x–y coordinate distribution at $z = 0$ is also shown in Fig. 12. It is seen that stronger particle trapping occurs when injection is employed, as compared with Figs. 8 and 9 without injection. Now the direct conversion efficiency is $12.11/(9+2+20) = 39.06\%$, a value higher than that for a cold beam without injection (see Fig. 2).

Harmonic injection also benefits co-generation for the case where the TE_{11} mode is killed beyond its first minimum. Again, for 2.0 MW of 20-GHz power injected at $z = 0$, results are shown in Figs. 13–15. The magnetic-field profile chosen is similar to that in Fig. 7, with a resonant profile followed by two straight-line segments. In Fig. 13 it is seen that the seventh-harmonic power grows to 15.96 MW at $z = 87.5$ cm, for a net gain of 3.76 MW over the case with no injection. The direct conversion efficiency is $15.96/(20+2+9) = 51.48\%$. This improvement can also be understood as due to improved particle trapping, as shown in Figs. 14 and 15. The energy distribution is shown in Fig. 14, and the instantaneous x–y distribution at $z = 0$ and $z = 87.5$ cm are shown in Fig. 15. These distributions are not as narrow as those shown in Figs. 11 and 12, but nevertheless do indicate improved trapping, with concomitant improvement in seventh-harmonic generation efficiency.

D. Spent-Beam Energy Recovery Using a Single-Stage Depressed Collector

In a configuration requiring a large number of sources, such as a high-energy electron-positron collider, one could interconnect neighboring sources in tandem, so that any 2.856-GHz output of one source would partially feed the next source; in that case, the "makeup" power required for each source (except for the first one) would be reduced. For the example shown in Fig. 10 it would be $20.0 - 9.27 = 10.73$ MW. The 2.0 MW of 20-GHz input power would be derived from the output of the preceding source. In this case, one can define the output efficiency of a single co-generation in the tandem

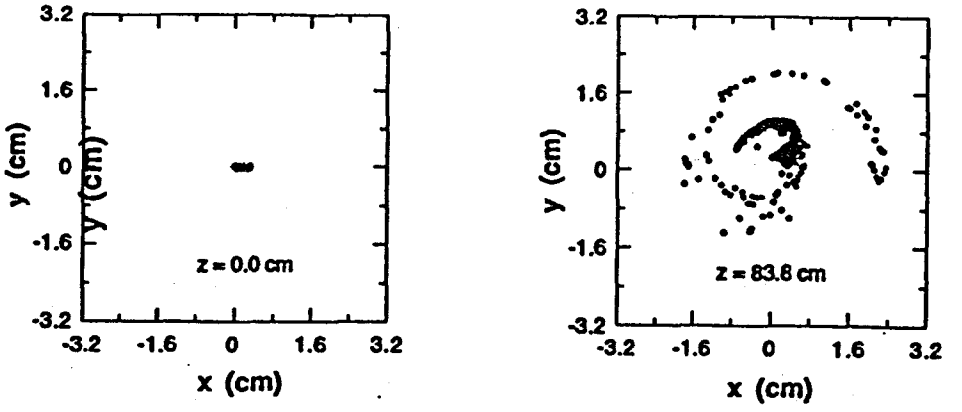

Fig. 9. Instantaneous transverse coordinates for the example shown in Fig. 4. At left is shown the distribution for 512 particles at $z = 0$, to illustrate the finite guiding center spread. At right is shown the distribution at $z = 83.8$ cm, where for many particles a large migration in relative phases is evident. Failure to achieve good phase trapping is responsible for the low level of 20-GHz power shown in Fig. 4.

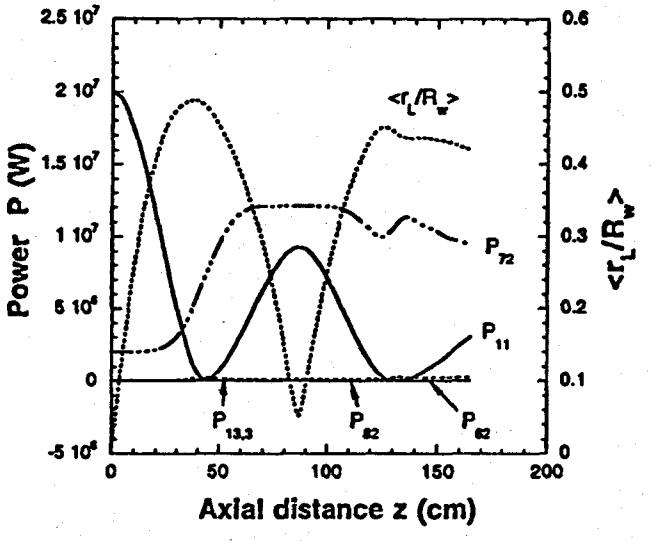

Fig. 10. Seventh-harmonic co-generation at 20 GHz with injection of 2.0 MW of 20-GHz power, for the same parameters as in Fig. 4. 20-GHz output is seen to rise to 12.11 MW at $z = 86.5$ cm, for an additional net power gain of 10.11 MW, as compared with 5.52 MW in Fig. 4.

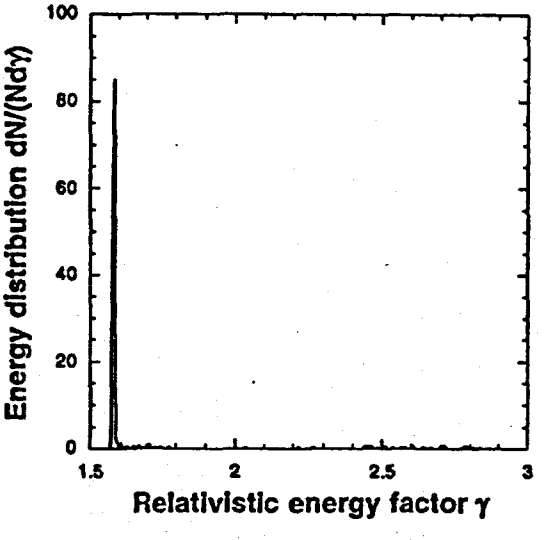

Fig. 11. Energy distribution at $z = 86.5$ cm for the co-generation example shown in Fig. 10. Distribution is much sharper than for the case without injection shown in Fig. 8.

sequence as

$$\eta_{\text{output}} = \frac{P_{72}(\text{out})}{P_{11}(\text{makup}) + P_{72}(\text{in}) + P_{\text{beam}}(\text{in})}. \quad (11)$$

Now for the example shown in Fig. 10, we find $\eta_{\text{output}} = 12.11/(10.73 + 2 + 9) = 55.73\%$, which is higher than the 51.48% found for the example in Fig. 13.

The sharper energy distribution found in Fig. 11 suggests that a higher efficiency can be achieved for recovery of spent-beam energy if a depressed collector is employed. This is done by operating the beam collector at a negative voltage, so as to retard the spent beam—thus delivering energy to the collector circuit. It is probably impractical to incorporate into a compact microwave generator a collector terminal to be held at a dc potential of 300 kV or more. Therefore, the energy-recovery concept envisioned here is pulsed, with the recovered beam current charging a pulse-forming network that could feed a step-down pulse transformer, thereby delivering the recovered energy at lower voltage for recirculation to the gun modulator.

The design of the collector, pulse-forming network, and pulse transformer would be akin to the inverse of what is used at the gun end of the device. However, it is beyond the scope of this paper to discuss a design for the energy-recovery circuit, but rather to show the benefit that would accrue from beam-energy recovery in enhancing co-generator efficiency. Indeed, development of the appropriate energy-recovery circuit, be it for a co-generator or for some other rf source, is a design challenge in and of itself. However, a co-generator can differ from other rf sources in that the energy distribution of the spent beam can be relatively narrow, as shown in Fig. 11, so that energy recovery efficiency can be relatively high.

Inclusion of beam energy recovery leads to a definition of an enhanced efficiency, defined as

$$\eta_{\text{enhanced}} = \frac{P_{72}(\text{out}) + \eta_{\text{rec}} P_{\text{beam}}(\text{in})}{P_{11}(\text{makup} + P_{82}(\text{in}) + P_{\text{beam}}(\text{in})} \quad (12)$$

where η_{rec} is the efficiency for recovery of spent beam power, and $P_{\text{beam}}(\text{out})$ is the beam power at the end of the co-generator. The quantity η_{rec} can be found from the ratio of

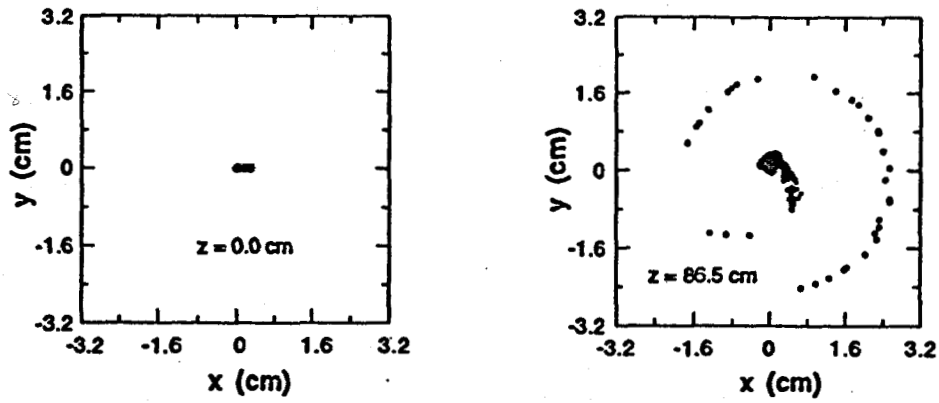

Fig. 12. Instantaneous transverse coordinates for the example of Fig. 10 with injection of 2.0 MW of 20-GHz power. As in Fig. 9, left diagram shows initial distribution at $z = 0$, while right diagram shows distribution at $z = 86.5$ cm. Phase trapping is seen to be improved, as compared with that in Fig. 9. As a result, net 20-GHz power gain is higher with injection than without.

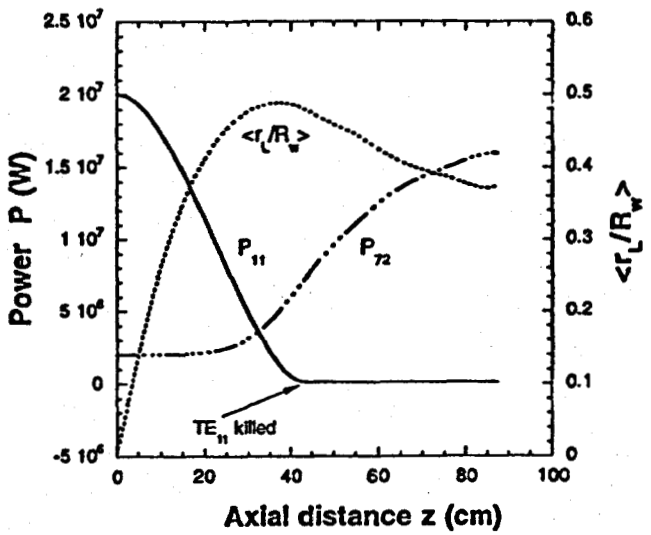

Fig. 13. Seventh-harmonic co-generation with injection of 2.0 MW of 20-GHz power for the example shown in Fig. 7. Seventh-harmonic power grows to 15.96 MW at $z = 87.5$ cm, for a net gain of 3.76 MW, as compared to the case without injection.

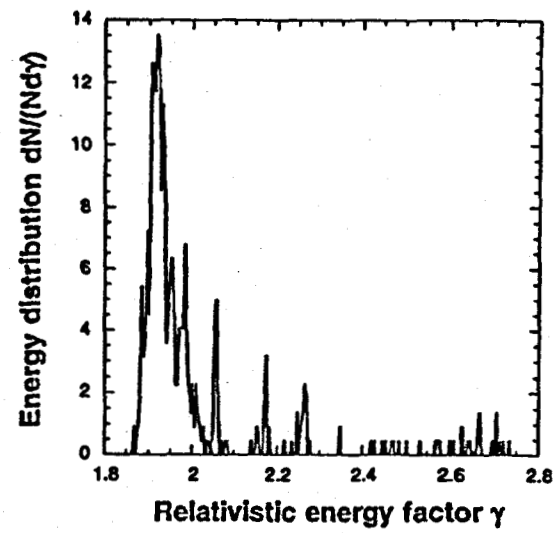

Fig. 14. Energy distribution function at $z = 87.5$ cm for the example shown in Fig. 13. Comparison with Fig. 11 suggests that maintaining the fundamental frequency TE_{11} mode throughout the interaction can improve phase trapping.

beam power to the collector after retardation, to the beam power at the end of the co-generator prior to retardation. This ratio must be multiplied by η_{coll}, the efficiency of beam interception by the collector. Thus one finds

$$\eta_{rec} = \frac{\gamma_r - 1}{\langle\gamma\rangle - 1}\eta_{coll} \tag{13}$$

where $\gamma_r = 1 + e|V_r|/m_oc^2$ is the relativistic energy factor corresponding to the collector retarding potential V_r, and $\langle\gamma\rangle$ is the ensemble average energy factor of the beam particles. In the idealized estimates that follow, it is assumed that the collector is designed to retard and intercept all primary beam electrons with kinetic energy above $e|V_r|$, as well as all scattered and secondary electrons; thus $\eta_{coll} = 1$. In practice, of course $\eta_{coll} < 1$. It is further assumed that the particles have zero velocity parallel to the collector. The retarding potential V_r is taken to correspond to the lowest kinetic energy of electrons in the beam, so that all beam current is collected, so as to avoid undesirable reflections prior to interception.

Table II shows comparisons for four configurations of co-generation at 20 GHz. For the Fig. 4 case with a detuned resonant magnetic field, there is no injection harmonic power, and TE_{11} and TE_{72} modes always coexist. For the Fig. 7 case with a resonant magnetic field before $z = z_{min}$ and a segmented straight-line magnetic field after that, there is no injection either, and the TE_{11} mode is killed after $z = z_{min}$. The Fig. 10 case is the same as the Fig. 4 case, and the Fig. 13 case is the same as the Fig. 7 case, except that the two former cases have a harmonic injection power of 2.0 MW at 20 GHz. Effects of mode suppression and magnetic field adjustment on efficiencies can be found by comparing the Fig. 4 case with the Fig. 7 case, and by comparing the Fig. 10 case with the Fig. 13 case. Effects of injection power at 20 GHz on efficiencies can be found by comparing the Fig. 4 case with the Fig. 10 case, and by comparing the Fig. 7 case with the Fig. 13 case. The Fig. 13 case has the maximum direct efficiency 51.48%, with 15.96-MW output at 20 GHz; the Fig. 10 case has the maximum enhanced efficiency 96.5%, with 12.11-MW output at 20 GHz. Effects of beam energy recovery on efficiencies

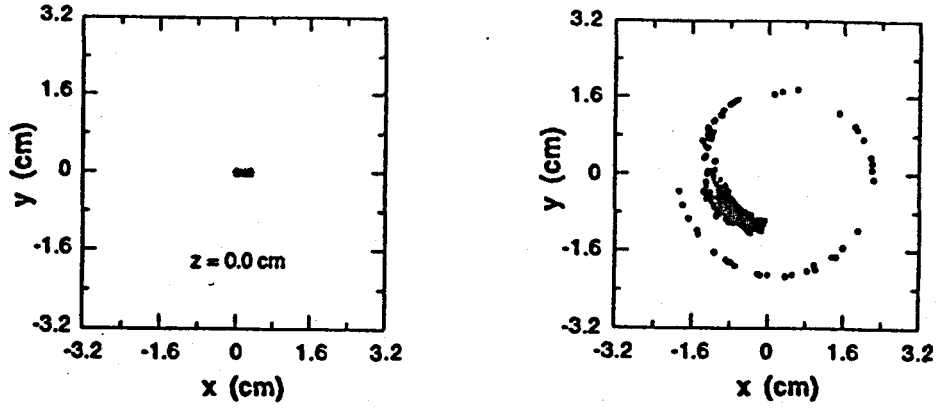

Fig. 15. Instantaneous transverse coordinates for the example of Fig. 13. Left diagram shows initial distribution at $z = 0$, while right diagram shows distribution at $z = 87.5$ cm. Phase trapping is seen to be better than that shown in Fig. 9, but not as good as that in Fig. 12. This is additional evidence to suggest that maintaining the fundamental frequency TE_{11} mode throughout the interaction can improve phase trapping.

TABLE II
PARAMETERS FOR FOUR CONFIGURATIONS OF CO-GENERATION OF 20 GHz. IN ALL CASES, INPUT POWER AT 2.856 GHz IS 20 MW, AND THE INJECTED BEAM IS 300 kV, 30 A WITH 0.02% rms AXIAL VELOCITY SPREAD AND 10% GUIDING CENTER SPREAD. FOR THE FIGS. 7 AND 13 CASES, FUNDAMENTAL POWER DOES NOT REGENERATE BEYOND $z = z_{min}$. FOR THE FIGS. 10 AND 13 CASES, INJECTED POWER AT 20 GHz IS 2.0 MW

	$P_{72\text{-out}}$ (MW)	$P_{11\text{-out}}$ (MW)	$P_{beam\text{-out}}$ (MW)	η_{direct} (%)	η_{output} (%)	η_{rec} (%)	$\eta_{enhanced}$ (%)
Fig. 4	5.52	10.45	12.85	19.03	29.75	69.1	77.6
Fig. 7	10.20	-	18.55	35.17	35.17	78.6	85.4
Fig. 10	12.11	9.27	9.40	39.06	55.73	94.4	96.5
Fig. 13	15.96	-	14.73	51.48	51.48	90.2	94.4

can be found from comparison between η_{output} and $\eta_{enhanced}$. From Table II we see that the efficiency is increased by 48% for the Fig. 4 case, 50% for the Fig. 7 case, 41% for the Fig. 10 case, and 43% for the Fig. 13 case, respectively, if beam energy recovery is employed.

IV. CONCLUSIONS

Gyroharmonic conversion as presented in the paper is based on the newly discovered phenomenon of co-generation [20], where a near-degeneracy in group velocity takes place between the TE_{11} mode at frequency ω and the TE_{72} mode at frequency 7ω in the cylindrical waveguide. This near-degeneracy causes the two modes to have nearly equal resonant magnetic fields in the CARA interaction, and helps the seventh harmonic to be excited preferentially, resulting in efficient power transfer between the TE_{11} mode at 2.856 GHz that energizes a gyrating electron beam, and the TE_{72} mode at 20 GHz. It has been analytically shown that the electron's gyration radius normalized to waveguide radius can be as large as 0.5431 in the CARA interaction, where a resonant guide magnetic field is imposed. This analytic prediction has been well confirmed by computer simulation. For co-generation with a 300-kV, 30-A electron beam driven by 20-MW rf power at 2.856 GHz, several axial magnetic-field and rf circuit configurations have been examined for maximizing 20-GHz power output, and for minimizing power lost in the conversion process. Particle simulation studies indicate that harmonic power injection is an effective means of improving particle trapping. This is because that TE_{72}-mode fields vary for seven periods when an electron makes one revolution around the waveguide axis, while TE_{11}-mode fields vary but one period. The injected harmonic power flowing into TE_{72} mode plays a role in constraining particle gyrophases when electrons experience the TE_{72}-mode fields. Recovery of power from the spent electron beam also has been shown to be an attractive means of enhancing the overall device efficiency. This is partly because the spent beam can have a comparatively narrow-energy distribution in co-generation. All results discussed in this paper neglect dc space-charge forces within the gyrating beam, an issue that is analyzed in [21]. However, it can be expected that the strong rf trapping forces provided by the ubiquitous intense TE_{11} mode fields may inhibit beam degradation below that estimated in [21] for a freely propagating beam. Thus this paper has given a detailed analysis for a novel seventh-harmonic generation mechanism based on mode degeneracy in a cylindrical waveguide. Taken together, the stratagems discussed for improving particle trapping and the recovery of spent-beam power have been shown in this paper to allow co-generators to achieve overall efficiencies of over 90%.

REFERENCES

[1] B. G. Danly, "RF source for linear colliders," in *Advanced Accelerator Concepts, AIP Conf. Proc. 335*, New York, Amer. Inst. Phys., 1995, pp. 25–38.

[2] G. Caryotakis, "'High-power microwave' tubes: in the laboratory and on line," *IEEE Trans. Plasma Sci.*, vol. 22, pp. 683–691, 1994.

[3] D. Sprehn, R. M. Phillips, and G. Caryotakis, "Performance of a 150-MW S-band klystron," in *Pulsed RF Sources for Linear Colliders, AIP Conf. Proc. 337*, New York, Amer. Inst. Phys., 1995, pp. 43–49.

[4] J. Haimson, B. Mecklenburg, and B. G. Danly, "Initial performance of a high gain, high efficiency 17 GHz traveling wave relativistic klystron for high gradient accelerator research," in *Pulsed RF Sources for Linear Colliders, AIP Conf. Proc. 337*, New York, Amer. Inst. Phys., 1995, pp. 146–161.

[5] R. B. Palmer, R. C. Fernow, J. Fischer, J. C. Gallardo, H. G. Kirk, S. Ulc, H. Wang, Y. Zhao, B. Danly, W. Herrmannsfeldt, R. Miller, K. Eppley, and T. Lee, "Status of the BNL-MIT-SLAC cluster klystron project," in *Pulsed RF Sources for Linear Colliders, AIP Conf. Proc. 337*, New York, Amer. Inst. Phys., 1995, pp. 94–102.

[6] H. Wang, R. B. Palmer, Y. Zhao, J. C. Gallardo, H. G. Kirk, and R. C. Fernow, "Beam aberration considerations and simulations for the cluster klystron," in *Pulsed RF Sources for Linear Colliders, AIP Conf. Proc. 337*, New York, Amer. Inst. Phys., 1995, pp. 103–117.

[7] J. P. Calame, W. Lawson, J. Cheng, B. Hogan, P. E. Latham, M. Castle, V. L. Granatstein, and M. Reiser, "100 MW gyroklystron development for linear collider applications," in *Pulsed RF Sources for Linear Colliders, AIP Conf. Proc. 337*, New York, Amer. Inst. Phys., 1995, pp. 195–199.

[8] O. Nezhevenko, "Magnicons," in *Pulsed RF Sources for Linear Colliders, AIP Conf. Proc. 337*, New York, Amer. Inst. Phys., 1995, pp. 172–173.

[9] S. H. Gold, B. Hafizi, and A. W. Fliflet, "X-band magnicon amplifier research at the Naval Research Laboratory," in *Pulsed RF Sources for Linear Colliders, AIP Conf. Proc. 337*, New York, Amer. Inst. Phys., 1995, pp. 184–192.

[10] J. L. Hirshfield, C. Wang, and A. K. Ganguly, "Design of multimegawatt millimeter-wave converters for operation at high gyroharmonics," *IEEE Trans. Plasma Sci.*, vol. 24, pp. 825–837, 1996.

[11] J. L. Hirshfield, A. K. Ganguly, and C. Wang, "Gyroharmonic converter as a high power cm-wavelength RF source for future $e^- - e^+$ colliders," in *Pulsed RF Sources for Linear Colliders, AIP Conf. Proc. 337*, New York, Amer. Inst. Phys., 1995, pp. 200–212.

[12] A. K. Ganguly and J. L. Hirshfield, "Linear and nonlinear theory of gyroharmonic radiation into modes of a cylindrical waveguide from spatiotemporally modulated electron beams," *Phys. Rev. E*, vol. 47, pp. 4364–4380, 1993.

[13] A. J. Balcum, D. B. McDermott, K. C. Leou, F. V. Hartmann and N. C. Luhmann, Jr., "Theory and design of a high-harmonic gyrofrequency multiplier," *IEEE Trans. Plasma Sci.*, vol. 22, pp. 913–919, 1994.

[14] C. S. Kou, D. B. McDermott, N. C. Luhmann, Jr., and K. R. Chu, "Prebunched high-harmonic gyrotron," *IEEE Trans. Plasma Sci.*, vol. 18, pp. 343–349, 1990.

[15] K. R. Chu, D. S. Furuno, N. C. Luhmann, Jr., D. B. McDermott, P. Vitello, and K. Ko, "Theory, design and operation of large-orbit high-harmonic gyro-klystron amplifiers," *IEEE Trans. Plasma Sci.*, vol. PS-13, pp. 435–443, 1985.

[16] D. B. McDermott, D. S. Furuno, and N. C. Luhmann, Jr., "Production of relativistic, rotating electron beams by gyroresonant RF acceleration in a TE111 cavity," *J. Appl. Phys.*, vol. 58, pp. 4501–4508, 1985.

[17] H. R. Jory and A. W. Trivelpiece, "Charged-particle motion in large amplitude electromagnetic fields," *J. Appl. Phys.*, vol. 39, pp. 3053–3060, 1968.

[18] G. S. Nusinovich and V. L. Granatstein, "On the optimal choice of microwave systems for future linear colliders," in *Pulsed RF Sources for Linear Colliders, AIP Conf. Proc. 337*, New York, Amer. Inst. Phys., 1995, pp. 16–24.

[19] P. B. Wilson, "RF pulse compression for future linear colliders," in *Pulsed RF Sources for Linear Colliders, AIP Conf. Proc. 337*, New York, Amer. Inst. Phys., 1995, pp. 293–302.

[20] C. Wang and J. L. Hirshfield, and A. K. Ganguly, "Efficient co-generation of seventh-harmonic radiation in cyclotron autoresonance acceleration," *Phys. Rev. Lett.*, vol. 77, pp. 3819–3822, 1986.

[21] B. Hafizi, P. Sprangle, and J. L. Hirshfield, "Electron beam quality in a cyclotron autoresonance accelerator," *Phys. Rev. E*, vol. 50, pp. 3077–3086, 1994.

[22] C. Wang and J. L. Hirshfield, "Energy limit in cyclotron autoresonance acceleration," *Phys. Rev. E*, vol. 51, pp. 2456–2464, 1995.

[23] M. A. LaPointe, R. B. Yoder, C. Wang, A. K. Ganguly, and J. L. Hirshfield, "Experimental demonstration of high efficiency electron cyclotron autoresonance acceleration," *Phys. Rev. Lett.*, vol. 76, pp. 2718–2721, 1996.

[24] Hirshfield, M. A. LaPointe, A. K. Ganguly, R. B. Yoder, and C. Wang, "Multimegawatt cyclotron autoresonance accelerator," *Phys. Plasmas*, vol. 3, pp. 2163–2168, 1996.

[25] K. Sakamoto, M. Tsuneoka, A. Kasugai, T. Imai, T. Kariya, K. Hayashi, and Y. Mitsunaka, "Major improvement of gyrotron efficiency with beam energy recovery," *Phys. Rev. Lett.*, vol. 73, pp. 3532–3535, 1994.

[26] V. L. Granatstein and W. Lawson, "Gyro-amplifiers as candidate RF drivers for TeV linear colliders," *IEEE Trans. Plasma Sci.*, vol. 24, pp. 648–665, 1996.

[27] P. B. Wilson, "Scaling linear colliders to 5 TeV and above," SLAC-PUB-7449, 1997.

J. L. Hirshfield, photograph and biography not available at the time of publication.

Changbiao Wang, photograph and biography not available at the time of publication.

A. K. Ganguly, photograph and biography not available at the time of publication.

Author: Please supply short biographies and photographs of yourself and your coauthors. Otherwise, the above squibs will appear in print. Also, please check reference call-outs in text. The IEEE style does not allow for multiple entries under one reference number. Hence, the references have been renumbered and appropriate changes made in the text. Thank you.

MULTI-MEGAWATT W-BAND RF SOURCE BASED ON GYROHARMONIC CONVERSION AT THE EIGHTH HARMONIC*

Changbiao Wang[1], J. L. Hirshfield[1,2], and O. A. Nezhevenko[2]
[1]Physics Department, Yale University, New Haven, Connecticut 06520-1820
[2]Omega-P, Inc., 202008 Yale Station, New Haven, Connecticut 06520

Abstract

A new version of an eighth-harmonic converter is analysed, which consists of a TE_{111}-mode cavity and an adjacent TE_{81}-mode cylindrical waveguide. Driven by 40 MW of rf power at 11.424 GHz, a 500 kV, 60.5 A Brillouin beam is accelerated in the cavity and generates up to 13 MW of output power at 91.392 GHz.

1 INTRODUCTION

Gyroharmonic conversion as a process for efficient production of high-power radiation has been discussed in a number of publications [1-6] and various approaches have been proposed. In one approach [1], low frequency rf drive power is used to accelerate an electron beam using the TE_{11} mode in a cylindrical waveguide by means of cyclotron autoresonance acceleration (CARA). The beam then passes through a transition region into a converter section, where it can selectively emit coherent radiation at a harmonic of the drive frequency. To allow the accelerated beam from CARA to fulfill the synchronous and grazing conditions in the converter section, the magnetic field in the transition region is tapered up. The operating harmonic index is specified by proper choice of converter circuit parameters and magnetic field profile. One deficiency in this approach is degradation in beam quality when the beam passes through the transition region where trapping in the strong rf fields is absent.

Another approach to gyroharmonic conversion is co-generation [5,6], which exploits a near-degeneracy for cylindrical waveguide, where nearly equal phase and group velocities prevail for the TE_{11} mode at frequency ω and the TE_{72} mode at frequency 7ω. As a result, gyroresonant interactions in the two modes require essentially the same resonant magnetic field profile. Thus efficient transfer of rf energy from the fundamental to the seventh-harmonic can occur in the self-same structure. The harmonic index is selected by the synchronous interaction mechanism itself, instead of through the circuit parameters. The near-degeneracy in cylindrical waveguide referred to above does not exist for an eighth-harmonic TE-mode interaction.

A new approach to eighth-gyroharmonic conversion is described here. Here the CARA drive section uses a TE_{111}-mode cavity and the converter section uses a TE_{81} waveguide where the TE_{11} mode is cutoff and the resonance with the eighth-harmonic is maintained by a proper choice of waveguide radius. Accordingly, no transition region is required between the CARA section and the converter section. A cavity is shorter than a waveguide would be for similar beam and rf parameters, and does not require a terminating absorber; both features help in preserving good beam quality.

In this paper, we present preliminary simulation results for the eighth-harmonic converter.

2 BASIC PRINCIPLES

Conditions for sustaining resonance for a beam at the end of CARA and the beginning of eighth-harmonic converter section are given by

$$\omega = \frac{\Omega_1}{\gamma_1} + k_{z1} c\beta_{z1}, \quad \text{and} \quad 8\omega = \frac{8\Omega_2}{\gamma_2} + k_{z2} c\beta_{z2}, \qquad (1)$$

where the electron gyrofrequency is $\Omega = eB_0/m$ with e the electron charge in magnitude, m the rest mass, and B_0 the axial magnetic field, k_z is the axial wavenumber, and the relativistic energy factor is $\gamma = (1-\beta_\perp^2-\beta_z^2)^{-1/2}$ with $\beta_\perp$ and β_z the transverse and axial velocities normalized to the vacuum light speed c. The parameters with subscript 1 are for the end of CARA and 2 for the beginning of converter section. Since the eighth-harmonic output section is directly adjacent to the CARA cavity, the continuity of magnetic field, particle energies, and velocities (that is, $\Omega_1 = \Omega_2$, $\gamma_1 = \gamma_2$, and $\beta_{z1} = \beta_{z2}$) requires $8k_{z1} = k_{z2}$. From dispersion equations for TE_{111} and TE_{81} modes, we obtain

$$\frac{R_2}{R_1} = \frac{j'_{81}}{8j'_{11}} = 0.65498, \qquad (2)$$

where R_1 and R_2 are, respectively, the TE_{111}-cavity radius and TE_{81}-waveguide radius, and $j'_{11} = 1.84118$ and $j'_{81} = 9.64742$ are the Bessel function roots. It can be noted that an equation similar to the above, but for the TE_{72} mode at frequency 7ω could be nearly satisfied with $R_1 = R_2$, since $j'_{72}/7 = 1.84748$; this fact is responsible for the near-degeneracy mentioned previously that can make seventh-harmonic co-generation in the CARA waveguide an efficient process.

Eq. (2) insures that a beam exiting the TE_{111}-mode cavity at frequency ω remains resonant with the TE_{81} mode at frequency 8ω. According to selection rules for axisymmetric beams [2], TE_{11} mode at the fundamental is the most competitive to the TE_{81} mode in the converter section. It can be shown that a proper choice of the cavity radius R_1 insures that the TE_{11} mode at the fundamental (or the TE_{72} mode at the seventh harmonic) is cutoff. If the fundamental frequency f_1 is 11.424 GHz

* The work was supported by the U. S. Department of Energy, Divisions of High Energy Physics and Advanced Energy Projects.

0-7803-5573-3/99/$10.00@1999 IEEE.

($\lambda_1 = 2.626$ cm), and the eighth-harmonic frequency f_8 is 91.392 GHz ($\lambda_8 = 0.328$ cm). Taking the cavity radius $R_1 = 0.798$ cm, from Eq. (2) we have the converter section radius $R_2 = 0.522$ cm. The cutoff wavelengths of TE_{11} mode at f_1 and TE_{81} mode at f_8 are, respectively, 1.783 cm and 0.340 cm, which means that TE_{81} is a propagating mode while TE_{11} is cutoff.

3 SIMULATION RESULTS

A preliminary simulation study has been performed for this harmonic converter configuration. The design parameters are chosen to accommodate as initial conditions at the CARA entrance a Brillouin beam. The beam radius r_b, beam current I, guide magnetic field B_0, and beam energy factor γ_0 are related by [7]

$$r_b = \frac{1}{B_0}\left[\frac{2m}{\pi\varepsilon_0 ec}\frac{I}{\left(\gamma_0^2-1\right)^{1/2}}\right]^{1/2}. \qquad (3)$$

For the example that was analyzed, a 500 kV, 60.5 A Brillouin beam with a radius of 0.35 mm is injected along the axis of a TE_{111} CARA cavity with a radius of 0.798 cm and a length of 4.95 cm. The cavity resonates at 11.424 GHz and is driven with a power of 40 MW; the unloaded cavity quality factor Q_0 is 5000. The TE_{81}-mode output waveguide has a radius of 0.522 cm and a length of 3.0 cm, following which a gentle up-taper in wall radius accompanies a linear down-taper to zero in guide magnetic field, allowing the beam to be collected on the wall. The simulation parameters are given in Table I.

Table I: Parameters in simulation

Beam energy	500 keV
Beam current	60.5 A
Beam radius	0.35 mm
Input rf power	40 MW
Drive frequency	11.424 GHz
TE_{111} cavity radius R_1	0.798 cm
Cavity length L	4.95 cm
Unloaded cavity quality factor Q_0	5000
Loaded cavity quality factor Q_L	100
TE_{81} waveguide radius R_2	0.522 cm
TE_{81} waveguide length	3 cm
Final collector radius	0.6 cm
Collector length	10 cm

Fig. 1 shows the rf structure outline and orbits of 8 sample particles in the $r-z$ plane, and Fig. 2 shows the relativistic energy factors for the particles. In the CARA section (from $z=0$ to 4.95 cm), the electrons are accelerated and their energies are increased. In the output section including the TE_{81} waveguide and collector (from $z=4.95$ to 17.95 cm), the electrons lose energy to TE_{81} mode at the eighth harmonic and then the wall intercepts all the electrons, because the axial magnetic field is linearly reduced to zero between $z=7.95$ and 17.95 cm.

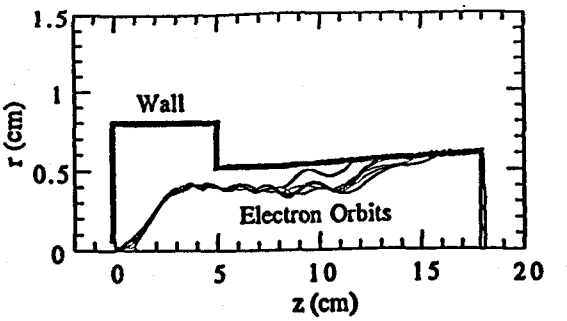

Figure 1: Wall profile for CARA cavity, output waveguide and tapered collector, and orbits throughout device for 8 sample electrons of 512 taken in simulation, including those orbits with extreme excursions.

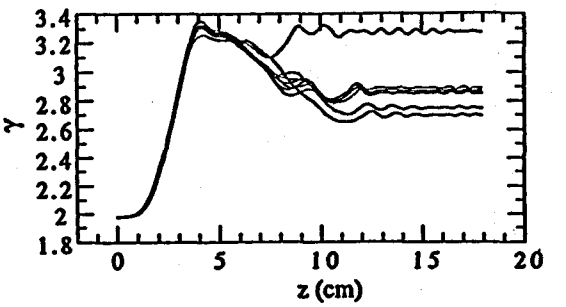

Figure 2: Energy factors for the 8 electrons in Fig. 1.

Fig. 3 shows the rf power levels and axial magnetic field profile along the full 17.95-cm length of the device. With a power of 40 MW at 11.424 GHz, the beam is accelerated initially from 500 keV to 1.15 MeV at the end of the cavity; this corresponds to an acceleration efficiency of 98% and an loaded cavity quality factor of 100; the magnetic field varies from 6.2 to 12.5 kG. In the output section, the eighth-harmonic rf power at 91.392 GHz is gradually increased and then reaches a maximum of 14.9 MW at $z=11$cm. Because of wall loss after about $z=13$cm where no net energy exchange takes place, the power is slightly reduced with a final output power of 13.1 MW. The magnetic field is resonantly decreased from 11.6 kG ($z=4.95$cm) to 10.3 kG ($z=7.95$cm), and then linearly to zero ($z=17.95$cm).

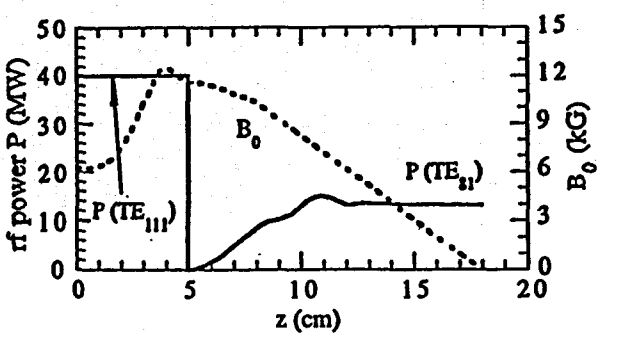

Figure 3: rf power levels in CARA and in output section (solid line), and magnetic field profile (dashed line).

Peak field strengths and ohmic power loss in the structure have been computed as well, and have been found to be well below the accepted levels for carefully built high power structures at X-band and W-band [8]. Results of these computations are shown in Figs. 4 and 5.

Fig. 4 shows the dependence of peak radial rf field strength at the walls in CARA and output section on axial distance. The maximum electric field in the CARA is 0.326 MV/cm and 0.266 MV/cm in the output section, well below the accepted breakdown limits for copper with $1-2\,\mu$sec pulses [9].

Fig. 5 shows the dependence of peak wall loss power P_{wall} and power density dP/dA on axial distance z for the output waveguide. Note that for a duty cycle less than 10^{-3}, the maximum average power density to be dissipated at the walls of the output waveguide would be less than 30 W/cm^2. The cavity must dissipate an average power of 800 W at this duty cycle.

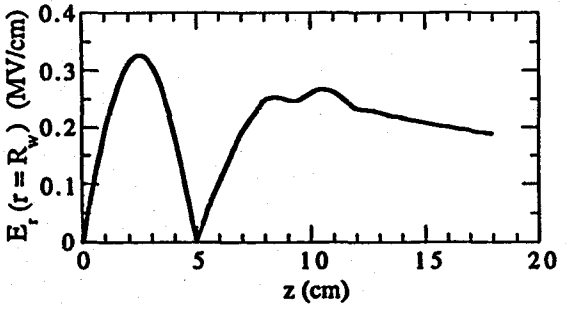

Figure 4: Peak radial rf field strength at the walls in CARA and in the output waveguide.

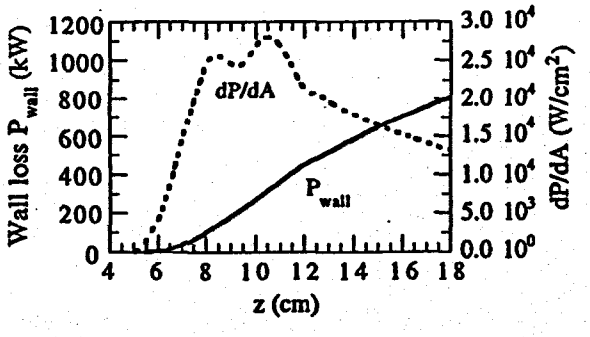

Figure 5: Cumulative peak power (solid line) and power density to be dissipated on the walls of the output waveguide (dashed line).

4 REMARKS

By simulation, we have analyzed an eighth-harmonic converter which uses a TE_{111}-mode cavity as the drive section and a TE_{81}-waveguide as the output section, without any required transition region. With an input power of 40 MW at 11.424 GHz and a 0.35-mm radius, 500-kV, 60.5-A Brillouin beam, a net output power of 13 MW at 91.392 GHz is obtained. As beam current and beam radius increase, the efficiency for eighth-harmonic conversion falls, although the absolute magnitude of output power can increase; likewise, an increase in rf drive power level can be tolerated at higher current, thereby also making higher output power possible.

Mode competition which is not taken into account in the simulation can occur in an overmoded rf structure as used in such a harmonic converter. In the CARA cavity, co-generation of seventh-harmonic power could arise, should it turn out that one of the TE_{72m} modes of the cavity were to resonate at 79.968 GHz. For a perfect cylinder with $R_1 = 0.798$cm, $L = 4.95$cm, probably the most dangerous (i. e., nearest) eigenmode is the TE_{721}, whose eigenfrequency is 80.222 GHz. But if the loaded Q for the TE_{721} mode is much larger than $80.222/2(80.222-79.968) = 158$, it should be possible to avoid excitation of the seventh harmonic because of detuning. Mode competition might also pose a problem in the output waveguide, since the TE_{61} and TE_{71} modes are not cutoff at the sixth and seventh harmonics. In the extreme, it is possible to operate with a cavity in place of the output waveguide, in order to discriminate against frequencies other than the design frequency of 91.392 GHz. In a preliminary simulation for a TE_{811}-mode output cavity, whose ohmic Q for copper cannot be higher than about 5000, and for the beam parameters and 40 MW-11.424 GHz drive level used in Figs. 1-5, a power of 12.06 MW is obtained. But 4.28 MW of this is dissipated in wall losses in the output cavity where $Q_L = 1774$; so the net output is 7.78 MW. These considerations suggest that strategies to avoid serious mode competition, and to operate insofar as possible without undue ohmic wall losses, will probably be the major challenges for further investigations.

5 REFERENCES

[1] J. L. Hirshfield, C. Wang, and A. K. Ganguly, *IEEE Trans. Plasma Sci.* PS-24, 825 (1996).

[2] A. K. Ganguly and J. L. Hirshfield, *Phys. Rev. E* 47, 4364 (1993).

[3] A. J. Balcum, D. B. McDermott, K. C. Leou, F. V. Hartmann, and N. C. Luhmann, Jr., *IEEE Trans. Plasma Sci.*, PS-22, 913 (1994).

[4] H. R. Jory and A. W. Trivelpiece, *J. Appl. Phys.* 39, 3053 (1968).

[5] C. Wang, J. L. Hirshfield, and A. K. Ganguly, *Phys. Rev. Lett.* 77, 3819 (1996).

[6] J. L. Hirshfield, C. Wang, and A. K. Ganguly, *IEEE Trans. Plasma Sci.*, PS-26, 567 (1998).

[7] M. Reiser, *Theory and Design of Charged Particle Beams* (Wiley, New York, 1994).

[8] J. W. Wang and G. A. Loew, *SLAC-PUB-7684*, Stanford University (1997).

[9] D. G. Myakishev, M. A. Tiunov, and V. P. Yakovlev, *Int. J. Mod. Phys. A*, 915 (1993).

LASER-DRIVEN CYCLOTRON AUTORESONANCE ACCELERATOR*

Changbiao Wang[1] and J. L. Hirshfield[1,2]
[1]Physics Department, Yale University, New Haven, Connecticut 06520-1820
[2]Omega-P, Inc., 202008 Yale Station, New Haven, Connecticut 06520

Abstract

Theory is developed for the cyclotron autoresonance acceleration of electrons in a gently-focused Gaussian laser beam and a gently tapered axial magnetic field. Numerical simulation shows, for example, acceleration from 50 MeV to 178 MeV over a distance of 148 cm, using a 10.6 μm CO_2 laser with a minimum spot size of 0.1 cm.

1 INTRODUCTION

Electron acceleration using intense lasers has engendered significant attention within the accelerator research community. This interest stems from the enormous optical electric field strengths E_0 that can be obtained with a focused laser, i.e. of the order of $E_0 = 3\times10^{-9}\sqrt{I}$ TV/m, where the intensity I is in W/cm^2 [1]. Since compact terawatt focused lasers can have $I > 10^{18}$ W/cm^2, field strengths of the order of teravolts/m are possible. Of course, since this field is transversely polarized, it can not give much net acceleration to a charged particle directly, so a number of indirect means have been devised to achieve net acceleration. For example, in the laser wake field accelerator [2] an intense laser pulse is used to locally polarize a plasma, thus creating a strong longitudinally-polarized plasma wake field for acceleration. In another example, the vacuum beat-wave accelerator [3], two laser pulses of differing frequencies are combined to create a slow optical ponderomotive beat wave that can exert a strong force for acceleration.

Originally a microwave interaction, the cyclotron autoresonance acceleration (CARA) of a low energy electron beam has been studied and demonstrated experimentally to operate with efficiencies exceeding 95% for transforming microwave energy into directed beam energy [4]. For acceleration of a high energy beam, however, the magnetic field required in the microwave CARA becomes so strong that it is not practical.

An alternative CARA is laser-driven cyclotron autoresonance accelerator (LACARA) [5]. The refractive index in LACARA is so close to unity that the upper energy limit for acceleration [6] is removed, and for acceleration of a high energy electron beam the magnetic field required is realizable. Furthermore, the group velocity in LACARA exceeds the axial particle velocity, so operation with strong pump depletion is possible without causing energy spread for the beam. The acceleration gradient in LACARA can be as high as $E_0(v_\perp / v_z)_{max}$, with $v_\perp$ and v_z the particle transverse and axial velocities respectively.

Recently, by simulation we have studied LACARA for acceleration of electron beams. Here we present the theory and preliminary numerical results.

2 OUTLINE OF LACARA THEORY

The preliminary analysis presented here is for a traveling Gaussian laser beam focused by two spherical mirrors. The laser fields in cylindrical coordinates (r,θ,z) for the lowest-order mode with circular polarization are [7]

$$E_r = cB_\theta = E_0\frac{w_0}{w}\exp\left(-\frac{r^2}{w^2}\right)\cos(\psi-\theta), \quad (1)$$

$$E_\theta = -cB_r = E_0\frac{w_0}{w}\exp\left(-\frac{r^2}{w^2}\right)\sin(\psi-\theta), \quad (2)$$

$$E_z \approx -\frac{2}{kw}\frac{r}{w}\left(E_\theta + \frac{z}{z_R}E_r\right), \quad (3)$$

$$B_z \approx -\frac{2}{kw}\frac{r}{w}\left(B_\theta + \frac{z}{z_R}B_r\right), \quad (4)$$

where c is the vacuum light speed, $w = w_0(1+z^2/z_R^2)^{1/2}$ is the spot size, w_0 is the waist radius (minimum spot size), and z_R is the Rayleigh distance. The waist radius and Rayleigh distance are related by $w_0 = (\lambda z_R/\pi)^{1/2}$, with λ the laser wavelength. The laser phase is $\psi = \omega t - kz + \tan^{-1}(z/z_R) - kr^2/2R$, with ω the laser angular frequency, $k = \omega/c$, and $R = z + z_R^2/z$ the radius of curvature of the ray normals. The axial and radial effective refractive indices (group velocities normalized to c) are given by

$$n = n_z = 1 - \frac{1}{2}\frac{w_0^2}{Rz} + \frac{1}{2}\frac{(z_R^2 - z^2)r^2}{(Rz)^2} \quad \text{and} \quad n_r = \frac{r}{R}. \quad (5)$$

The non-zero n_r means that there is diffraction loss for the Gaussian beam. The condition for resonance between wave and particles is $\Omega_0 = \gamma\omega(1 - n_z\beta_z - n_r\beta_r)$, where the non-relativistic gyrofrequency is $\Omega_0 = eB_0/m$ with e the electron charge in magnitude and m the rest mass, the relativistic energy factor is $\gamma = (1-\beta_\perp^2-\beta_z^2)^{-1/2}$ with $\beta_\perp = v_\perp/c$ and $\beta_z = v_z/c$, and β_r is the radial velocity normalized to c. Usually, the radial dimension of electron motion in LACARA is much less than the Rayleigh distance. Thus the resonance condition can be written as $\Omega_0 \approx \gamma\omega(1-n\beta_z)$, with $n \approx 1 - w_0^2/(2Rz)$.

The laser power is related to the electric field amplitude by $P_L = 0.5\pi w_0^2 E_0^2/\eta_0$, with $\eta_0 = (\mu_0/\varepsilon_0)^{1/2}$ the wave impedance of a plane wave in free space.

* The work was supported by the U. S. Department of Energy, Divisions of High Energy Physics and Advanced Energy Projects.

0-7803-5573-3/99/$10.00@1999 IEEE.

Eqs. (1)-(4), together with the relativistic equations of motion for the electrons

$$\frac{d}{dt}(\gamma v) = -\frac{e}{m}(E + v \times B) \qquad (6)$$

allow solutions to be found for single-particle orbits. In the results of computations to be shown below, iterative solutions for the position, velocity and energy of the particles are found at each computational stage by specifying the change in guide magnetic field value necessary to maintain resonance.

3 SIMULATION RESULTS

The simulation results presented below are for three LACARA examples. The laser power is from a CO_2 laser at a wavelength of 10.6 μm. Example 1 is for a 50 MeV cold electron beam driven by a laser power of 4 TW. The interaction length or mirror separation is 148 cm (5 Rayleigh distances). The simulation parameters are given in Table I and the results are shown in Figs. 1-4. In Example 2, the interaction length and the mirror radius are both 59.28 cm (2 Rayleigh distances), and all the other parameters are the same as those in Example 1. The result is shown in Fig. 5. Example 3 is for a 0.5 GeV cold beam driven by a laser power of 4 PW. Simulation parameters are given in Table II and the result is shown in Fig. 6. In all simulations, 8 computational particles initially uniformly distributed over one laser period are taken, and all electrons experience the same acceleration history. Beam loading is neglected.

Table I: Parameters in simulation for Example 1

Input cold beam energy	50 MeV
Laser power P_L	4.0 TW
Waist radius w_0	0.1 cm
Field amplitude E_0	31.0 GV/m
Rayleigh distance z_R	29.64 cm
Mirror radius	85.95 cm
Mirror separation	148 cm

Table II: Parameters in simulation for Example 3

Input cold beam energy	0.5 GeV
Laser power P_L	4.0 PW
Waist radius w_0	0.3 cm
Field amplitude E_0	326.5 GV/m
Rayleigh distance z_R	267 cm
Mirror radius	889 cm
Mirror separation	1600 cm

Fig. 1 shows average axial and transverse normalized velocities versus axial distance. The maximum $<\beta_\perp>$ is 0.0063; the initial $<\beta_z>$ is 0.999949 (minimum) and the final $<\beta_z>$ is 0.999984 (maximum), only 0.0035% change. From this, it is seen that the velocity ratio $\beta_\perp/\beta_z$ is quite small for a high energy beam in the LACARA, compared with a low energy beam in the microwave CARA [8]. This insures that all the electrons have very small transverse displacements, as shown in Fig. 2. The laser waist radius is 0.1 cm; so all the orbits of the 8 particles are within the minimum spot size.

Fig. 3 shows normalized axial group velocity and average axial electron velocity, plotted as $1-n$ and $1-<\beta_z>$, versus axial distance. It can be seen that the group velocity everywhere exceeds the axial particle velocity, allowing for rapid replenishment of laser energy that is given to the beam. This fact bodes well for achievement of an accelerated beam with low energy spread, even with significant beam loading. This allows efficient use of laser power without loss of beam quality.

Fig. 4 shows the dependence of average relativistic energy factor and axial magnetic field on axial distance. It is seen that the beam energy rises monotonically from 50 MeV to 178 MeV in a distance of 148 cm, corresponding to an average acceleration gradient of 86.6 MeV/m. The resonance magnetic field required rises from 52 kG to about 80 kG near the laser focus, and then falls back to about 60 kG. It is the fall in magnetic field that allows continuous acceleration without stalling; the fall in field can be traced to the fall in $(1-n)$ after the focus. This demonstrates that LACARA is not limited to be a γ-doubler, as in the microwave CARA.

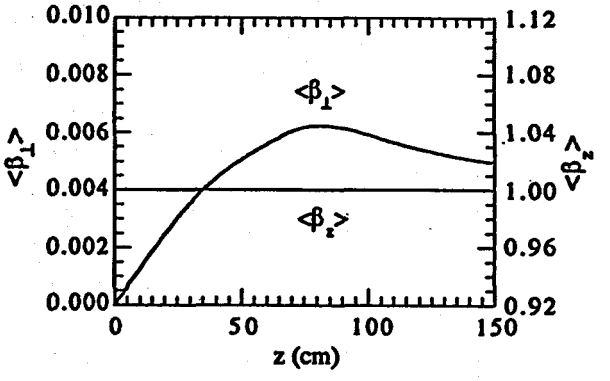

Figure 1: Average axial and transverse normalized velocities for Example 1 with a $5z_R$ interaction length. Initial beam energy is 50 MeV, z_R = 29.64 cm, w_0 = 0.10 cm, and P_L = 4.0 TW.

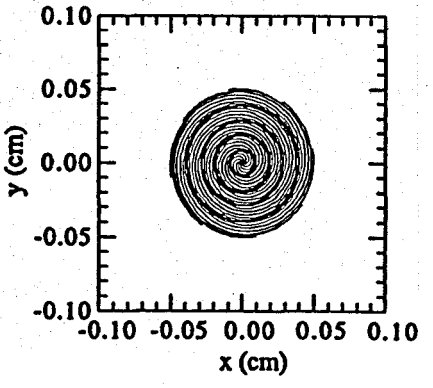

Figure 2: Projection in $x-y$ plane of orbits of 8 computational particles for Example 1. It is seen that the maximum transverse excursion is not greater than $w_0/2$.

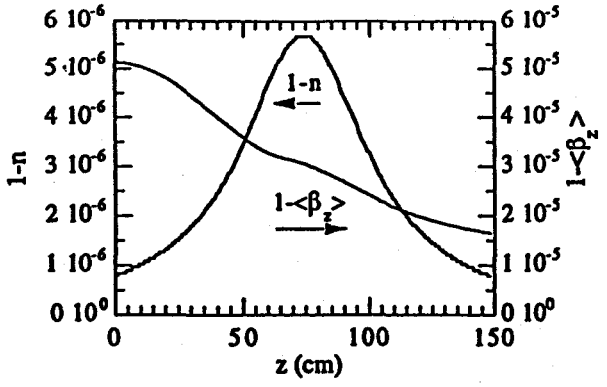

Figure 3: Variation in normalized axial group velocity plotted as $1-n$ (left scale), and normalized average axial velocity plotted as $1-<\beta_z>$ (right scale), for parameters of Example 1. It is seen that n exceeds $<\beta_z>$ throughout the interaction.

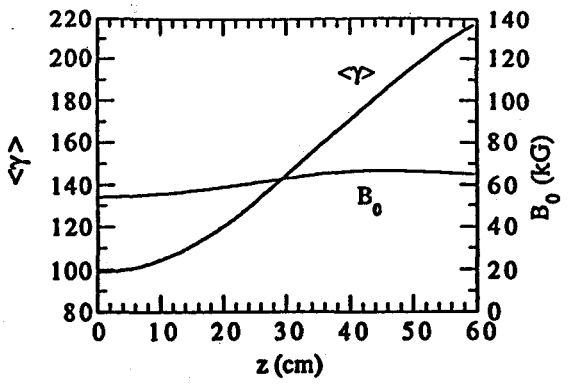

Figure 5: Variation in average relativistic energy factor $<\gamma>$ and axial magnetic field B_0 along LACARA for Example 2. Parameters are the same as Example 1, except for a LACARA of length $2z_R$ with a mirror radius of curvature 59.28 cm.

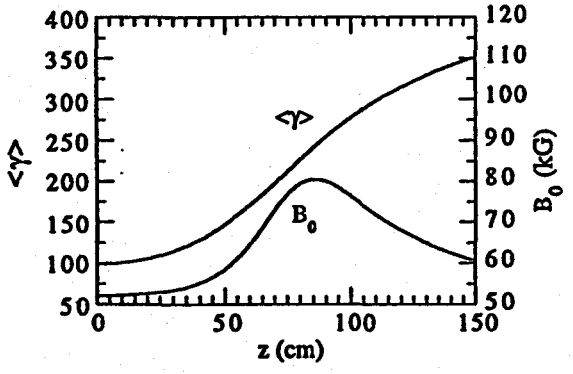

Figure 4: Variation in average relativistic energy factor $<\gamma>$ and axial magnetic field B_0 along LACARA, for parameters of Example 1.

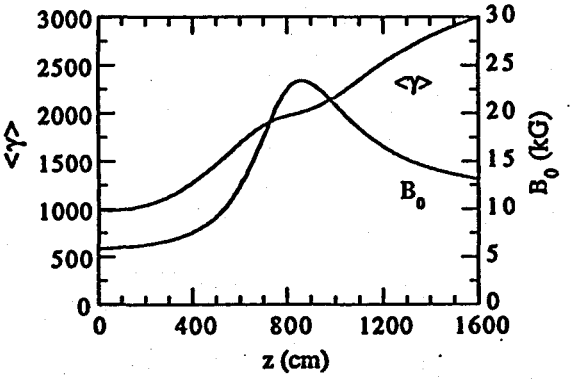

Figure 6: Variation in average relativistic energy factor $<\gamma>$ and axial magnetic field B_0 along LACARA for Example 3. The beam is accelerated from 0.50 GeV to 1.53 GeV within a $6z_R$ interaction length.

Fig. 5 shows the dependence of average relativistic energy factor and axial magnetic field on axial distance for Example 2. It is seen that the energy rises monotonically from 50 MeV to 110 MeV in a distance of 59.28 cm ($2z_R$), corresponding to an average acceleration gradient of 100 MeV/m. The resonance magnetic field required rises from 54 kG to about 67 kG near the laser focus, and then falls back to about 65 kG. This example shows that a shorter interaction region has a larger average acceleration gradient, since the laser field is weaker in the region far away from the focus.

Fig. 6 shows the dependence of average relativistic energy factor and axial magnetic field on axial distance for Example 3. It is seen that the energy rises from 0.5 GeV to 1.53 GeV in a distance of 16 m ($6z_R$), corresponding to an average acceleration gradient of 64.4 MeV/m. The orbit in this case was seen in the computations to execute only about one full gyration over its 16-m length, with a maximum displacement from the axis of less than 3.0 mm. The magnetic field is seen to vary from 6 kG, up to 24 kG, then down to 13 kG. This example shows that a lower magnetic field is required for a higher energy beam, as expected, in rough proportion to $1/\gamma$.

4 CONCLUSIONS

It is shown by simulation that in a LACARA driven by a power of 4 TW at 10.6 μm, a 50 MeV electron beam is accelerated to 178 MeV in a distance of 148 cm, corresponding to an average acceleration gradient of 87 MeV/m. The magnetic field varies from 52 kG to 80 kG.

5 REFERENCES

[1] P. Sprangle, et al., *AIP Conf. Proc.* 398, New York, Amer. Inst. Phys., 96 (1996).

[2] K. Nakajima, et al., *Phys. Rev. Lett.* 74, 4428 (1995).

[3] E. Esarey, et al., *Phys. Rev.* E 52, 5443 (1995); P. Sprangle, et al., *Opt. Commun.* 124, 69 (1996); B. Hafizi, et al., *Phys. Rev.* E 55, 5924 (1997).

[4] M. A. LaPointe, et al., *Phys. Rev. Lett.* 76, 2718 (1996).

[5] P. Sprangle, et al., *IEEE Trans.* NS-30, 3177 (1983).

[6] J. L. Hirshfield, et al., *Phys. Plasmas* 3, 2163 (1996).

[7] B. Hafizi (private communication).

[8] C. Wang and J. L. Hirshfield, *Phys. Rev.* E 51, 2456 (1995).

Laser-driven electron cyclotron autoresonance accelerator with production of an optically chopped electron beam

J. L. Hirshfield[1,2] and Changbiao Wang[1]
[1]*Department of Physics, Yale University, New Haven, Connecticut 06520-8120*
[2]*Omega-P, Inc., Suite 100, 345 Whitney Avenue, New Haven, Connecticut 06511*
(Received 15 October 1999)

Analysis is presented of the gyroresonant acceleration of electrons in a vacuum using a focused laser. Continuous and equal acceleration is shown for electrons injected at all optical phases over an interaction length of tens of centimeters. Beam stalling is avoided as beam energy increases. Acceleration from 50 to 178 MeV is predicted for a 4 TW, 10.6-μm laser focused to a waist radius of 1.0 mm; these parameters correspond to a planned experiment. A beam stop with an off-axis hole after acceleration is shown to create a train of optically chopped bunches with 3-fs bunch lengths and a 35-fs period.

PACS number(s): 41.75.Jv, 41.75.Lx, 96.50.Pw

Electron acceleration using intense lasers has engendered widespread attention within the accelerator research community, stimulated mainly by the enormous optical electrical field strengths E that can be obtained with a focused laser in a vacuum, i.e., of the order of $E=3\times10^{-9}\sqrt{I}$ TV/m, where the intensity I is in W/cm^2 [1]. Since compact terawatt-focused lasers can have $I>10^{18}$ W/cm^2, field strengths of the order of TV/m are possible. Of course, since this field is transversely polarized, it cannot give much net energy gain directly to a charged particle, so a number of indirect means have been devised to achieve cumulative acceleration. For example, in the laser wake field accelerator [2], an intense laser pulse is used to create a strong longitudinally polarized plasma wake field for acceleration. In the vacuum beat-wave accelerator [3], two laser pulses of different frequencies are combined to create a slow optical ponderomotive beat wave that can exert a strong force for acceleration. Electron acceleration to over 100 MeV has been observed in laser wake field accelerator experiments, corresponding to an acceleration gradient of the order of 30 GeV/m [4]. The energy spread of electrons that are accelerated in this manner is usually not small, since particles are acted upon throughout the nonuniform plasma wake. Moreover, the acceleration length is limited to a few Rayleigh lengths, usually less than a few millimeters for tightly focused optical radiation. These facts have led to experiments in which an optically prebunched beam is created, so that injected electrons in an inverse Čerenkov accelerator might all enjoy nearly the same acceleration [5,6]; or by exploitation of an injection mechanism (laser ionization and ponderomotive acceleration), wherein an energetic highly directed bunched beam is born within the optical focus [7]. Channeling has been suggested as a means to allow acceleration over many Rayleigh lengths [8]. Progress in the wide field of laser-based accelerators is summarized in a recent review [9].

This Brief Report describes a laser-driven acceleration mechanism in a vacuum that does not require a prebunched beam; nevertheless, all injected electrons can enjoy nearly the same acceleration history, regardless of their initial optical phase. A tight laser focus is not required, so the Rayleigh length can be tens of centimeters for a 10.6-μm laser wavelength, and continuous acceleration over meter-length paths is predicted. Furthermore, since the accelerated beam gyrates in a transverse plane at the laser frequency, an interposed beam stop with a judiciously placed off-axis hole can be employed to produce a transmitted beam comprising a train of optically chopped bunches with bunch lengths below 1 μm (3 fs). An example is presented of the acceleration of a beam from 50 to 178 MeV using a 4 TW, 10.6-μm wavelength laser in a nonuniform magnetic field peaking at 81 kG; a rf linear accelerator and a CO_2 laser with these parameters are to be available for a proposed experiment at Brookhaven National Laboratory [10].

The underlying mechanism, cyclotron autoresonance acceleration (CARA), has heretofore been studied mainly as a microwave interaction, where theory predicts and experiments show efficiencies exceeding 95% for transforming microwave energy into directed beam energy [11]. Phase bunching—but not spatial bunching—occurs in CARA, so that all injected electrons can be arranged to experience nearly the same magnitude of accelerating fields. However, a microwave CARA is in practice only a "γ doubler," in that the relativistic energy factor $\gamma=W/mc^2$ cannot in practice be increased much beyond a factor of 2 in a single stage, due to stalling of the electron beam in the required up-tapered guide magnetic field. In this expression, W is the electron rest energy mc^2 plus kinetic energy. It will be shown below that the CARA stalling limit can be circumvented when a focused optical field is used in place of a guided microwave field since, in the optical case, the axial magnetic need not necessarily be continuously up-tapered. Another feature of the laser-driven CARA, hereafter dubbed LACARA, is the relatively low level of magnetic field required for the cyclotron resonance interaction: for high beam energies, the magnetic field scales roughly as $1/\gamma\lambda$, where λ is the optical wavelength. As a result, state-of-the-art superconducting solenoid magnets are suitable for a 100-MeV demonstration of LACARA operating at $\lambda=10.6\,\mu$m.

Laser acceleration based on cyclotron resonance was first analyzed by Sprangle, Vlahos, and Tang [12] using fields approximating a focused Gaussian. These authors identified the need for a nonuniform guide magnetic field to preserve gyroresonance, and gave an example with an acceleration

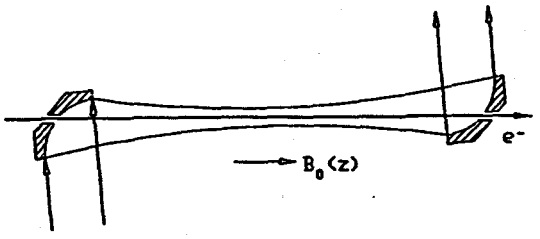

FIG. 1. Schematic diagram of LACARA. The incoming Gaussian CO_2 laser beam is focused by the left mirror, travels with the accelerating electron beam, and is deflected out of the beam path by the right mirror. Gyrations of the beam orbit are too small to be seen on the scale of this diagram.

gradient of 31 MeV/m for a $\lambda=10.6$-μm, $I=1\times10^{13}$ W/cm^2 laser. More recently, other authors have analyzed acceleration that is based on cyclotron resonance [13–15]. However, none of this prior analysis considered acceleration into and beyond a laser focus, and thus failed to show that the magnetic field will fall in magnitude after the focus, thereby avoiding stalling so that no upper limit to acceleration is imposed.

The analysis presented below is for a traveling Gaussian laser beam focused by a parabolic mirror, as shown in Fig. 1. The second mirror is solely to direct the spent laser beam away from the beam axis. The electron beam is taken to be injected and extracted through holes in each mirror. An axisymmetric nonuniform magnetic field is imposed on the system, as provided by a system of surrounding coils not shown in the figure. The form of this magnetic field is determined self-consistently by requiring that gyroresonance be maintained along the particle orbits. The electromagnetic fields in cylindrical coordinates (r,θ,z) for the lowest-order Gaussian mode in such a configuration excited with circular polarization are given by [3]

$$E_r=cB_\theta=E_0\frac{w_0}{w}\exp(-r^2/w^2)\cos(\psi-\theta), \tag{1}$$

$$E_\theta=-cB_r=E_0\frac{w_0}{w}\exp(-r^2/w^2)\sin(\psi-\theta), \tag{2}$$

$$E_z\approx-E_0\frac{2}{kw}\frac{w_0}{w}\frac{r}{w}\exp(-r^2/w^2)\times\left[\sin(\psi-\theta)+\frac{z}{z_R}\cos(\psi-\theta)\right], \tag{3}$$

$$B_z\approx-\frac{E_0}{c}\frac{2}{kw}\frac{w_0}{w}\frac{r}{w}\exp(-r^2/w^2)\times\left[\cos(\psi-\theta)-\frac{z}{z_R}\sin(\psi-\theta)\right], \tag{4}$$

where the waist radius w_0 in the focal plane $(z=0)$ and the Rayleigh length z_R are related by $w_0=(\lambda z_R/\pi)^{1/2}$, with $\lambda=2\pi/k$ the radiation wavelength. The radius of the radiation pattern for $z\neq0$ is $w(z)=w_0[1+(z/z_R)^2]^{1/2}$, the phase is $\psi(z,r,t)=\omega t-kz+\tan^{-1}(z/z_R)-kr^2/2R$, and the radius of the curvature of the rays' normal surfaces is given by $R(z)=z+z_R^2/z$. The coordinates (r,z) on surfaces of constant phase, i.e., where $d\psi/dt=0$, lead to $\omega=k_z v_{p,z}+k_r v_{p,r}$, with axial and radial phase velocities $v_{p,z}=dz/dt$ and $v_{p,r}=dr/dt$. The effective axial and radial wave numbers, found from $k_z=-\partial\psi/\partial z$ and $k_r=-\partial\psi/\partial r$, are

$$k_z=k-\frac{z_R}{z_R^2+z^2}+\frac{k}{2}\frac{(z_R^2-z^2)r^2}{(z_R^2+z^2)^2},\quad k_r=\frac{kzr}{z_R^2+z^2}. \tag{5}$$

Laser power P_L is related to the electric-field amplitude E_0 by $P_L=\pi\sqrt{\varepsilon_0/\mu_0}E_0^2w_0^2/2$. Some prior analyses [13,14] of gyroresonant acceleration consider uniform optical fields, thereby neglecting both diffraction and axial components.

The condition to be met for gyroresonance between electrons and the electromagnetic wave is given by the relation $\omega-k_{z0}v_z-\Omega_0/\gamma=0$, where v_z is the axial component of the electron velocity, $k_{z0}=k_z(z,r=0)$, and where the gyrofrequency on the axis is $\Omega_0(z)=eB_0/m$ with $B_0=B_z(z,r=0)$ the axially symmetric static magnetic field. The on-axis field can be used in the resonance condition in this case since radial excursions are much smaller than both the Rayleigh length and the scale length $|\partial\ln B_z/\partial r|^{-1}$. Clearly, resonance can be maintained along the orbit for an accelerated electron if the magnetic field is tailored in space to track the variations in γ and v_z. An equivalent way to write the resonance condition is $\Omega_0=\gamma\omega(1-n\beta_z)$, where $\beta_z=v_z/c$ and $n(z)=ck_{z0}/\omega=1-w_0^2/2zR(z)$ are the normalized axial velocity and effective index of refraction, respectively. When ensembles of particles with narrow variances are considered, the resonance condition can be approximated as $\Omega_0/\omega=\langle\gamma\rangle(1-n\langle\beta_z\rangle)$, where the angle brackets indicate ensemble average values.

The above field equations, Eqs. (1)–(4) together with the relativistic equation of motion for the electrons,

$$\frac{d}{dt}(\gamma\mathbf{v})=-\frac{e}{m}(\mathbf{E}+\mathbf{v}\times\mathbf{B}), \tag{6}$$

allow solutions to be found for single-particle orbits. In the results of computations, to be shown below, iterative solutions for the position, velocity, and energy of the particles are found at each computational stage by specifying the change in guide magnetic-field value necessary to maintain resonance. This insures that the solutions are internally consistent.

An example of predicted LACARA performance is shown in Fig. 2 for an incident 10.6-μm CO_2 laser power of 4 TW, an initial electron-beam energy of 50 MeV, a current of 1 A, and an initial normalized beam rms emittance of

$$\varepsilon_{nx}=\sqrt{(\gamma^2-1)(\langle x^2\rangle\langle x'^2\rangle-\langle xx'\rangle^2)}=\varepsilon_{ny}=\sqrt{(\gamma^2-1)(\langle y^2\rangle\langle y'^2\rangle-\langle yy'\rangle^2)}=2.0\text{ mm mrad}$$

[10]. In the computation, a total of 904 computational particles were injected, uniformly distributed in the optical phase and transverse phase spaces within emittance ellipses having major and minor axes r_b and $\beta_{\perp\max}$, with the beam radius $r_b=0.1$ mm and $\beta_{\perp\max}=\max\sqrt{\beta_x^2+\beta_y^2}$. The waist radius w_0 was chosen to be 1.0 mm, or approximately 100 optical wavelengths. This leads to a Rayleigh length z_R

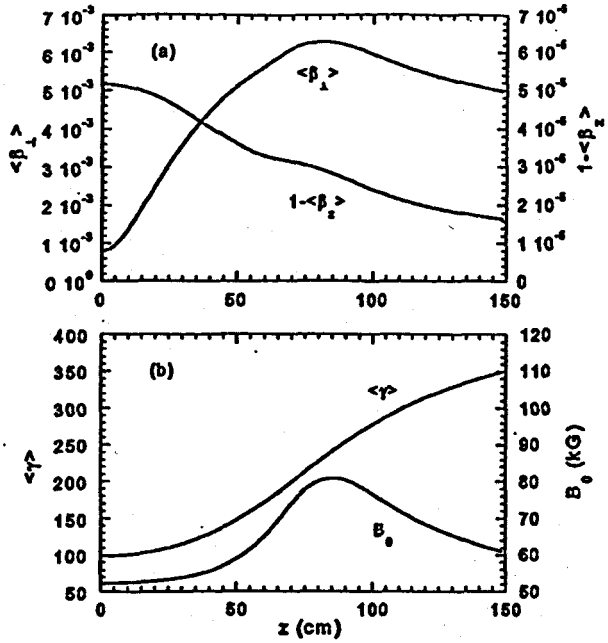

FIG. 2. (a) Average normalized transverse velocity $\langle\beta_\perp\rangle$ and normalized axial velocity, plotted as $1-\langle\beta_z\rangle$; (b) average relativistic energy factor $\langle\gamma\rangle$ and axial magnetic field B_0; (a) and (b) as functions of axial coordinate z in LACARA. For this example, the initial beam energy is 50 MeV, beam current is 1 A, Rayleigh length $z_R=29.64$ cm, laser-beam waist $w_0=1.0$ mm, interaction length $5z_R=148.2$ cm, and laser power $P_L=4.0$ TW. The acceleration gradient at $z=75$ cm is 147 MeV/m.

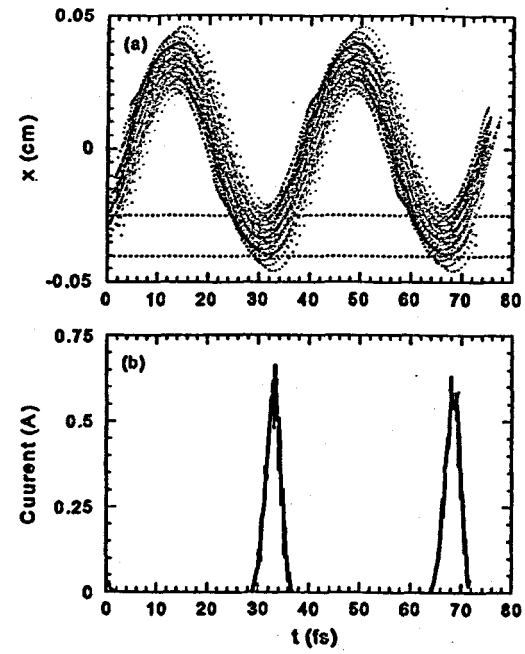

FIG. 3. (a) Phase plot for two optical cycles in the x-t plane at $z=2z_R=59.3$ cm for an ensemble of beam particles with initial normalized rms emittance $\varepsilon_{nx}=2.0$ mm mrad after acceleration from 50 to 110 MeV. Horizontal dashed lines show limits in x of the aperture in the beam stop. A similar plot, shifted one quarter-cycle in phase, depicts the y-t phase space. (b) Current transmitted through the 0.08-mm radius tunnel in a 2-cm beam stop. Incident current is 1.0 A. Microbunches in this example have FWHM widths of 3 fs, with an interbunch spacing of 35 fs. See text for details.

$=29.64$ cm. A mirror separation of $5z_R=148.2$ cm was chosen, with a mirror radius of 85.95 cm. Figure 2(a) shows the computed mean axial and transverse normalized velocities $1-\langle\beta_z\rangle$ and $\langle\beta_\perp\rangle$ as functions of distance along the axis, showing that the transverse momentum never exceeds 0.63% of the axial momentum; this insures that the motion remains well within the 2-mm-diam optical waist. Furthermore, $n>\beta_z$ throughout the interaction. The electrons execute about five gyrations in traversing the 148-cm intermirror distance, reflecting the strong Doppler down-shifted laser frequency experienced by the electrons, due to the small value of $1-n\langle\beta_z\rangle$. Figure 2(b) shows both the mean relativistic energy factor $\langle\gamma\rangle$ and the magnetic-field strength $B_0(z)$ versus axial distance. It is seen that the mean beam energy is predicted to rise monotonically from 50 to 178 MeV in a distance of 148 cm, corresponding to a maximum acceleration gradient at $z=75$ cm of 147 MeV/m and an average acceleration gradient of 86.6 MeV/m. The resonance magnetic field required rises from 52 to about 81 kG near the laser focus, and then falls back to about 60 kG. It is the fall in magnetic field beyond the focus that allows acceleration to continue without stalling; this fall in magnetic field can be traced to the fall in $(1-n)$ beyond the focus. This example demonstrates that LACARA is not limited to being a γ doubler. In fact, indefinite acceleration beyond the focus is possible—albeit with an ever-diminishing acceleration gradient.

In general, computations for a range of laser power levels, waist radii, and acceleration lengths show that energy gain increases as laser power increases, but more slowly than linearly; that energy gain falls with increasing initial beam energy; that energy gain is approximately independent of waist radius when the overall interaction length is held constant; and that the average acceleration gradient increases as waist radius decreases, provided the overall acceleration length contains a constant number of Rayleigh lengths. For example, with $P_L=4.0$ TW, $w_0=0.60$ mm, $L=5z_R=53.4$ cm, and an initial beam energy of 50 MeV, one finds an energy gain of 65.6 MeV and an average acceleration gradient of 123 MeV/m. For $P_L=1.0$ TW, with the other parameters unchanged, the average acceleration gradient falls to 46.9 MeV/m. For $P_L=4.0$ TW, with the initial beam energy increased to 80 MeV and other parameters unchanged, the average acceleration gradient falls to 42.5 MeV/m. In yet another example, acceleration from 0.50 to 1.50 GeV is predicted for a 4.0-PW, 10.6-μm laser with a waist of 0.30 cm over a distance of $6z_R=16$ m, for an average acceleration gradient of 64.4 MeV/m. The magnetic field for this example varies from 6 kG up to about 24 kG, then down to 13 kG.

An accelerated beam emerges from LACARA with electrons on helical orbits. The number of gyrations executed by a single electron during the interaction is few, but the gyration phases for orbits of successive electrons advance rapidly, i.e., at the laser frequency. Thus if a beam stop with an off-axis hole is interposed after acceleration, the transmitted beam will be chopped at a frequency equal to the laser frequency. A phase plot that illustrates this possibility is shown in Fig. 3(a), where two cycles of the $x-\omega t$ coordinates are plotted for an ensemble of 18 080 electrons after acceleration through an interaction length of $2z_R=59.28$ cm, with other

parameters the same as in the example shown in Fig. 2. The correlation between coordinate and time is evident, so that if an aperture limits beam transmission in x, then a temporally chopped beam will emerge. Similar considerations apply in y. A computed example of such an optically chopped beam is shown in Fig. 3(b), which shows the two cycles of beam current after transmission through a 0.08-mm radius hole in a 2-cm-thick tungsten beam stop. In this example, the beam is accelerated from 50 to 110 MeV (corresponding to an average acceleration gradient of 100 MeV/m) while the resonance magnetic field varies between 54 and 67 kG. The entrance aperture in the beam stop is centered at $x=-0.32$ mm, $y=0$; the exit is centered at $x=-0.305$ mm, $y=-0.11$ mm; so the beam channel is inclined at an angle of 0.32° with respect to the z axis. These limits of x are shown in Fig. 3. As is seen in Fig. 3(b), the peak transmitted current is 0.6 A (out of an incident 1.0 A) in a train of 3-fs [full width at half maximum (FWHM)] bunches with a period of 35 fs, or equivalently 0.9-μm bunches spaced by 10.6 μm. Such an optically chopped beam could find an application as an injector for other laser-based accelerators in a harmonic generator of optical radiation, in the generation of femtosecond x-ray pulses, or in studies of excitation and lifetimes in electron-induced nuclear reactions.

This Brief Report has presented computed predictions for the acceleration of electrons in a circularly polarized, focused CO_2 Gaussian laser beam, under conditions where gyroresonance is maintained along the electron trajectory. For currently achievable CO_2 laser power levels in the multi-TW range, acceleration gradients of over 100 MeV/m and overall acceleration in 150 cm of a 50-MeV beam to 178 MeV have been shown to be achievable for a mild laser focus with a beam waist of 1.0 mm. The parameters selected for the examples presented correspond to those soon to be available for a proposed experiment [10]. This laser-based accelerator treats all electrons in a bunch nearly identically, providing the laser pulse width exceeds the bunch width. The acceleration occurs in a vacuum, without any proximate material medium—except for a mirror to focus the laser. Experience with the microwave CARA where high efficiency (>95%) for the transfer of rf power to beam power has been observed [11], suggests that the laser-driven version of LACARA could be similarly efficient. It has also been shown that if a beam stop with a small slightly inclined beam tunnel is interspersed after acceleration with LACARA, then an optically chopped beam can be produced that consists of a train of femtosecond bunches spaced by the laser period. This simple idea is, to the author's knowledge, the only mechanism yet proposed for production of a beam fully chopped on an optical time scale.

Constructive discussions with B. Hafizi, T. C. Marshall, M. A. LaPointe, and V. L. Bratman are acknowledged. This research was supported by the U.S. Department of Energy under SBIR Grant No. DE-FG02-99ER82846 to Omega-P, Inc.

[1] P. Sprangle, E. Esarey, B. Hafizi, R. Hubbard, J. Krall, and A. Ting, in *Advanced Accelerator Concepts*, edited by S. Chattopadhyay, J. McCullough, and P. Dahl, AIP Conf. Proc. No. 398 (AIP, Woodbury, NY, 1996), p. 96.

[2] K. Nakajima *et al.*, Phys. Rev. Lett. 74, 4428 (1995).

[3] E. Esarey, P. Sprangle, and J. Krall, Phys. Rev. E 52, 5443 (1995); P. Sprangle, E. Esarey, J. Krall, and A. Ting, Opt. Commun. 124, 69 (1996); B. Hafizi, A. Ting, E. Esarey, P. Sprangle, and J. Krall, Phys. Rev. E 55, 5924 (1997).

[4] K. Nakajima *et al.*, in *Advanced Accelerator Concepts* (Ref. [1]) p. 83; D. Gordon, *et al.*, Phys. Rev. Lett. 80, 2133 (1998).

[5] W. D. Kimura *et al.*, in *Advanced Accelerator Concepts* (Ref. [1]), p. 608.

[6] W. D. Kimura *et al.*, in *Advanced Accelerator Concepts*, edited by W. Lawson, C. Bellamy, and D. F. Brosius, AIP Conf. Proc. No. 472 (AIP, Woodbury, NY, 1998), p. 563.

[7] C. I. Moore, A. Ting, S. J. McNaught, J. Qiu, H. R. Burris, and Sprangle, Phys. Rev. Lett. 82, 1688 (1999).

[8] P. Sprangle, B. Hafizi, and P. Serafin, Phys. Rev. Lett. 82, 1173 (1999); C. B. Schroeder, D. H. Whittum, and J. S. Wurtele, *ibid.* 82, 1177 (1999); F. Dorchies *et al.*, *ibid.* 82, 4655 (1999).

[9] E. Esarey, P. Sprangle, and A. Ting, IEEE Trans. Plasma Sci. 24, 252 (1996).

[10] Experiments based on the analysis presented in this Brief Report have been proposed to Brookhaven National Laboratory Accelerator Test Facility; I. Ben-Zvi (private communication).

[11] J. L. Hirshfield, M. A. LaPointe, A. K. Ganguly, R. B. Yoder, and C. Wang, Phys. Plasmas 3, 2163 (1996); M. A. LaPointe, R. B. Yoder, C. Wang, A. K. Ganguly, and J. L. Hirshfield, Phys. Rev. Lett. 76, 2718 (1996).

[12] P. Sprangle, L. Vlahos, and C. M. Tang, IEEE Trans. Nucl. Sci. 30, 3177 (1983).

[13] A. Loeb and L. Friedland, Phys. Rev. A 33, 1828 (1986).

[14] C. Chen, Phys. Rev. A 46, 6654 (1986).

[15] C. Wang and J. L. Hirshfield, Phys. Rev. E 51, 2456 (1995); 57, 7184 (1998).

10-MW, W-Band RF Source for Advanced Accelerator Research

J. L. Hirshfield,[*,†] O. A. Nezhevenko,[†] Changbiao Wang,[*]
V. P. Yakovlev,[†] A. A. Bogdashov,[¶] V. L. Bratman,[¶] A. V. Chirkov,[¶]
G. G. Denisov,[¶] A. N. Kuftin,[¶] S. V. Samsonov,[¶] and A. V. Savilov[¶]

Beam Physics Laboratory, Yale University, 272 Whitney Ave., New Haven, CT 06511
†Omega-P, Inc., 345 Whitney Ave., New Haven, CT 06511
¶Institute of Applied Physics, Russian Academy of Sciences, 603600 Nizhny Novgorod, Russia

Abstract. A conceptual design is presented for a W-band RF source that should be suitable for testing advanced accelerator structures and related components. The source is an 8th-gyroharmonic converter, in which 28 MW of X-band power at 11.424 GHz is used to energize and spin up an injected 500 kV, 40 beam in a TE_{111} cavity; and in which over 10 MW of W-band power at 91.392 GHz is extracted from the beam in a TE_{811} output cavity. A mode converter is employed to provide a Gaussian output beam.

INTRODUCTION

Efforts have been directed at design and fabrication of accelerating structures to operate at W-band (91.4 GHz) because of the expectation of achieving an acceleration gradient ~1 GeV/m, based on empirical scaling [1]. This gradient allows a 5 TeV electron/positron collider to be built within a length of 5 km, not including the final focus region. It is this dramatic reduction in size of a future multi-TeV collider that has provided much of the stimulus for the W-band work. But to test the susceptibility of accelerating structures and components at high-power to rf breakdown and fatigue, it is apparent that a high-power W-band source will be required.

No megawatt-level W-band source exists for this task. Some moderate power sources at W-band are presently available, and others are under design. Notable are the W-band gyro-klystron amplifiers developed at Naval Research Laboratory (NRL) [2] and at Institute of Applied Physics in Nizhny Novgorod, Russia [3]. These devices currently deliver peak output powers of over 100 kW and over 200 kW, respectively. Design of a W-band multi-beam klystron that embodies several 100 kW "klystrinos" is also currently underway [4]. Furthermore, a preliminary design has been published for

a 7.5 MW, W-band three-cavity second-harmonic gyro-klystron [5]. No other W-band amplifier has been designed heretofore with a peak power of more than 10 MW.

CONCEPTUAL DESIGN

A design for an 8th-harmonic frequency multiplier is described here that is predicted to have 40% efficiency for power conversion from 11.424 GHz up to 91.392 GHz. A conceptual drawing of the heart of the device is shown in Fig. 1. Computations described below show a peak output power of 11.3 MW at W-band, for an input of 28 MW at X-band. This converter could be driven from an X-band SLAC klystron [6], or from the Omega-P/NRL 60-MW, X-band magnicon [7]. Either driver would allow one to obtain a 1-3 μsec W-band output pulse with a repetition rate determined by the available modulator. The 11.3 MW output power level is not an absolute upper limit, but is set in the present design by the beam current (40 A) from the available modulator at NRL. Features of the tube include:

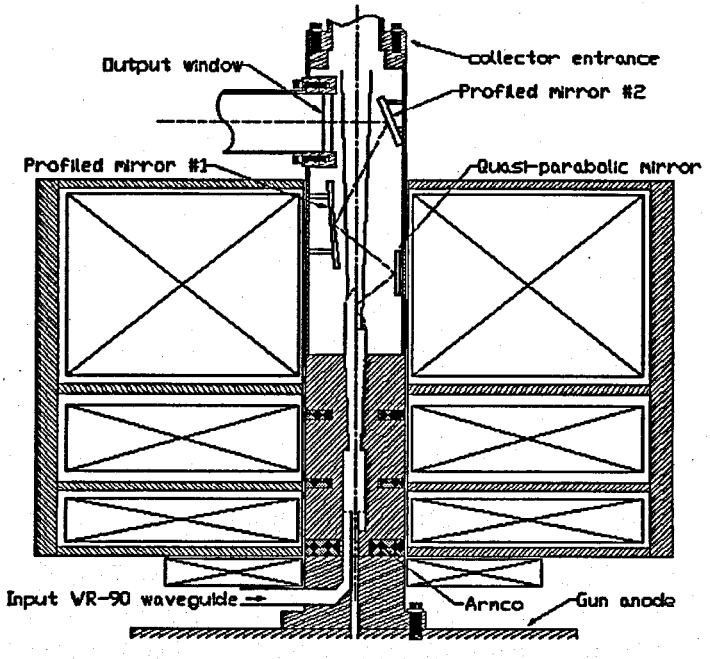

Figure 1. Conceptual design of W-band source.
Not shown are the gun at bottom, and the beam collector at top.

a. Two WR-90 input waveguides, with an H-plane miter-bend to feed a coupling aperture in the bottom face of the TE_{111} input drive cavity. The second input waveguide is disposed at 90° with respect to the first, and is not seen in the drawing. Opposite each input waveguide is an aperture in the cavity wall with a tuning section to symmetrize fields in the drive cavity. Each waveguide is to carry 14 MW of 11.424 GHz input power from the rf driver, a level well below the waveguide breakdown limit.

b. A four-coil room-temperature magnet structure, with three carefully tailored Armco rings that help produce the steeply contoured axial magnetic field required for achievement of high efficiency in this device. Such a steep contour may be difficult to produce with a cryomagnet of the same room-temperature inner bore diameter as this coil system (70 mm). The entire magnet structure can be raised up over the top of the tube without breaking vacuum, to allow bakeout and other adjustments. The lowest coil is to provide the field needed to match the beam emerging from the gun anode and pole piece as it flows through the long beam tunnel to the input cavity.

c. An input drive cavity that supports a rotating TE_{111} mode at 11.424 GHz, as fed by the two input waveguides phased in time-quadrature. Cavity radius and length are 8.10 mm and 40.9 mm. The ratio of ohmic-to-beam-loaded quality factors for this cavity is 136, indicating that the efficiency for imparting rf drive power to the beam is 99.2%. Peak surface rf electric field in this cavity at rated drive power is 250 kV/cm, far below the breakdown limit at 11.4 GHz. A short cut-off section is inserted between the drive cavity and the output cavity, with radius 4.6 mm and length 12 mm.

d. A TE_{811} mode output cavity, with radius and length 5.07 mm and 14.7 mm, ending in a gently up-tapered output waveguide. Output power is 11.3 MW at 91.392 GHz, with only 0.85 MW in spurious modes at higher harmonics. Lower harmonic spurious modes are suppressed by careful circuit design. Peak surface rf electric field in this cavity is 727 kV/cm, safely below the breakdown limit at 91.4 GHz.

e. A quasi-optical mode converter for producing a Gaussian output wave beam, consisting of a helical cut in the output waveguide, a quasi-parabolic mirror, two profiled mirrors, and an output window. In addition to producing the low-transmission-loss Gaussian beam, the mode converter separates the wave beam from the spent electron beam, which passes to the collector above. Spurious modes are not focused by the mode converter.

Further detail on each of these elements is given below.

The modulator that could be used to power the W-band tube is rated at 500 kV, 250 A, in 1.1 μsec pulses at a 10 Hz rep rate. This modulator now powers the 11.4 GHz magnicon that can furnish rf drive power for the W-band tube, so that the driver and converter will be operated in parallel on the same modulator. Since the magnicon requires 210 A to run the tube at rated output and gun voltage, only 40 A will be left over for the W-band tube.

Fig. 2 shows the optimum result found for design of the gun, using the code Super-SAM [8]. The beam is seen to be in nearly ideal laminar flow. Maximum electric field on the focus electrode is found to be 195 kV/cm, which is well below the 230-420 kV/cm fields that are sustained by SLAC X-band klystron gun focus electrodes [7]. Cathode loading of 8 A/cm^2 is well within an acceptable range for dispenser cathodes. Geometric emittance is below the irreducible thermal emittance value of 6π mm-mrad; 500:1 electrostatic compression produces a beam with a diameter of 1.1 mm, and subsequent magnetic area compression of about 5:1 in the gradually-increasing field of the input cavity gives a beam diameter computed to be about 0.5 mm. But to provide a margin of safety, simulations of converter performance shown

below are for a beam with diameter of 0.8 mm, corresponding to an overall area compression of ~1000:1.

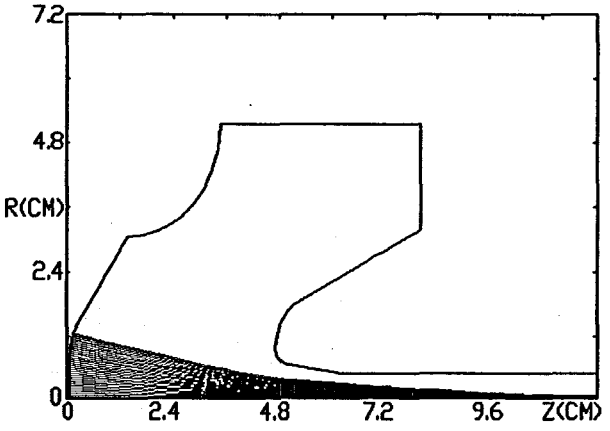

Figure 2. Optimum conceptual design of electron gun for W-band source.

The mechanical design for this gun will be very similar to a gun already delivered from Budker INP for the 34 GHz magnicon now under development by Omega-P, Inc. The only significant design difference between the gun for the W-band source and the 34 GHz gun is the cathode diameter, the corresponding focus electrode changes, and small modifications in anode shape. The existing gun is designed for 200 A with a cathode diameter of 50 mm, while the new gun will be designed for only 40 A with a cathode diameter of 25 mm. The low perveance value of 0.12×10^{-6} A - $V^{-3/2}$ for the new gun will allow a long focal length into the 11.4 GHz drive cavity, perhaps allowing room between the gun and the first iron pole piece for a gate valve.

Designs were optimized of three linked sub-systems of the W-band source, namely magnet, drive cavity, output cavity and mode converter. Fig. 1 shows these elements together. The highest tolerable 11.4 GHz input power level was found to be 28 MW for the available beam current of 40 A; the beam is accelerated in the drive cavity by 700 keV to produce a 1.2 MeV beam at the entrance of the output cavity. For rf drive power above 28 MW, beam energy spread increased and output power decreased. The output cavity, with radius of 5.07 mm and length of 14.7 mm, and a tapered output waveguide, has a diffraction Q of about 400. Suppression of harmonics below the eighth was achieved in the design shown here because the cavity radius is such that these are cutoff. To study the device in detail, a self-consistent system of equations for the electromagnetic fields and electron motions was applied, using time-tested interaction codes.

Fig. 3 shows the optimum magnetic field profile, the structure of the two-cavity/up-tapered output system, and resulting electron trajectories. The power that emerges from the cavity and passes along the following up-taper is shown in Fig. 4; it is seen to be about 11.3 MW. Some power (totaling about 0.85 MW) is radiated into other harmonics, also shown in Fig. 4. But these harmonics are not expected to be focused

into a Gaussian output beam by the output converter optics that are designed for the TE_{81} mode.

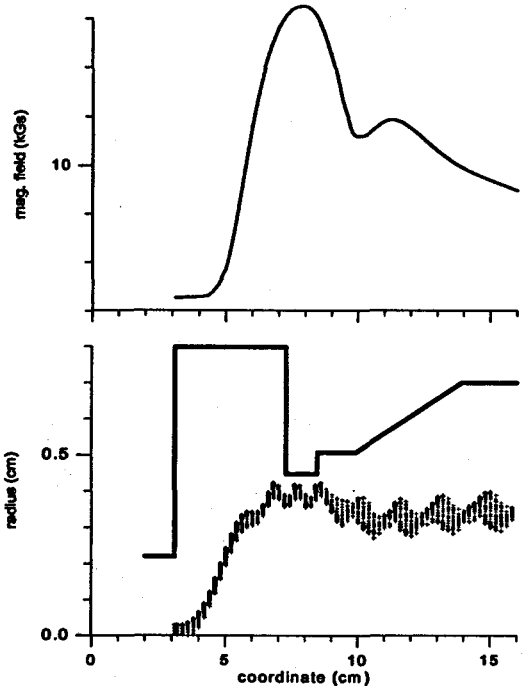

Figure 3. Electron-wave interaction region, showing (top) magnetic field profile; and (bottom) rf structure profile and radii of electron trajectories.

The magnet system is shown in Fig. 5; it has been designed to provide the required magnetic field profile, as shown in full in Fig. 6. The room-temperature coil system consists of three axially symmetric solenoids with independent current control. The solenoids are to be wound with copper wire of rectangular cross-section, and are to be equipped with a two-stage oil-water cooling system. The primary cooling circuit (whose coolant is transformer oil) consists of a heat exchanger and a pump. The secondary circuit of the heat exchanger is cooled by chilled water. Influence of the first coil near the gun, introduced to match the beam into the fields at the input cavity, is neglected in studying the electron dynamics in the interaction regions, but its influence upon fields in the interaction region should be small. Design parameters for the main coils include the following:

coil # 1:	$j = 2.15$ A/mm^2,	$I = 37$ A (or 306 A), $P = 0.21$ kW.
coil # 2:	$j = 18.0$ A/mm^2,	$I = 306$ A, $P = 24.9$ kW.
coil # 3:	$j = 6.43$ A/mm^2,	$I = 109$ A (or 306 A), $P = 7.2$ kW.
coolant flow rate (transformer oil):		3.6 m^3/h, 3-4 atm.
water flow rate for oil cooling:		4 m^3/h, 2 atm.

The total power required is seen to be 32.3 kW, but this figure depends on coil temperature and thus on oil-cooling water flow rates, and may vary within ±10%.

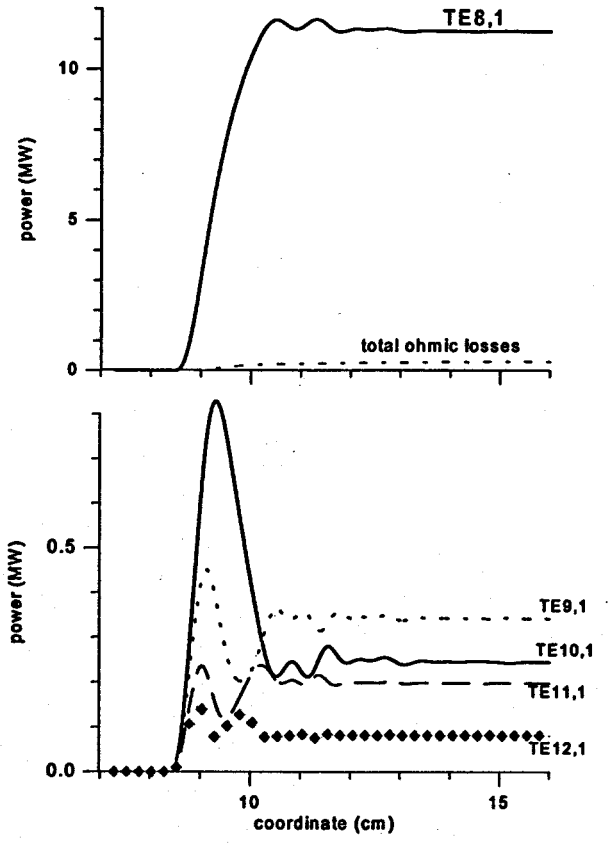

Figure 4. Output power of operating mode and ohmic losses (top); and power in parasitic modes (bottom); as functions of distance along the device.

To convert the $TE_{8,1}$ 91.4 GHz output mode into a nearly Gaussian wave beam that can be transported to a load with negligible loss, a quasi-optical mode converter has been designed. This mode converter consists of a special waveguide cut, a quasi-parabolic mirror, and two profiled turning mirrors, as shown in Fig. 7. The quasi-parabolic mirror transforms the radiation into a paraxial wave beam. The following shaped mirrors maximize the Gaussian mode content in the beam. The shaped mirrors are shown in Fig. 8. The output structure ends with 40 mm diameter window. The mode converter is supported within a 70 mm diameter pipe, so it is possible to hoist the magnet off the W-source so as to bake out the source or to make other adjustments. Fig. 9 shows the intensity and phase variations of the output Gaussian wave beam at the output window.

Collector design is essentially the same as that of a collector already designed and built by Omega-P, Inc. for the 34 GHz magnicon [7].

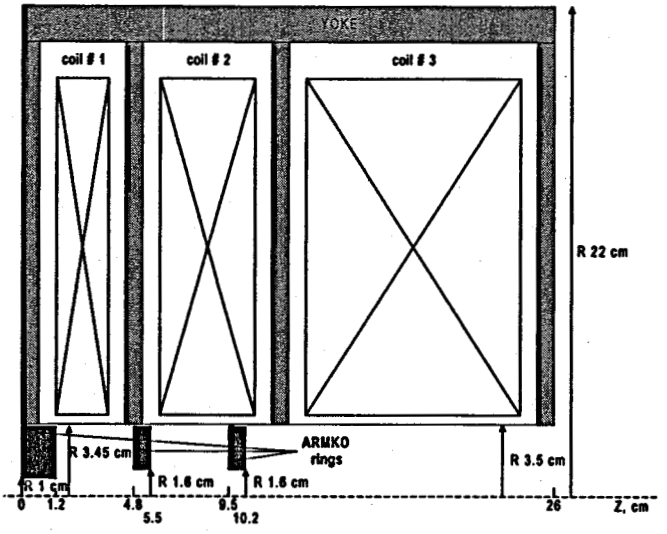

Figure 5. Schematic of the room-temperature magnet system. Shown are the dimensions of the three coils, and of the Armco rings and iron yoke structure. This structure, mounted vertically, is designed to allow removal from the tube without breaking vacuum.

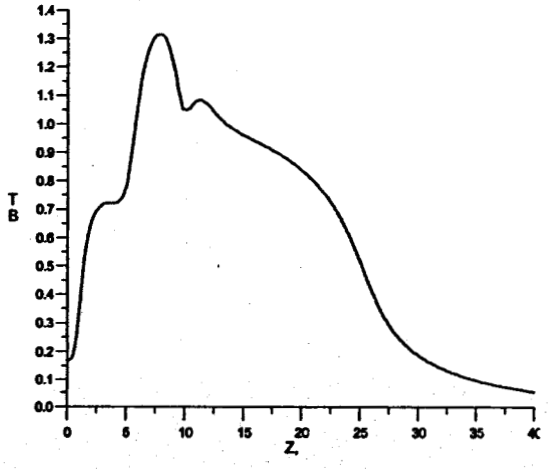

Figure 6. Computed guide magnetic field profile for the structure shown in Fig. 5.

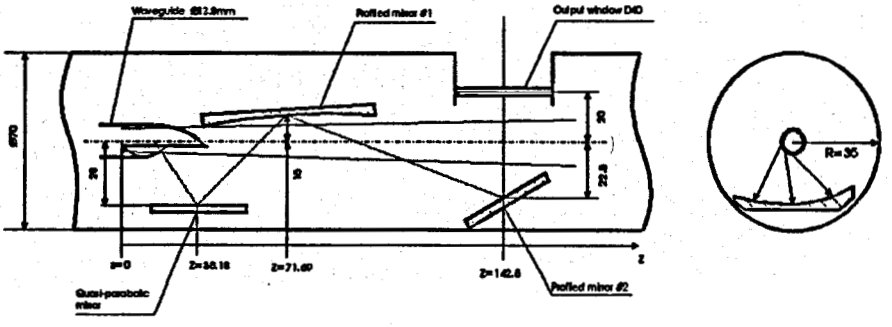

Figure 7. Quasi-optical output structure to convert TE_{81} mode to Gaussian wave beam.

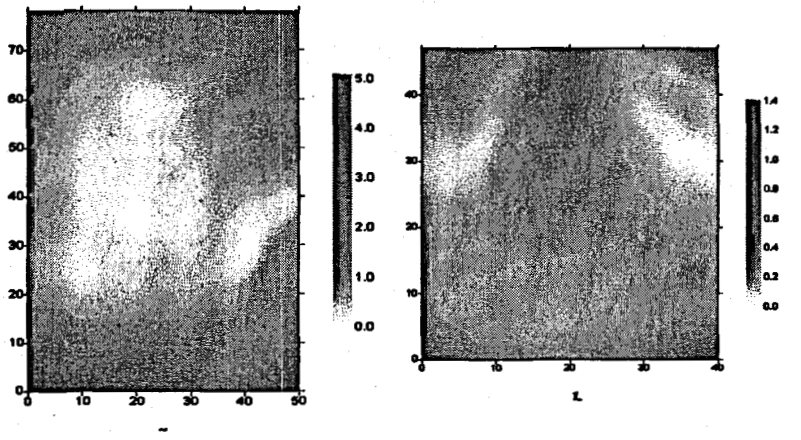

Figure 8. Synthesized mirrors for the quasi-opical mode converter.
The first mirror (*a*) is 50×77.9×5.46 mm; the second mirror (*b*) is 40×46.7×1.48 mm.

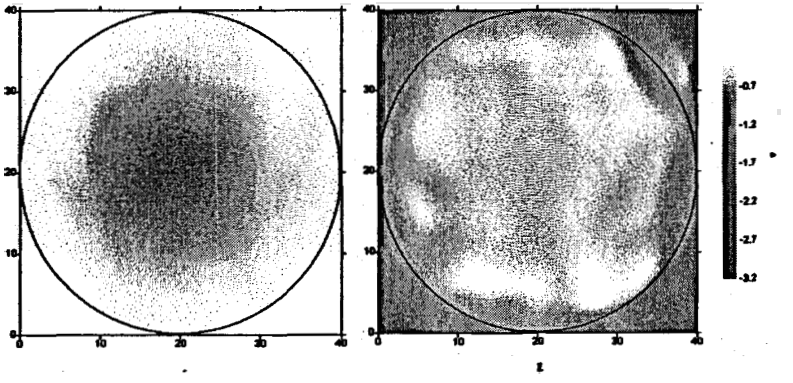

Figure 9. Intensity (*a*), and phase (*b*) patterns at the output window. Gaussian content: $\eta_a = 99.15\%$, $\eta_{a,\varphi} = 98.56\%$; Gaussian parameters: $a_x = 8.26$ mm, $a_y = 7.99$ mm, $S_x = -2.68 \cdot 10^3$ mm, $S_y = 4.66 \cdot 10^3$ mm; Diffraction losses: ≈ 8%.

A summary of the main parameters embodied in the 10-MW W-band source design is given in Table I.

For higher applied rf power, higher beam current is needed, and higher W-band output can be obtained. Indeed, the W-band source described above is designed for a 40 A beam since that is the highest current that can be derived from the NRL modulator operating in parallel with the 11.4 GHz magnicon. Drive power at 11.4 GHz of over 50 MW is expected to be available, but no more than 28 MW of this can be used because of the current limitation. But there is no fundamental limitation to achievement of higher W-band output from this type of source. Study of the performance of the 8th gyroharmonic W-band source reveals, for example, that operation at 80 A should be possible with only minor modifications of the device. Of course, a new gun—similar to that described above—would have to be built with

beam voltage	480 kV
beam current	40 A
gun perveance	0.12×10^{-6} A-$V^{-3/2}$
cathode diameter	25 mm
maximum cathode loading	8 A/cm^2
beam area compression	1000:1
maximum E-field in gun	195 kV/cm
rms beam thermal emittance	6π mm-mrad
rms beam geometrical emittance	0.5 π mm-mrad
11.4 GHz drive power	28 MW
91.4 GHz output power	11.3 MW
Output mode purity	$\eta_a = 99.15\%$, $\eta_{a,\varphi} = 98.56\%$
Output beam radii	$a_x = 8.26$ mm, $a_y = 7.99$ mm
power in spurious harmonics*	0.85 MW
peak magnetic field	13.1 kG
total magnet power	32.3 kW

Table I. Main parameters for proposed 10-MW, W-band source.
*Spurious modes are not focused by output mode converter.

larger cathode and with suitably modified focus electrode and anode. Furthermore, the output cavity would have to be shortened slightly to reduce the diffraction Q to below its present value of 400. The 80 A beam would have a Brillouin diameter of about 0.8 mm, and would thus pass the beam tunnel and interact well in the existing drive cavity. With twice the present drive power, or 56 MW at 11.4 GHz, it is estimated that the W-band output power would be greater than 20 MW.

SUMMARY

The 10-MW W-band source described here embodies several attractive features:

- A high-convergence diode electron gun that is similar to one already built for Omega-P 34 GHz magnicon is employed, so no significant new gun development is needed.
- A high-power beam collector that is similar to one built for the Omega-P 34 GHz magnicon is to be employed, so no significant new collector development is needed.
- An existing X-band magnicon will serve as the rf driver.
- Modulator requirements are to be satisfied by adding a second socket to the existing NRL modulator that powers the Omega-P/NRL X-band magnicon, thereby operating both the driver and the harmonic converter in parallel from the same power supply.
- The required magnetic field is to be provided by room-temperature (non-cryogenic) coils.

- The W-band tube design allows removal, without breaking vacuum, of surrounding magnet structure for high-temperature bakeout and other external adjustments.
- W-band output is in the form of a Gaussian wave beam, suitable for low-loss transmission to a wide class of loads, such as test accelerator structures and associated components.
- For an 80 A beam and 56 MW of 11.4 GHz drive power, it is estimated that a W-band output of about 20 MW could be obtained from this device.

ACKNOWLEDGMENT

This work was sponsored by the US Department of Energy.

REFERENCES

[1] P. J. Chou *et al*, *Advanced Accelerator Concepts, AIP Conf. Proc.* 398, New York, Am. Inst. Phys., (1996) pp. 501-517; D. T. Palmer, at *AAC'98*, Baltimore, 1998; P. B. Wilson, *SLAC-Pub-7449, April 1997*; R. B. Palmer, "Pulsed rf sources for linear colliders," *AIP Conf. Proc.* 337, New York, Am. Inst. Phys. (1994) pp. 1-15.

[2] M. Blank *et al*, *Phys. Rev. Lett.* 79, 4485 (1997).

[3] E. V. Zasypkin *et al*, *IEEE Trans. Plasma Sci.* 24, 666 (1996).

[4] G. Caryotakis *et al*, "High power W-band klystrons," in *High Energy Density Microwaves*, R. M. Phillips, ed., CP474, Am. Inst. Phys. (1999) pp. 59-73.

[5] M. R. Arjona and W. Lawson, to be pub. In *Proc. EPAC'98*, Stockholm (1998); see also "Design of a 10 MW, 91.392 GHz Gyroklystron for Advanced Accelerators," by W. Lawson, R. L. Ives, J. Neilsen, M. E. Read, *abstract submitted to EPAC2000.*

[6] E. Wright *et al*, "Design of a 50-MW-Klystron at X-band," *Proc. RF'94*, AIP Conf. Proc. 337, pp. 58-66 (Am.Inst. Phys., New York 1995).

[7] O. Nezhevenko, *Phys. Plasmas* 7, 2224 (2000).

[8] D.G. Myakishev, M.A. Tiunov and V.P. Yakovlev, "Code SuperSAM for Calculation of Electron Guns with High Beam Area Convergence", XV-th Int. Conf. on High Energy Accelerators, 1992, Hamburg. *Int. J. Mod. Phys.* A (proc. Suppl.) 2B (1993), v-2, pp.915-917.

Multi-Stage, High-Gradient, Cyclotron Resonance Proton Accelerator Concept

J. L. Hirshfield,* Changbiao Wang,* and Robert Symons¶

*Beam Physics Laboratory, Yale University, 272 Whitney Ave., New Haven, CT 06511
¶Litton Electron Devices Division, 960 Industrial Road, San Carlos, CA 94070-4194

Abstract. Simulations are presented that show the possibility of high-gradient, high-efficiency cyclotron-resonance acceleration of protons that drift through a cascade of cavities in a uniform axial magnetic field. Means to maintain phase synchronism with a pulsed proton beam are discussed, with resonance frequencies for successive cavities in the cascade lowered by a fixed frequency interval. In an illustrative example, acceleration of a 114 mA (average current) beam by nearly 118 MeV is predicted for a cascade of two cavities at 100 MHz and 94 MHz in a 6.7 T magnetic field, with an efficiency of over 75% and an average acceleration gradient of over 20 MeV/m. Extension of this concept to ~12 stages could allow design of an accelerator to generate a 1.0 GeV, high-power proton beam.

INTRODUCTION

A preliminary design study has been conducted for a novel high current, high gradient, high efficiency, multi-stage proton cavity cyclotron accelerator. As will be shown below, this concept uses available technology to provide energy gains of over 50 MeV/stage, at an acceleration gradient exceeding 20 MV/m in room temperature cavities, with currents of over 100 mA and efficiency over 75%. Acceleration is provided *via* cyclotron resonance, so a strong static magnetic field is required. An innovation in design is described to minimize the diameters of the cavities and the corresponding diameters of the cryomagnets.

Recent developments in high-intensity proton accelerators, and new applications of high-intensity proton beams, have been reviewed by W. T. Weng [1]. It is possible that the high-gradient proton accelerator concept described in this paper could lead to machines for some of the same applications as existing proton linacs [2], but without need for the substantial real estate associated with conventional acceleration gradients of only ~2 MeV/m. These applications include: injectors into synchrotrons for acceleration to multi-TeV energies for fundamental particle physics research; basic studies in condensed-matter physics, materials science, chemistry, polymer science,

and structural biology; radiography; materials characterization; medical isotope production; nondestructive evaluation; tomographic surveillance; burning of plutonium, energy amplifier, burning of commercial nuclear waste, and production of tritium. Staged cavity cyclotrons might also be used for acceleration of muons, and an example of this is given to illustrate.

A considerable body of material has been published on the design and operation of *electron* accelerators that invoke cyclotron resonance. These include a 400 keV, 12 MW cyclotron autoresonance accelerator (*CARA*) [3]; a 1.2 MeV, 35 MW *CARA* [4]; and a 150 MeV laser-driven *CARA* (*LACARA*) [5]. *CARA* is a microwave-driven electron accelerator and *LACARA* is laser-driven. In contrast, the proton accelerator described here would be a VHF-band rf machine, operating at frequencies in the range 40-120 MHz for acceleration up to about 0.5-1.0 GeV. *CARA* and *LACARA* operate with non-uniform magnetic fields having spatial profiles designed to preserve cyclotron resonance along the acceleration path, while the proton accelerator described here employs a uniform magnetic field in which slippage in and out of resonance phase occurs in each stage. The magnetic field in the proton accelerator must be uniform across all stages, since—as protons drift from one stage to the next—an increasing field would lead to loss of axial momentum and stalling, while a decreasing field would lead to an unmanageable increase in orbit radius. Successive cavity stages of the proton accelerator operate at successively-lower rf frequencies, to maintain approximate resonance as the proton mass increases: acceleration from 10 keV to 1.0 GeV requires a frequency reduction between the first and last stages of approximately a factor-of-two. This diminution in frequency is opposite to the temporally-increasing frequency variation typical for synchrotrons [6], where the magnetic field also increases. Electron cyclotron accelerators in laboratory tests have be shown to be capable of operation with rf-to-beam power efficiencies of over 90% [3]. High efficiency is also possible in proton cavity cyclotron accelerators, as will be shown below. These superficial comparisons suggest that the accelerator described here is qualitatively different from existing proton machines, most notably in its high acceleration gradient and high efficiency. However, it must be stressed that results shown here are preliminary and are not optimized with respect to any particular system parameter. Clearly, additional design computations, and construction and operation of a prototype, should be carried out to show that the presently-perceived virtues of the concept can be realized in practice.

Results are presented in this paper of a preliminary computational study to illustrate the new concept for proton acceleration. Computations have been carried out for a two-stage system that seems to embody much of the relevant physics; extension to a large number of stages is straightforward. The rf structure for computations described here is shown in Fig. 1. It consists of back-to-back TE_{111} rotating mode room temperature cavities immersed in a strong uniform axial magnetic field. Protons are injected at 10 keV directly from an ion source. The cavities are driven with rf power at different frequencies, with the resonant frequency of the second cavity lower than that of the first. Phase slip of up to ±3-4% occurs in each cavity during acceleration.

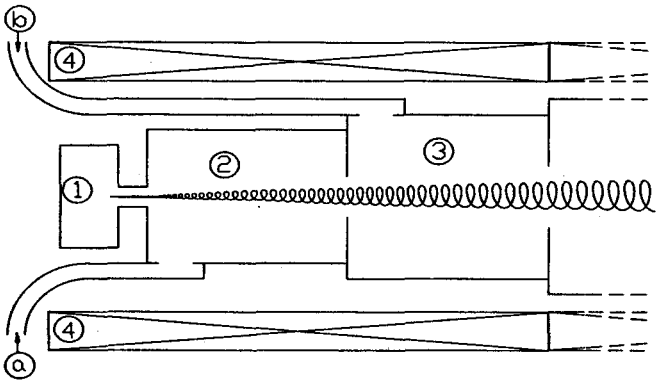

Figure 1. Sketch of two stages in a multi-stage high-gradient cavity proton accelerator. (1) ion source; (2) 100 MHz cavity; (3) 94 MHz cavity; (4) solenoid coil. (a) and (b) are input feeds for the cavities. A proton orbit is also sketched.

RESULTS OF COMPUTATION

For the illustrative example to be presented here, the first cavity is driven with 10 MW of rf power at 100 MHz, the second with 7.7 MW at 94 MHz. The unloaded and beam-loaded quality factors for the first cavity are Q_o = 100,000 and Q_L = 30,000; while for the second cavity they are Q_o = 100,000 and Q_L = 17,000. These values imply that 70% of the incident rf power is absorbed by the proton beam in the first cavity, and 83% in the second cavity; the beam power after the second stage is 13.4 MW. A uniform magnetic field of 67.0 kG threads both cavities. The injected proton beam energy is 10 keV, the final proton energy is 114.0 MeV and the proton current is 117.6 mA. The beam is taken—for purposes of this illustration—to have zero initial emittance and zero initial energy spread. Sixteen computational particles to simulate the beam are injected at time intervals of 1.25 nsec, corresponding to rf phase intervals of $\pi/4$ over two cycles at 100 MHz and to a pulse width of 20 nsec; the injected particles have zero initial radial coordinate. The histories of average energy gain and axial velocity variation along the first cavity are shown in Fig. 2, for three values of axial guide magnetic field B_z = 66.8, 67.0, and 67.2 kG. This cavity has a radius of 110 cm. The energy gain at the end of the cavity (z = 249 cm) is maximum for 67.0 kG, where the decrease in axial velocity within the cavity is not as severe as for the 67.2 kG case. Further increase in B_z is found to lead to a reversal of the sign of axial velocity, i.e. to particle reflection. This stalling effect is attributable to a ponderomotive axial force, which evidently depends on the precise details of the proton orbit. For B_z = 67.0 kG, a net energy gain $\overline{U} - \overline{U}_o$ = 59.5 MeV (γ = 1.063) is found during passage through the cavity, where $\overline{U}$ and $\overline{U}_o$ are the ensemble average final and initial proton energies. The small diminution in particle energy for z > 200 cm is attributable to excessive phase slip, since the cyclotron frequency of the protons has fallen to below 94% of the rf frequency at this stage. The average acceleration

gradient in the first cavity is 23.8 MeV/m. With a beam current of 117.6 mA, the efficiency of the first cavity is 70%. The strong axial acceleration gradient is possible since protons make a large number of gyrations, and follow a long path moving nearly parallel to the rotating rf electric field. For this example, the protons execute about 48 turns in the first cavity, and reach a final gyration radius of about 17 cm. This rapid,

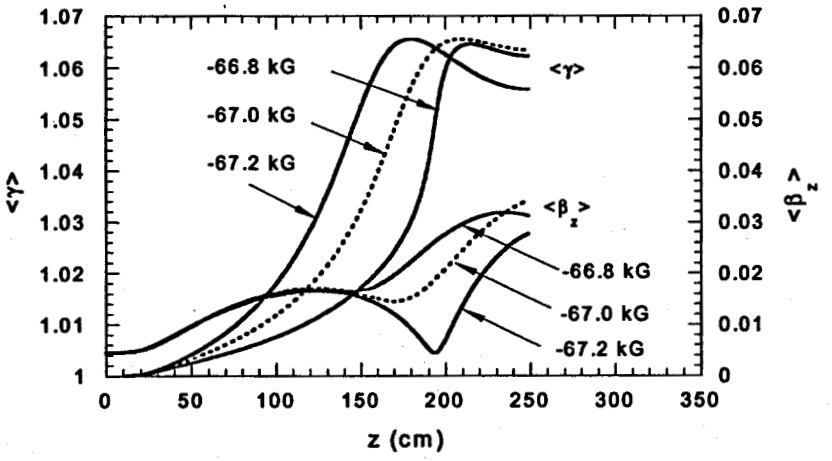

Figure 2. Computed variations of mean proton energy, in units of $\langle\gamma\rangle = 1 + \overline{U}[\mathrm{MeV}]/938$, and mean axial velocity $\langle\beta_z\rangle = \overline{v}_z/c$, as functions of axial coordinate z within the first cavity. Examples are for $I = 117.6$ mA and for other parameters as described in text, and for three values of B-field.

efficient cyclotron resonance acceleration of protons in a TE_{111} cavity with a uniform magnetic field is reminiscent of similar results reported for electrons by Jory and Trivelpiece [7], who showed evidence of acceleration by 100's of keV.

Fig. 3 shows the energy gain and axial velocity for two cavities operated in tandem. The second cavity, operating at 94 GHz, has a radius of 110 cm and a length of 302 cm. The relative phase difference between fields in the first and second cavities

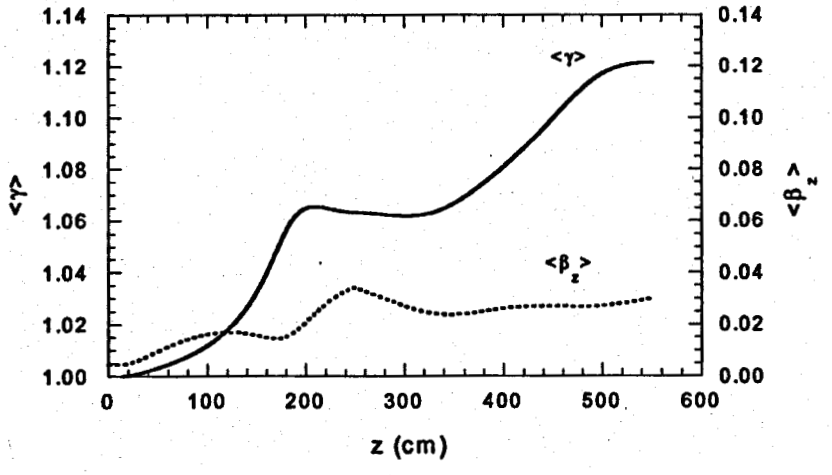

Figure 3. Energy gain for protons in traversing two cavities. Final proton energy is 114 MeV, beam current is 117 mA, average acceleration gradient is 20.7 MeV/m, and rf-to-beam efficiency is 75.6%.

(reckoned at the initial time) is set at 0.70π. This phase difference allows gyrating protons to enter the second cavity with their velocity vectors aligned nearly parallel to the rotating rf electric field; phase synchronism is discussed in the next section of this paper. From Fig. 3, it is seen that the energy gain in the two cavities together reaches 113.96 MeV ($\gamma = 1.1215$), while the axial velocity remains sensibly constant throughout the second cavity. The beam-loaded Q (17,000) and rf drive power (7.7 MW) were adjusted to accommodate the same current (117.6 mA) as in the first cavity; this adjustment required several steps of computational iteration. The protons execute about 43 turns in the second cavity, and reach a final gyration radius of about 22 cm. The average acceleration gradient for both cavities is 20.7 MeV/m. Figs. 4 and 5 show projections in the transverse (x-y) and longitudinal (x-z) planes of the orbit of a single proton during the course of its acceleration.

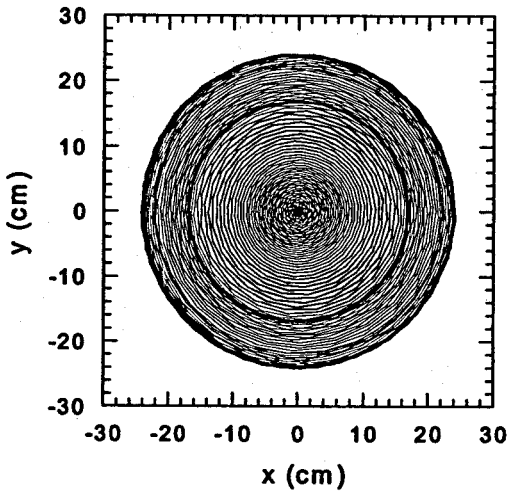

Figure 4. Projection in the transverse plane of the orbit of a proton undergoing acceleration, as in Fig. 3.

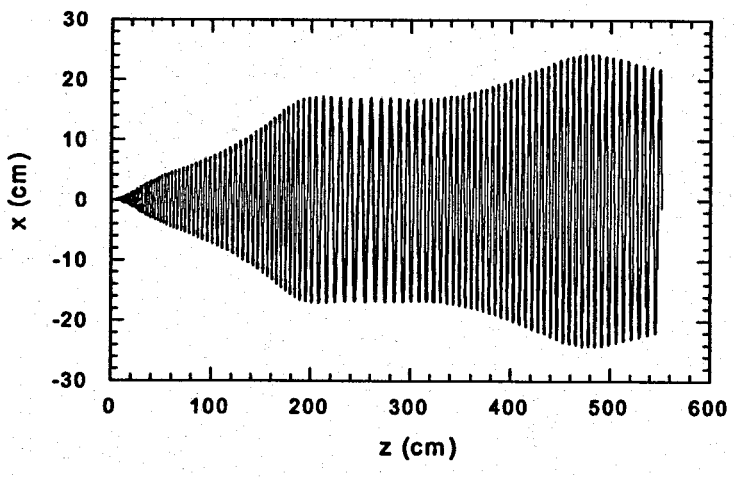

Figure 5. Projection in a longitudinal plane of the orbit of a proton undergoing acceleration as in Figs. 3 and 4. The proton executes 91 turns during acceleration. At $z = 550$ cm, $\beta_\perp/\beta_z \approx 15$.

The same principle that is shown in the above example for acceleration of protons can also be applied to acceleration of other charged species, namely electrons [7], muons, or heavy ions. In view of the current strong interest in muon accelerators [8], it may be instructive to provide an example of muon acceleration at cyclotron resonance using cavities in a strong uniform magnetic field. Fig. 6 shows an example for two cavities in a uniform 67.0 kG B-field, for parameters as follows.

1st cavity: $f = 850$ MHz, $P = 10$ MW, $Q_o = 40{,}000$, $Q_L = 20{,}000$, $R = 13$ cm, $L = 29$ cm;
2nd cavity: $f = 700$ MHz, $P = 4.0$ MW, $Q_o = 40{,}000$, $Q_L = 10{,}000$, $R = 15$ cm, $L = 39$ cm.

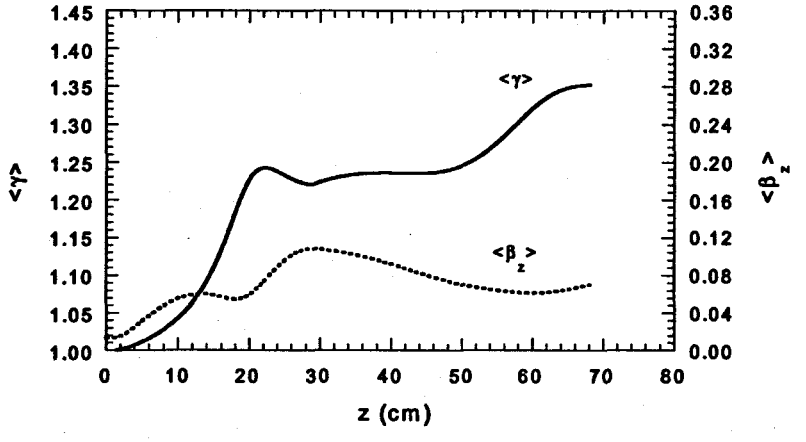

Figure 6. Normalized mean energy $\langle\gamma\rangle = 1 + \overline{U}[\text{MeV}]/105.7$ and axial velocity $\langle\beta_z\rangle$ for muons in the two-cavity cyclotron accelerator described above.

Acceleration in the first cavity is from 10 keV to 23.24 MeV, and in the second cavity to 37.1 MeV. The beam current is 215 mA, maximum orbit radius is 3.8 cm, average acceleration gradient is 54.4 MeV/m, and overall efficiency is 57%. These values compete favorably with conventional muon linacs.

PHASE SYNCHRONISM CONSIDERATIONS

In the cavity cascade concept described here, protons drift from one TE_{111} cavity to the next, but successive cavities must have lower resonance frequencies in order to effect cumulative acceleration, since the imposed axial magnetic field is uniform and the effective proton mass is increasing. Thus, the issues of phase synchronism and stability must be examined carefully. For a single narrow bunch of protons, it is not difficult to imagine acceleration through a cascade of cavities, provided the phases for fields in each cavity are properly adjusted. Specifically, as the proton bunch arrives at each cavity, if the orientation of the electric vector of the rotating TE_{111} mode is parallel to the proton momentum, maximum acceleration is afforded. However, uniform acceleration of a train of proton bunches can occur only if the phases of disparate frequencies in successive cavities are judiciously sequenced, to insure that

all bunches have identical histories as they progress through the cascade. This can be arranged if the cavity frequencies decrease in equal increments. For example, suppose the frequency decrease between cavities is 5 MHz, and the cavity frequencies are 100, 95, 90, 85, 80...50 MHz. Also suppose that the initial phases of the fields in each cavity are such as to provide optimized cumulative acceleration to the first proton bunch. If successive bunches are injected at time intervals of $(5\ \text{MHz})^{-1} = 200$ nsec, then the fields seen by each bunch are identical to those seen by the first bunch. This is so since, after each 200 nsec interval, fields in the respective cavities will have advanced by precisely 20, 19, 18, 17, 16...10 cycles, and will thus reconstruct the sequence seen by the first bunch. Since precise reconstruction only occurs at 200 nsec intervals (in this example), protons in a finite width bunch experience slightly different acceleration histories, leading to a finite energy spread for the bunch. However, careful choice of the median phase difference between successive cavities can minimize this spread. Moreover, phase focusing can also occur. In these regards, the cavity cascade has features in common with a conventional rf linac.

Examples of the effects of finite proton bunch width are shown in Fig. 7. Within the first cavity, acceleration is independent of the time of injection. But, due to the phase

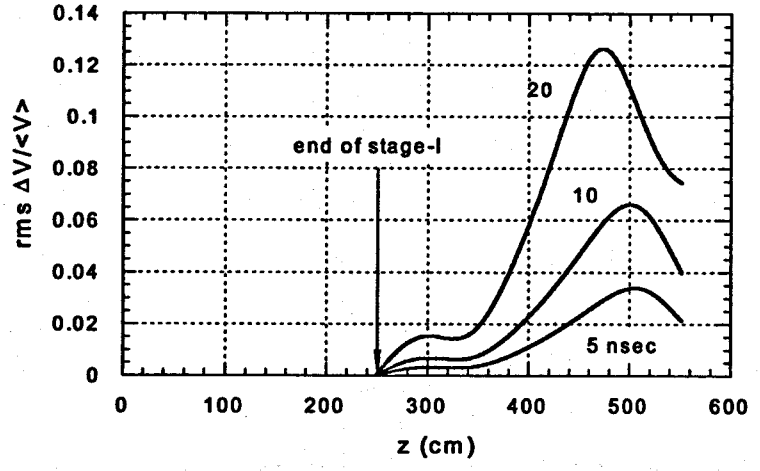

Figure 7. Influence of finite bunch width on beam rms energy spread, for parameters described in text. The examples shown correspond to duty factors of 3%, 6%, and 12%.

dependence of acceleration in the second cavity, energy spread increases with pulse width. For this example, parameters for the first cavity at 100 MHz are as in Figs. 2-5. In the second cavity at 94 MHz, parameters are also as in Figs. 2-5, except for small variations in Q_L and final average beam energy. For the 5, 10, and 20 nsec examples these are 13,200, 13, 600, and 17,000; and 116.2, 116.0, and 114.0 MeV, respectively. The relative initial phase difference between fields in the two cavities is 0.70π. For the 5 nsec case, the final energy spread is seen to be about 2%.

Fig. 8 illustrates the influence of relative phase difference upon beam energy spread. Here, for a 5 nsec pulse width (3% duty factor), acceleration history and evolution of beam rms energy spread are plotted for three values of relative phase shift, namely 0.65π, 0.70π, and 0.75π. It is seen that a final rms energy spread of about 0.7% is

found for the 0.75π case, lower by nearly a factor-of-3 than the 0.70π case. Here, the second cavity Q_L and final average beam energies are 16,500, 13,200, and 11,600; and 114.2, 116.2 and 117.3 MeV, respectively. The facts that energy spread decreases significantly after $z \approx 500$ cm, and that minimum spread accompanies maximum final energy, strongly suggest that longitudinal phase focusing is occurring, a phenomenon that is sensitive to small changes in relative phase between cavities.

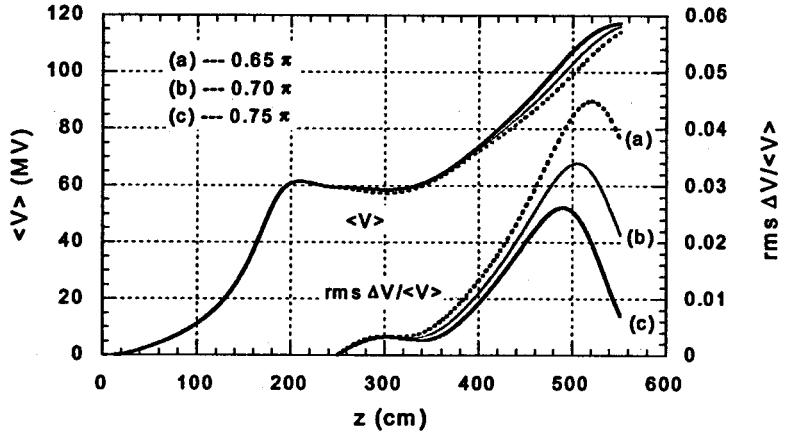

Figure 8. Acceleration history and evolution of rms energy spread in a two-cavity proton accelerator for three values of relative initial phase between fields in the two cavities. Note the significant diminution in energy spread for case (c) towards the end of the trajectory.

It is also instructive to illustrate the bunch shape during acceleration. Figs. 4 and 5 show the orbit for a typical proton, but the instantaneous distribution of charge for a finite-length bunch does not lie along this curve, since orbits of successive protons are rotated in the x-y plane at the rf frequency. To illustrate, Figs. 9(a) and 9(b) show the

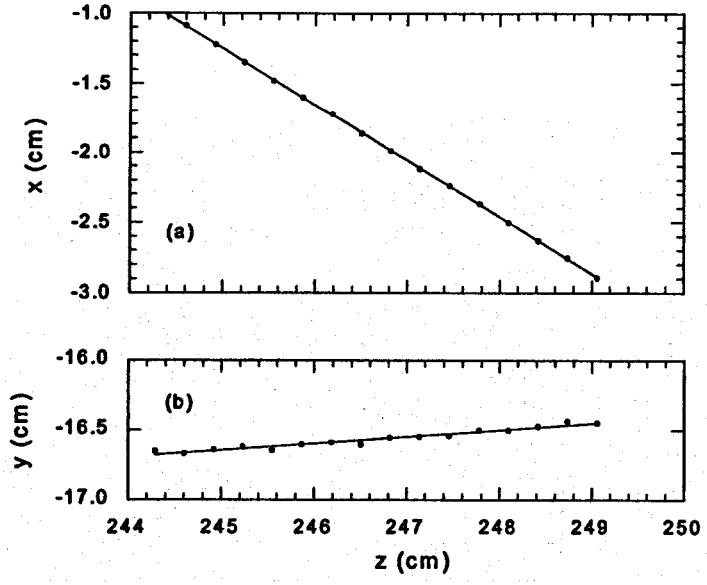

Figure 9. Loci in x-z and y-z for protons in a 5 nsec bunch, at the end of the first cavity. The bunch is seen to be a straight line of charge that gyrates as a whole about the cavity axis.

x-z and *y-z* loci for 16 protons injected on axis within a 5 nsec long bunch, at the instant (671.5 nsec after injection) that the head of the bunch reaches the end of the first cavity at $z = 249.06$ cm. The particles are seen to lie along a nearly straight line ~4.8 cm long, with a deviation from linearity of less than 0.4 mm. These particle loci can be contrasted with the trace in *x-z* for the first particle during its final 4.8 cm of travel, which is a half-cycle of oscillation with radius ~17 cm, as shown in Fig. 5. During acceleration, the proton bunch advances in *z* and rotates about *z* nearly as a straight rigid object. The small deviations from linearity arise from phase slip between proton momenta and the rf electric field, and from small energy differences during acceleration between the head and tail of the bunch. The near-uniformity of the axial charge distribution within such a long bunch should mitigate against longitudinal instability.

CAVITY DESIGN CONSIDERATIONS

The 100 MHz and 94 MHz TE_{111} cavities for the example of the first two stages of the proton accelerator discussed above have diameters of 220 cm, yet the maximum proton orbit diameters are only 34 and 44 cm. At least in these first stages, most of the cavity volume is not traversed by the proton beam, but is permeated with magnetic flux lines from the surrounding coils. The 67 kG cryomagnet would need a room-temperature bore diameter of perhaps 240 cm (to allow room for the rf feeds, as sketched in Fig. 1); while this is probably within the present state-of-the-art, it would be highly desirable if a means were found to reduce this bore diameter. One such means to achieve this is to employ thick radial vanes in the cavity that provide capacitive loading and thereby reduce the cutoff frequency for the desired dipole modes. When four symmetric vanes are used, the structure resembles that for a radio-frequency quadrupole, except that it is the two degenerate dipole modes that are of interest, rather than the quadrupole modes. To obtain a rotating ("circularly polarized") field, the two dipole modes must be excited in time-quadrature. A simple example of such a structure has been analyzed using the HFSS structure simulation code; the structure outline and computed *E*-field flux lines are shown in Fig. 10.

For the structure shown, with an outer diameter of 130 cm, a ridge width of 15 cm, and a central gap between opposing ridges of 30 cm, the cutoff frequency for the dipole mode is found to be 73.7 MHz, while the cutoff frequency for the quadrupole mode is 78.97 MHz. Thus a section of structure 222 cm in length would have a dipole resonance frequency of 100 MHz, and a quadrupole resonance frequency of 104 MHz. Operation with Q_L of the order of 1,000-10,000 should thus be possible purely in the dipole mode, without significant coupling by the beam to the quadrupole mode. This idealized example is shown to illustrate the possibility of devising an all-metal structure for the cavities that will have an outer diameters significantly smaller than for a simple TE_{111} cylindrical cavity. Clearly, it is required to refine the analysis of such structures, including optimizing the shape of the vanes, rounding of sharp corners

to reduce surface field strengths, and provision of input coupling for excitation of both degenerate dipole modes in time quadrature.

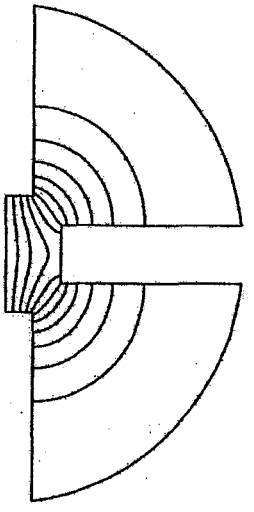

Figure 10. Example of cross-section of 4-vaned cavity structure for proton cyclotron accelerator. Note that only one-half of the structure is shown, after cutting along the vertical axis of symmetry. Electric field lines shown for the dipole mode are seen to be nearly uniform near the axis.

CONCLUSIONS

Preliminary computations indicate that a cavity cascade can be designed and built for cyclotron resonance acceleration of an intense proton beam to energies in the range of 1 GeV. This new concept is characterized by high acceleration gradient for room-temperature cavities (~20 MV/m), high rf-to-beam efficiency (~75%), and high average beam currents (~100 mA). A design innovation is introduced to minimize the diameters of the cavities, and the diameters of the associated cryomagnets.

REFERENCES

[1] W. T. Weng, "Ultra-high intensity proton accelerators and their applications," *Proc. 1997 Particle Accelerator Conf. (Vancouver)* vol. 1, pp. 42-46 (IEEE, 1998).

[2] See, for example, J-M. Lagniel, S. Joly, J-L. Lemaire, and A. C. Mueller, *Proc. 1997 Particle Accelerator Conf. (Vancouver)* vol. 1, pp. 1120-1122 (IEEE, 1998).

[3] J. L. Hirshfield, M. A. LaPointe, A. K. Ganguly, R. B. Yoder, and C. Wang, "Multi-megawatt cyclotron autoresonance accelerator," *Phys. Plasmas* 3, 2163 (1996); see also "Experimental demonstration of high efficiency electron cyclotron autoresonance acceleration," *Phys. Rev. Lett.* 76, 2718 (1996).

[4] M. A. LaPointe, C. Wang, and J. L. Hirshfield, "Cyclotron autoresonance accelerator for electron beam dry scrubbing of flue gases," in CP475 *Applications of Accelerators in Research and Industry*, J. L. Duggan & I. L. Morgan, eds., pp. 945-948 (Am. Inst. Phys., 1999).

[5] J. L. Hirshfield and C. Wang, "Laser-driven cyclotron autoresonance accelerator," *Proc. 1999 Particle Accelerator Conf. (New York)* vol. 5, pp. 3630-3632 (IEEE, 1999); "Laser-driven electron cyclotron autoresonance accelerator with production of an optically chopped electron beam," *Phys. Rev.* E 61, pp. 7252-7255 (2000).

[6] See, for example, E. J. N. Wilson, "Synchrotrons and storage rings," in *Handbook of accelerator physics & engineering*, A. W. Chao & M. Tigner, eds. (World Scientific, Singapore, 1999), pp. 42-44.

[7] H. R. Jory and A. W. Trivelpiece, "Charged-particle motion in large amplitude electromagnetic fields," *J. Appl. Phys.* 39, pp. 3053-3060 (1968).

[8] Y. Zhao, R. Palmer, R. Fernow, J. Gallardo, and H. Kirk, "A normal conducting accelerator for a muon collider demonstration machine," *Proc. 1997 Particle Accelerator Conf. (Vancouver)* vol. 1, pp. 408-410 (IEEE, 1998).

GYRORESONANANT ACCELERATION OF ELECTRONS, MUONS AND PROTONS*

J. L. Hirshfield**
Department of Physics, Yale University, New Haven, CT 06520 & Omega-P, Inc. New Haven, CT 06511

Abstract. Gyroresonant acceleration of charged particles is explored in light of much that has been learned about the interaction of electromagnetic radiation and electron beams during decades of development of gyro-amplifiers and gyro-oscillators. Examples are shown for high-gradient acceleration of electrons, muons, and protons.

INTRODUCTION

Gyroresonant acceleration of charged particles has been re-examined, wherein infrared lasers, cm-wavelength microwaves or m-wavelength rf furnish the excitation, and where the species considered include electrons, muons and protons. Published experiments for electron autoresonance acceleration show the production of multi-MW gyrating electron beams, where rf-to-beam efficiencies >90% have been found [1]. In this paper several theoretical examples are given. (*i*) Microwave cavity excitation is shown to provide a compact high-power, high efficiency, cyclotron accelerator for a 5 MeV electron beam; this configuration is attractive for several industrial applications. (*ii*) Acceleration is shown over all optical phases and over meter-length paths for electrons in the fields of a gently focused TW-level CO_2 laser. It is shown that acceleration gradients of ~100 MV/m result. Optical chopping of the beam can provide a train of femtosecond bunches. (*iii*) Multi-cavity rf cyclotron acceleration of protons and muons is shown possible, with acceleration gradients of about 20 and 50 MV/m, respectively, or about one order-of-magnitude greater than with conventional room-temperature linacs. These studies illustrate how lessons learned from research on millimeter-wave gyrodevices can be translated into other fields.

MICROWAVE CAVITY ELECTRON CYCLOTRON ACCELERATOR

Fig. 1 shows the ensemble-average energy factor $\langle\gamma\rangle$ and the normalized axial velocity $\langle\beta_z\rangle$ for electron acceleration in a rotating-mode TE_{111} cavity in a uniform magnetic field. Here, a 1 keV, 13.69 A injected cold beam is accelerated to 5.26 MeV in a 5.2 kG uniform magnetic field, with 80 MW of pulsed rf power at 2.856 GHz absorbed in the cavity. The cavity radius and length are 5.0 and 6.66 cm, while the loaded and unloaded cavity Q's are 2,000 and 20,000. RF-to-beam efficiency is 90%, so final pulsed beam power is 72 MW. Peak and average acceleration gradients are 332 and 79 MV/m.

LASER AUTORESONANCE ACCELERATION (*LACARA*) [2]

Fig. 2 shows results of computation of electron acceleration by a focused 4-TW CO_2 laser in vacuum in a resonance magnetic field. The electrons execute about five gyrations in traversing the 148-cm inter-mirror distance, reflecting a strong Doppler down-shift. It is seen that the mean beam energy is predicted to rise monotonically from 50 MeV to 178 MeV in 148 cm, corresponding to a maximum acceleration gradient of 147 MV/m and an average acceleration gradient of 86.6 MV/m. The resonance magnetic field required rises from 52 to about 81 kG near the laser focus, and then falls back to about 60 kG. Few, if any, other laser-based schemes enjoy continuous acceleration over m-lengths at ~100 MV/m.

PROTON AND MUON CYCLOTRON RESONANCE CAVITY ACCELERATORS [3]

A preliminary computational study has been carried out to illustrate a new concept for proton and muon acceleration. The rf structure consists of a cascade of back-to-back TE_{111} rotating mode room temperature cavities immersed in a uniform 6.7 T axial magnetic field. For the illustrative 2-cavity proton example shown here, the first cavity is driven with 10 MW of rf power at 100 MHz, the second with 7.7 MW at 94 MHz. The unloaded and beam-loaded Q's for the first cavity are Q_o = 100,000 and Q_L =

30,000; while for the second cavity they are Q_o = 100,000 and Q_L = 17,000. These values imply that 70% of the incident rf power is absorbed by the proton beam in the first cavity, and 83% in the second cavity; the beam power after the second stage is 13.4 MW. The injected proton beam energy is 10 keV, the final proton energy is 114.0 MeV and the proton current is 117.6 mA. The average acceleration gradient in the first cavity is 23.8 MV/m. The rf-to-beam efficiency of this accelerator is 75.7%. Extension to ~12 cavities should allow proton acceleration to 1 GeV. Numerous applications exist for 100 MW, 1 GeV proton beams, including accelerator-based transmutation of nuclear waste.

A similar cavity cascade configuration can be used for acceleration of muons, as shown in Fig. 4, for parameters as follows: B_z = 6.7 T; f = 850 MHz, P = 10 MW, Q_o = 40,000, Q_L =20,000, R = 13 cm, L = 29 cm, for the first cavity; f = 700 MHz, P = 4.0 MW, Q_o = 40,000, Q_L =10,000, R = 15 cm, L = 39 cm, for the second cavity. Acceleration in the first cavity is from 10 keV to 23.24 MeV, and in the second cavity to 37.1 MeV. The beam current is 215 mA, average acceleration gradient is 54.4 MV/m, and overall efficiency is 57%. These values compete favorably with conventional muon linacs.

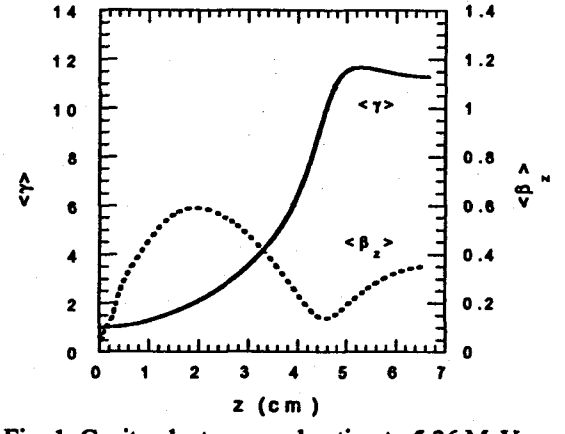

Fig. 1. Cavity electron acceleration to 5.26 MeV.

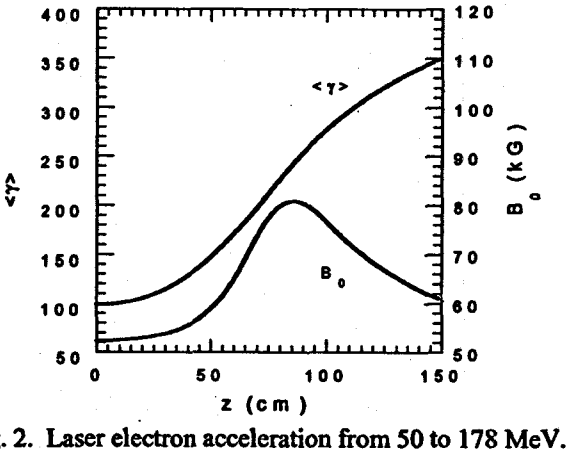

Fig. 2. Laser electron acceleration from 50 to 178 MeV.

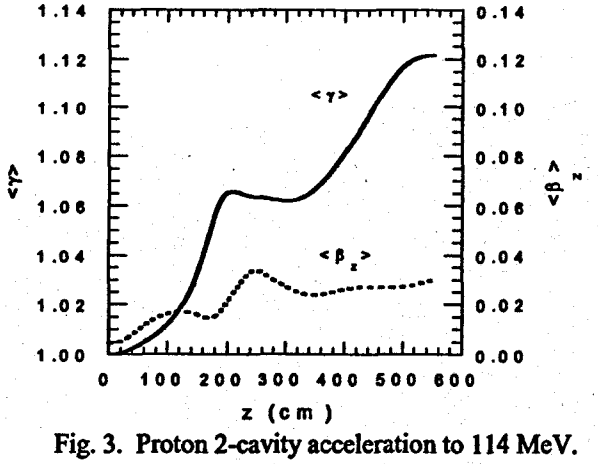

Fig. 3. Proton 2-cavity acceleration to 114 MeV.

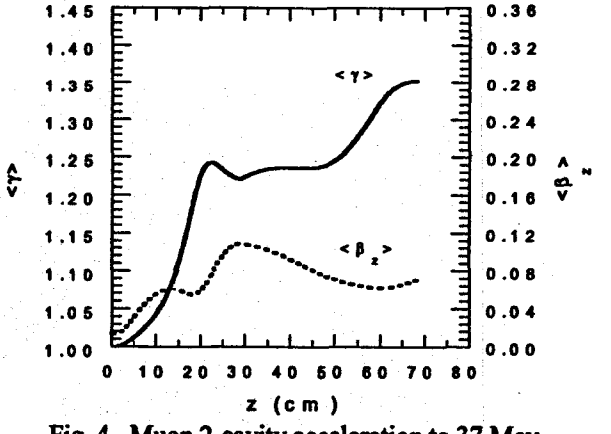

Fig. 4. Muon 2-cavity acceleration to 37 Mev.

*Research sponsored in part by US Department of Energy, Division of High Energy Physics.

**Computational results shown in this paper were obtained by Changbiao Wang of Yale University.

[1] M. A. LaPointe, R. Yoder, Changbiao Wang, A. Ganguly, and J. L. Hirshfield, *Phys. Rev. Lett.* 76, 2718 (1996).

[2] J. L. Hirshfield and Changbiao Wang, *Phys. Rev.* E 61, 7252 (2000).

[3] J. L. Hirshfield, Changbiao Wang, and R. Symons, in *Advanced Accelerator Concepts 2000* (to be published).